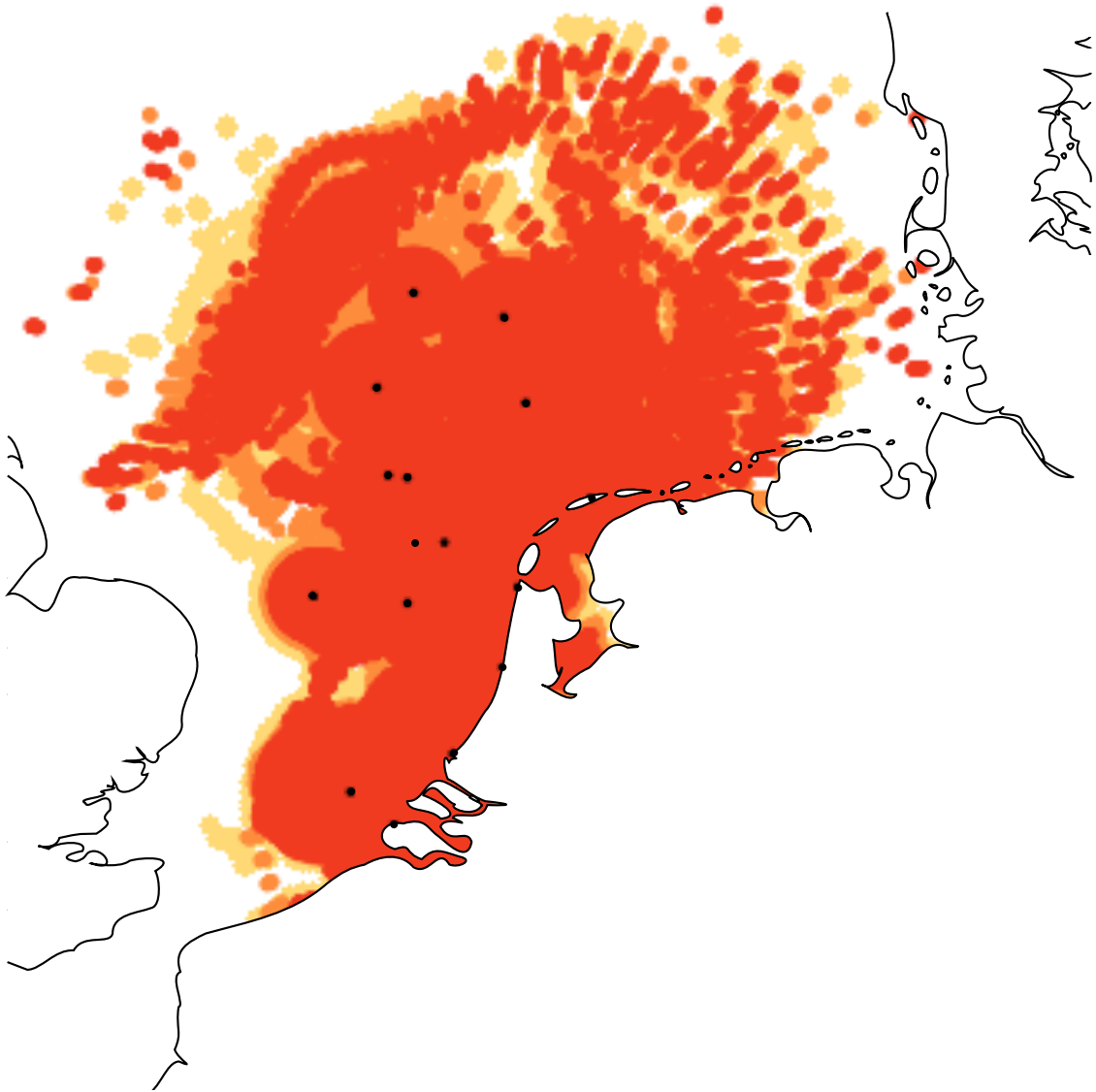# On propagation effects in Maritime Situation Awareness

Modelling the impact of North Sea weather conditions
on the performance of AIS and coastal radar systems

E.R. Bruin

Master of Science Thesis - Utrecht University

On propagation effects in Maritime Situation Awareness

Modelling the impact of North Sea weather conditions on the performance of AIS and coastal radar systems

AUTHOR

E.R. BRUIN
erikbruin@gmail.com
student number 3646173

SUPERVISED BY

DR. A.V. VAN LEIJEN
Kennis, Innovatie, eXperimenten en Simulatie (KIXS)
Ministry of Defence
PROF. DR. R. FERNANDEZ
Utrecht University
PROF. DR. IR. J.E. FRANK
Utrecht University

Utrecht University

Ministry of Defence

Disclaimer

This research was conducted during an internship at the Ministry of Defence. The primary goal of this research is complete the academical and educative objectives of the student. The conclusions and recommendations do not necessarily represent the opinion of the Ministry of Defence.

A full operational analysis of sensor coverage by the Netherlands Coastguard is a complex endeavour. This research focuses on one aspect only, which is the influence of prevailing weather conditions. As such, the results do not take into account issues such as technological limitations or limitations in line of sight due to physical mounting of sensor parts. Furthermore, this thesis documents results for simulated sensor infrastructure only.

The security classification for this document is UNCLASSIFIED.

Abstract

On propagation effects in Maritime Situation Awareness

**Modelling the impact of North Sea weather conditions
on the performance of AIS and coastal radar systems**

E.R. Bruin

This thesis studies the environmental impact on radio wave propagation of the Automatic Identification System (AIS) and coastal radar systems in the operational area of the Netherlands Coastguard, i.e., the exclusive economical zone (EEZ) of the Netherlands. In this part of the North Sea, the coastguard monitors marine traffic to maintain a safe and secure environment. For their situation awareness, they are depending on (Class A) AIS and (X-band) radar. However, the operators of these sensor systems often experience abnormal effects such as coverage gaps and different detection ranges for AIS and radar. An important and strongly fluctuating cause of these effects is the environmental impact on radio wave propagation. Therefore, the weather conditions on the North Sea and the impact of these different conditions are analysed and modelled.

In general, five common propagation conditions are known: standard atmosphere, evaporation ducts, standard surface ducts, surface-based ducts, and elevated ducts. The effects of these conditions and their occurrences on the North Sea were studied for AIS and radar.

It was found that elevated and surface ducts - most prominent during spring and summer - extend both AIS and radar detection ranges, whereas evaporation ducts - strongest at the end of summer - were found to only extend radar detection ranges. Standard atmospheric conditions lead, for both systems, to minimum detection ranges.

The modelling in this thesis is a proof of concept for the coastguard to make a forecast of the coverage of their systems on a daily basis, by using Numerical Weather Prediction (NWP) data. Such a daily forecast will support the coastguard in the deployment of mobile detection units, such as ships and aircraft. The modelling also enables operators to understand why targets appear either on AIS or radar, thus preventing that signals are wrongly considered false or suspicious.

Key words: Automatic Identification System; AIS; VHF; Radar; X-band; Ducting; Coastguard; Propagation; North Sea; Numerical Weather Prediction; NWP; AREPS;

Dedication

To my grandfather, who spent his life in the navy and was one of the greatest supporters of my studies.

Contents

List of Figures

List of Tables

Acknowledgements

Hereby I would like to thank everyone who has supported me during the writing of this thesis. However, some people I would like to thank in particular:

Chapter 1

Introduction

On a daily basis, hundreds of shipping movements take place on the Dutch continental shelf of the North Sea. From large oil tankers entering the port of Rotterdam to small sailing boats with families on holiday and from fishing vessels on their way to their fishing grounds to ferries sailing across to the United Kingdom, they all use the same sea area and together they make the area - with a total of over 250,000 shipping movements a year - one of the world's busiest shipping routes.

When safety and security in the Dutch part of the North Sea is considered, the Netherlands Coastguard play an important role. They are there to coordinate and carry out multiple operational tasks that concern both the provision of service and law enforcement.[1]

Provision of service tasks:

- Monitoring, handling, and coordinating national and international;
- Distress, urgency, and safety radio traffic;
- Maritime assistance and Search and Rescue;
- Limiting and dealing with the aftermath of disasters and incidents;
- Wherever necessary, implementing vessel traffic services (buoys, vessel traffic service, instructions);
- Maritime traffic research;
- Clearing out explosives.

Law enforcement tasks:

- Maintaining law and order (police);
- Monitoring import, export, and transit of goods (customs);
- Upholding laws regarding environment, sea fishing, nautical traffic, ships equipment, and offshore activities;
- Border control.

In order to perform these tasks, the coastguard is depending on far-reaching situation awareness on the North Sea. To this extent, multiple sensor systems to monitor shipping movement

---

[1]The operational tasks of the Netherlands Coastguard as they are stated in this section can be found online on http://www.kustwacht.nl/en/whatwedo.html.

and behaviour are used. The output of those sensors is analysed in order to pick out those ships that can cause either safety or security issues. Although various monitoring techniques can be practised, they all start with the detection of ships.

Two independent methods for detection which are currently used by the Netherlands Coastguard are coastal radar and the relatively recently introduced Automatic Identification System (AIS). Both techniques are based on radio signals, but whereas (coastal) radar receives the target reflection of its own transmitted signal, AIS depends fully on receiving the transmitted information from others. As a result, a combination of both could directly reveal targets that try to hide their position. Having two sensor systems is therefore beneficial to monitoring shipping movement.

Currently, the North Sea waters, stretching from the Dutch coast to the border of the Dutch exclusive economic zone (EEZ),[2] are covered with multiple AIS receivers and radar systems, which are placed on coastal infrastructure and oil platforms. Although they provide the coastguard with valuable information, coverage of the total territory is not guaranteed. On the one hand, this is due to the locations of the platforms containing the systems and their theoretical reach of the systems, together with signal blockage due to poor mounting locations. But a more dynamic cause is the change of weather circumstances that can influence the covered area. Weather types and the associated atmospheric layers can affect the propagation of radio signals severely. Without knowledge of these effects and their appearances on the North Sea, accurate detection can be difficult and unknown coverage gaps will exist, both of which can eventually lead to unsafe situations as well as concealment of illegal activity.

To know the extent of prevailing situation awareness, the coastguard - amongst others - is looking for a way to take into account the environmental impact on their systems. Therefore, their aim is to set up a system that, on a daily basis, analyses radar and radio wave propagation under the present conditions and displays the radar coverage area for both AIS and radar. Such a system would, when integrated in existing command and control systems, be highly beneficial for the Netherlands Coastguard as it would strongly increase their situation awareness. In addition, the same integrated system can be advantageous for other parties, such as the Royal Netherlands Navy.

1.1   Problem definition

To improve situation awareness, the Netherlands Coastguard together with the Maritime Warfare Center (MWC)[3] set up the KWC_2 ("Evolutie Kustwachtcentrum naar Commandocentrale") project.[4] The first phase of this project focuses on improving the understanding of the encountered AIS and radar performances. Part of this study, will focus on (the limitations of the) coverage area which can be influenced by three major components, namely, the limitations of the used technology (including for AIS: slot management), the poor mounting locations of the antennae which leads to blockage of the signals, and the propagation of the signals itself.

---

[2]The exclusive economic zone is a sea zone over which a state has special rights, jurisdiction, and duties primarily regarding its natural resources and exploitation (due to the United Nations Convention on the Law of the Sea) and stretches out to a maximum of 200 nautical miles of the coast [6].

[3]The Maritime Warfare Center is a department of the Royal Netherlands Navy with expertise on operational data analysis, doctrines, and naval tactics.

[4]The KWC_2 is a research project on behalf of the Ministry of Defense of the Netherlands conducted by the Maritime Warfare Center and the Netherlands Coastguard together with the research institutions TNO (Netherlands Organisation for Applied Scientific Research) and MARIN (Maritime Research Institute Netherlands) on the improvement of the coastguard's Maritime Operations Center.

Although this thesis is not a part of KWC$_2$, it will, simultaneously, look at one of these topics, namely, the impact of the atmosphere on the propagation of the signals.[5] For this specific topic, this thesis will look, based on modelling, at why this impact and the corresponding coverage takes place, whereas KWC$_2$ will look, based on historical data, at what coverage is experienced when all components are incorporated. Together, the outcome of KWC$_2$ and this thesis will, potentially, result in the addition of new radar and AIS stations.

At a certain area, radar coverage could change along with the weather and, as a result, assumed target detection could well be absent at a certain date and time. At the same time, radar coverage and the accompanied target detection could significantly be increased without it being used effectively. The (Dutch part of the) North Sea is no exception when it comes to the environmental impact on radio wave applications. Throughout the year, different detection ranges are encountered by sensor system operators that maintain the situation awareness for the coastguard.

For their current situation awareness, the Netherlands Coastguard relies on images of the shipping traffic composed by the reception of AIS and radar antennae spread out over the North Sea and its coastline. Based on assessment of the sensor systems, theoretical coverage could be determined relatively easy and is already known to some extent. However, knowledge of the coverage in real conditions is currently absent. Also, North Sea weather conditions in relation to radar application purposes were found not to be analysed extensively before, leaving no basis for specific conditions that are important to build on. To combine both topics, this thesis analyses North Sea weather conditions and coastguard sensor systems on a year-through timescale based on the question:

> "How do seasonal weather changes above the exclusive economic zone of the Netherlands influence the coverage of the existing Automatic Identification System and coastal radar infrastructure?"

1.2 Thesis goals and objectives

From the research question stated above, two main goals can be derived: assess North Sea weather (II) and assess North Sea coverage (IV). In order to allow for in-depth investigation of these goals, two prior supporting objectives are introduced, namely, identify relevant atmospheric propagation mechanisms (I) and model AIS (and coastal radar) systems (III).

In addition, a third goal is: Provide a proof of concept to forecast realistic sensor coverage in the North Sea (V).

I Identify relevant atmospheric propagation mechanisms.

In literature, radar and radio wave propagation mechanisms are described extensively. This will form the basis to determine important propagation mechanisms for both AIS and radar. Since the outcome of the propagation mechanisms can differ for distinct wavelengths, the differences per wavelength will be studied to compose an overview of the most important mechanisms - concerning impact on the propagation path - per system, which will be used throughout the rest of the study.

II Assess North Sea weather.

---

[5]This research is conducted on behalf of the Knowledge, Innovation, eXperimentation and Simulation (KIXS, "Kennis, Innovatie, eXperimenten en Simulatie") institute within the Ministry of Defence of the Netherlands.

Based on the results of the first objective, North Sea weather conditions will be studied to determine those conditions that could lead to significant (anomalous) propagation effects. The occurrence of the most important of those propagation effects will be investigated more thoroughly and on a monthly basis in order to determine seasonal variations.

III Model AIS (and coastal radar) systems.

Before coverage in particular cases can be studied, a general maximum detection range threshold has to be determined, which can be used as a benchmark. Since not many AIS related studies have been carried out, the threshold will not follow from literature and for that reason the AIS system need to be modelled so that the detection range can be determined based on real received data. For radar, a maximum detection range threshold will also be established, yet this will follow more directly from earlier conducted research.

IV Assess North Sea coverage.

To assess North Sea coverage, an analysis of different cases will be made. Specific targets, that are of interest to the coastguard, will be selected and parameterised. For those targets, the maximum range at which they are discovered will be determined using all existing radar and AIS platforms located on the Dutch coast and on the Dutch continental shelf. To increase understanding, all results will be combined per case and will be visualised together with geographical data of the area. Finally, the worst, best, and standard cases concerning coverage of both AIS and radar will be determined.

V Provide a proof of concept to forecast realistic sensor coverage in the North Sea.

The North Sea coverage can also be assessed for future weather conditions. This way, the coastguard can use the same method to forecast the reach of the sensors and plan deployment of non-static resources such as ships and aircraft. A proof of concept of an approach to make this forecast for both AIS and coastal radar will be made, based on the assessment method to that is used to assess North Sea coverage in general.

The three goals and two objectives described above together form the overall goal of this research. To address these goals and objectives, some background knowledge on radar systems, wave propagation, and modelling is required. Therefore, a major part of this thesis consists of combining various models in order to go from atmospheric conditions to radar coverage. Understanding sensor models, weather models, propagation models, and detection models, as well as their implementations is key to reach the research goals and objectives; especially since (to our knowledge) this is the first study in which these models are being considered to assess AIS performance. Although it is not considered an objective on its own, these models, including their (mathematical) background, will be explained in this thesis.

1.3   Related research

Radar coverage and the impact which the atmospheric conditions can have is common knowledge amongst researchers and described extensively in many radar books, e.g., [1] and [7]. But, how different that is for AIS. At the start of this research, two studies were found to analyse the impact of the atmospheric conditions on AIS performance; a 2011 study by Green et al. [8] which analyses the facets that could theoretically influence AIS performances and a 2007 report

by the International Telecommunications Union (ITU)[6] [9] which models the impact of some general propagation mechanisms on AIS to analyse extended detection ranges, but without looking at atmospheric conditions behind it.

The North Sea weather conditions were not found - by the author of this thesis and its supervisors - to be studied in relation to radar performance other than by providing some general statistics. However, prior to this thesis, within KIXS, another thesis has been written on "Radar propagation modelling" by Derksen which focuses on the minimum required grid resolution for radar coverage assessment, but uses North Sea weather data during its cases studies.

Finally, simultaneous to this research, an associated research is conducted by TNO and MARIN. This research is part of the earlier mentioned KWC$_2$ study. It focuses on the performance of the Netherlands Coastguard's sensor systems, i.e., AIS and radar, similar to this research, but its analysis is mainly based on sensor observations. This way, the approach is different than the modelling, which also aims to explain why questions, that is key in this thesis.

1.4   Outline

Knowledge of radar and radio technology used in both radar and AIS systems forms the basis for this study and is discussed in chapter 2. The chapter gives insight in all factors and associated parameters that are influencing radio waves and builds up the Radar Range Equation both in general and specifically for AIS. This chapter also reveals some general information about laws and regulations as well as practical information on AIS and radar usage, in order to establish some general parameters. In chapter 3, environmental aspects impacting radio wave propagation will be discussed, separating standard and anomalous propagation conditions. In chapter 4, the complete process to model atmospheric propagation is described, from the acquisition of environmental data to target detection, including a description of the mathematical background of the most important steps. After that, focus will be on the practical part of this research, starting with the methods and data, chapter 5, used to determine the importance of certain propagation effects as well as the introduction of the cases that are studied. (This cases included simulated sensor position and height data.) The results related to the propagation assessment will be presented in chapter 6. The first part of this chapter consists of a literature based analysis of the impact of different propagation mechanisms on AIS and radar. The second part consists of a North Sea weather analysis based on the most important propagation mechanisms. Chapter 7 will discuss the results of all studied cases that were introduced earlier. Finally, chapter 8 will state the conclusion of this research, discuss the impact of the results in practice, and state some recommendations for further research and the Netherlands Coastguard, emerging from this thesis.

Apart from this thesis, a classified annex will be delivered to the initiators of this research, i.e., KIXS, the Netherlands Coastguard, and the MWC, with analysis results obtained for real infrastructure data.

---

[6]The International Telecommunications Union ITU is "the United Nations specialized agency for information and communication technologies – ICTs." (http://www.itu.int/en/about)

Chapter 2

Physics of RADAR and AIS

In this thesis, two types of detection systems are studied: the Automatic Identification System (AIS) and navigation radar. In this chapter, their physical background is explained, starting with the radar range equation. The radar range equation can be used to link multiple general parameters involved in radar and to understand and describe general radar techniques. The second part of this chapter focuses on navigation radar and AIS specifically by explaining their applications and system specifications based on different forms of the radar range equation suitable for each system. The information stated in this chapter will thus provide a general understanding of (the physics of) both systems and thereby forms the basis of all further study of these systems throughout this thesis.

2.1 Derivation of the Radar Range Equations

Electromagnetic waves and their possibilities were discovered by Maxwell in the nineteenth century. The ability to transfer information through the air gave rise to the development of dozens of new technologies and applications. Since the beginning of the twentieth century, detection systems also started to make use of radio signals and thereby the first radar systems were constructed. Nowadays RADAR, which initially stood for RAdio Detection And Ranging, has many applications. Weather predictions and speed controls make use of the techniques, but also the safety of air and sea traffic depends on it. In this chapter, basic notions of general detection radar techniques and AIS are introduced. Their technological concepts are explained and made concrete by setting up the radar equation.

Since radar usage involves roughly three phases: the transmission, the medium, and the reception, the section's set-up will be based on this. All the physical parameters will be introduced per phase to ultimately combine to a general form of the radar range equation, RRE. This equation relates the range performance of a radar system to the characteristics of the transmitter/receiver, target, and medium. It thereby can be used to determine the received radio signal strength as well as the maximum detection range of a specific target.

The radio signal strength is based on the transmitted power, P_t, and is measured in W. For an isotropic antenna, i.e. an antenna for which the transmitted power is constant over the direction, the propagated signal strength will decrease in a spherical way. The power incident on the target, P_d in W/m², will then be:

$$P_d = \frac{P_t}{4\pi R^2},\tag{2.1}$$

where R is the range from the transmitter to the target in m. Note that P_d can also be seen as the power density of a square metre of the surface of a sphere with radius R.

Isotropic antennae are however inefficient and therefore unpractical. Antennae can be built and used in a more effective and directed way. As a measure for this gain is used. The gain of an antenna in a given direction is defined as "the ratio of the intensity, in a given direction, to the radiation intensity that would be obtained if the power accepted by the antenna were radiated isotropically" [10, p. 66]. In other words, the gain is a measure of how well an antenna performs in a specific direction compared to an antenna which performs equally in every direction. Because the gain is measured in comparison to an isotropic antenna it is in principle dimensionless, yet it is often denoted by dBi (decibel isotropic). The gain can also be expressed depending on the effective area, A in m^2, and wavelength, λ in m, of an antenna by using the formula

$$G = \frac{4\pi A}{\lambda^2}.$$

The effective area, also called effective aperture, is, like the gain, defined in a given direction and gives the ratio in which the power density of an incident radio wave is transferred to available power at the receiving antenna. In the RRE, G_t is used for the gain of the transmitter in the direction in which it is maximal.[1] Including the gain into P_d leads to the following equation:

$$P_d = \frac{P_t G_t}{4\pi R^2}.$$

After the propagation of the radar wave, it is received by an antenna again. Depending on the effective area of the receiving antenna, A_r, the power density can be converted to the received power, P_r:

$$P_r = \frac{P_t G_t}{4\pi R^2} A_r.$$

Using the relation between the gain and the effective area we can substitute:

$$A_r = \frac{G_r \lambda^2}{4\pi}$$

to get:

$$P_r = \frac{P_t G_t G_r \lambda^2}{(4\pi)^2 R^2}.$$

This equation states the one-way radar range equation, which will be revisited later for AIS. However most radar systems do not operate based on one-way radar wave propagation; the radar waves are being reflected or scattered back by a target before they reach the receiver's antenna. The extent to which the wave is reflected depends on the target and is measured by the *radar cross section* or RCS, σ, in m^2 which is defined as the intensity of the energy scattered back in the opposite direction of the incident wave [4].

Scattered back from the target, spherical spreading over distance R will lead the radio wave to return to its origin radar system. Including RCS and the returning spread gives:

$$P_r = \frac{P_t G_t G_r \lambda^2 \sigma}{(4\pi)^3 R^4}. \tag{2.2}$$

Assuming a monostatic and single antenna system, i.e. a system in which the same radar antenna at the same location is used for both transmission and reception, this can be simplified to:

$$P_r = \frac{P_t G_t^2 \lambda^2 \sigma}{(4\pi)^3 R^4}. \tag{2.3}$$

---

[1]By convention, if the direction of the gain or effective area is not specified it can be taken as the maximum value for the pointing direction.

In theory, this equation can be used to calculate the power that is received. Yet, in practice, other influences need to be taken into account. Decline of signal strength is not only due to the distance between transmitter and receiver, but can also occur inside the transmitting station. Due to non-ideal equipment and mounting the system's input power - the theoretical system power used as P_t - is not equal to the transmitted power. This ratio between the transmitted output power and the power delivered to the antenna is referred to as transmitter system loss, L_t. Similar effects occur for the returning signal. The ratio between the power received by the antenna and the actual received power to work with, P_r, is denoted by L_r. L_t and L_r can be combined into the total system loss, L_s [11]. L_s can be incorporated into the equation to get:

$$P_r = \frac{P_t G_t G_r \lambda^2 \sigma L_s}{(4\pi)^3 R^4}. \tag{2.4}$$

Secondly, both the fact that the target may not be in the maximum of the transmitted beam pattern - the target can be away from the center of the beam - and the fact that wave propagation mechanisms due to non-free space are not yet included, can lead to additional signal decline. The pattern propagation or propagation factor both from transmitter to target, F_t, and from target to receiver, F_r, are used to denote this and are included together [11].[2] It needs to be emphasised that those parameters also include location and height dependencies. By considering non-free space wave propagation, different, preferably more realistic types of wave propagation are used to consider propagation mechanisms such as refraction and multipath interference, yet these mechanisms do not at all have to be homogeneous throughout the medium. Chapter 3 elaborates on different radar wave propagation mechanisms over the earth's surface and through the earth's atmosphere. Including F_t^2 and F_r^2, the resulting radar range equation becomes:

$$P_r = \frac{P_t G_t G_r \lambda^2 \sigma L_s F_t^2 F_r^2}{(4\pi)^3 R^4}, \tag{2.5}$$

which is the general equation for an active two way radar system.

The equation can also be rewritten with range as its leading variable. This is especially interesting when the maximum detectable range, R_{max}, is considered. When P_r is replaced by the so called minimum detectable signal, S_{min}, which is the minimum power that the receiver needs in order to still detect the target, it is possible to give the maximum detectable range for a specific target. It needs to be noted that this power is not at all zero. Background noise that is always received by radar antennae will cause the target to remain undetected as long as its signal cannot be distinguished from noise signals. This relation can be best described by

$$S_{min} = k T_0 B F_n \left(\frac{S}{N}\right)_{min}, \tag{2.6}$$

where k is Boltzman's constant (1.38^{-23} J/deg), T_0 (K) the noise temperature of the receiver, and B (H) the bandwidth of the receiver. Together they form what is called the thermal noise of an ideal conductor. The thermal noise is multiplied by the noise figure of the receiver, F_n, defined as the noise out of the receiver compared to an ideal receiver. S/N is the signal-to-noise ratio. The subscript min is added, since the minimum signal-to-noise ratio, i.e. the minimum factor at which the signal needs to exceed the noise to constitute as a detection, is considered [11, 12]. To summarise, the maximum detectable range of a receiver can be

---

[2]Together with the loss due to spherical spreading, the pattern propagation is often called propagation loss (PL), as they account for all losses caused by propagation.

calculated by

$$R_{max} = \sqrt[4]{\frac{P_t G_t G_r \lambda^2 \sigma L_s F_t^2 F_r^2}{(4\pi)^3 k T_0 B F_n \left(\frac{S}{N}\right)_{min}}}. \tag{2.7}$$

In the scope of this thesis, an adaptation of RRE focusing on AIS will be useful. Since AIS is a one-way technique which does not involve reflection of the signal on a target, the RCS, the power decline of the returning signal, and single way pattern propagations can be erased to create the AIS radar range equation with the maximum range as leading parameter:

$$R_{max} = \sqrt{\frac{P_t G_t G_r \lambda^2 L_s F^2}{(4\pi)^2 k T_0 B F_n \left(\frac{S}{N}\right)_{min}}}. \tag{2.8}$$

in which F denotes the one-way pattern propagations from the transmitter to the receiver. Additional information on the physics of radar systems and the radar range equation in particular can be found in [1] and [12].

2.2 Studied radar systems

By elaborating the radar equation in the previous section (2.1), the most important parameters considering both radar theory and the practical usage of radar systems have been introduced and summarised. In short, it could be said that the RRE contains all information needed to calculate radar coverage and thereby answer the main question of this thesis. By filling in all other parameters, the maximum detectable range of every single AIS as well as navigation radar antenna can be determined. However, the question remains how to get reasonable values of all those parameters.

In this section, the two studied systems, AIS and navigation radar, are introduced. A basic understanding of their usage and background is given. More importantly, the values of most of the parameters concerning AIS and navigation radar are determined. By looking at general system information, regulations, and other literature parameters such as wavelength and transmitted power can be established. For other parameters such as the transmitter and receiver gain, and system losses, an indication can be given based on literature and the specific system. The same can be said about RCS when a specific target is selected. [3]

The pattern propagation is the variable fluctuating the most, because it depends on a specific time and place. This makes it hard to determine even when the time and place are known. A theoretical value or estimation based on literature will therefore not be given at this stage; instead it will be studied based on atmospheric data later on in this thesis (chapter 7). Important to note is that the pattern propagation is often ignored by manufactures which leads to operational radar system performances that differ severely from the expectations based on the system specifics. Therefore, pattern propagation, based on seasonal weather influences, will be studied extensively throughout this thesis.

For the minimum detectable signal or the related signal-to-noise ratio, similar specific knowledge of the system is required. Especially for AIS, this knowledge is not available. Hence, the minimum detectable signal will also not be discussed in this section. Instead, it will be approached from a more practical point of view later on in chapter 7 of this thesis, by linking it directly to real reception data and atmospheric conditions.

---

[3]Determining the RCS is a not to be underestimated process. However, since it is studied a lot in other literature, reasonable values can be adopted from there.

2.2.1   Automatic Identification System

Around 2000, AIS was introduced by the International Maritime Organisation (IMO) as a system to provide information from a ship to other ships and to coastal authorities in its surroundings. International regulations that came into effect on December 31, 2014, "require AIS to be fitted aboard all ships of 300 gross tonnage and upwards engaged on international voyages, cargo ships of 500 gross tonnage and upwards not engaged on international voyages and all passenger ships irrespective of size" [13].[4] The European Union extended this obligation to all fishing vessels longer than 15 meters in May 2014 [14]. Ships with the obligation to have mounted an AIS system must maintain it in operation at all times except for circumstances in which protection of navigational information based on international agreements, rules, or standards is provided.

The primary aim of AIS is to improve maritime safety and avoid ships collisions. In order to do so AIS systems send dynamic information about the ship such as the latitude, longitude and accuracy of the ships position, the time stamp corresponding to the moment the message was generated, the ships course, and the ships speed, combined with static information like the ships identification number (MMSI) and name, the type and call sign of the ship, and its dimensions as reference for its position. Voyage related information such as the current destination, expected time of arrival, draught, and cargo-type can also be added [15].

The dynamic information is frequently transmitted according to the reporter interval, which is the interval between the transmission of two messages. This interval is depending on the speed of the ship. At anchor, the reporter interval for the dynamic information is limited to 3 minutes, whilst at a speed above 23 knots, the reporter interval is 2 seconds. The static information is transmitted either once every 6 minutes or on request. The transmission at different intervals is driven by the so called Self-Organized Time Division Multiple Access (SOTDMA) multiplexing technology. At the same time, the SOTDMA technology also performs slot management, i.e. the management of the limited number of time slots AIS has available. For reception and transmission combined, an AIS system has a maximum number of 2250 time slots per frequency per minute. Since AIS uses two different frequencies (as explained in the next subsection), there is a maximum of 4500 time slots per minute, which limits the number of messages - each time slot corresponds to at most one message - that can be processed and therefore the number of ships that can be followed. If this limit is exceeded, ships will be prioritised based on range. This way, ships that are more close are detected, whilst ships that are further away, and therefore less important regarding safety, are left out. [15, 16] Although slot management is not taken into account in this thesis, it could limit the coverage area, since it leaves out certain ships.

Secondly, AIS can also be used to monitor all marine traffic within a certain area. Combining all vessel positions, courses, and speeds and projecting them on a map of the specific area will lead to an overview that can be used during monitoring. Online several of those maps can be found.[5] The application of AIS in this manner can be seen as the foundation of this research.

AIS parameters

AIS systems can primarily be divided into two classes, Class A and Class B. The Class A functions on a higher transmitter power than Class B, respectively 12.5 and 2 W. The Class A type systems are the systems that are compulsory for all ships specified in section 2.2.1. Therefore, all AIS systems mentioned in this thesis (including the ones described in the previous

---

[4]Regulations can also be found on the IMO website www.imo.org/en/OurWork/Safety/Navigation/Pages/AIS.aspx

[5]www.vesselfinder.com and www.fleetmon.com are examples of website containing these maps.

subsection) will considered to be Class A. However, this does not exclude AIS Class B from any of our data in any way. Class A and Class B AIS systems are completely compatible with each other, allowing them to receive and decode each other's messages. Class B messages generally contain less information than Class A messages; however essential safety information is provided by both.

Worldwide two frequency channels are designated for AIS. Both frequencies lay within the Very High Frequency (VHF) bandwidth. Other frequencies can be used locally. The two main worldwide frequencies are: (VHF 1) 161.975 MHz and (VHF 2) 162.025 MHz. Every single AIS system makes use of both of these channels. At all times, messages can be received on both, whilst in case of sending messages will be alternated, which means that if a message is sent on VHF 1 the next will be send on VHF 2 and vice versa [15].

The transmitter and receiver gain of an AIS antenna are system specific. No exact universal value (or values) can be given. Nevertheless an indication can be obtained by looking at the workings of an AIS antenna. AIS antennae aboard ships are designed to communicate with all other ships or coastal stations around. All communication takes place in the more or less horizontal plane. AIS is not meant for communication upwards (for instance to airplanes), nor downwards (for instance to submarines). On the other hand, all surrounding antennae have to be able to receive the transmitted signal. Since an AIS antenna is a static rod antenna, i.e. a non-rotating antenna in the shape of a fishing rod (see figure 2.1), signal transmission needs to be equal in every more or less horizontal direction. An AIS antenna will therefore have relatively low antenna gain compared to other radar systems, yet not as low as 1 dBi, the value of an isotropic antenna. Values encountered during this research ranged from 2 to 5 dBi [9, 8].

For AIS, system losses have to be taken into account either for transmission or for reception depending on the application. This thesis' focus will be on reception; therefore the total system losses, L_s, can be taken equal to the system losses at reception, L_r. The two most important system losses concerning AIS are plumbing loss and non-ideal equipment loss.

Plumbing loss accounts for all losses caused by compromises made considering the installation of the AIS system. Ideally, there is a direct connection between the antenna and the receiver. However, in practice elements are placed in between. For AIS, transmission lines are concerned as well as a duplexer, i.e. an apparatus used to switch between receiving and transmitting. Losses caused by the length of the transmission lines are low for low frequencies such as AIS. A loss of no higher than 0.1 dB for up to 30 m of transmission line can be used. More important are the losses caused by the duplexer, cable connections, and cable bends. Duplexer loss can be estimated at about 1 dB. Connection and cable irregularities can be estimated around 0.5 dB [4].

The equipment parameters used are based on theoretical performance of the AIS system. In practice equipment can suffer from on-ideal operating conditions. Parameters such as receiver sensitivity are an example of AIS characteristics that can differ in practice. Although various conditions will result in various equipment performances, in general a loss of approximately 2 dB can account for the losses caused by non-ideal equipment. In total a rough estimation of 3.6 dB can be considered as system loss of an AIS system [4].

An overview of all coastal radar parameters can be found in table 2.1.

---

[6]"Eierland Lighthouse texel" by Yornik Heyl. Licensed under CC BY-SA 3.0 via Commons - `commons.wikimedia.org/wiki/File:Eierland_Lighthouse_texel.jpg`

Table 2.1: General AIS parameter values for both classes.

Characteristic	Class A	Class B
Power (W)	12.5	2
Frequency (MHz)	161.975 and 162.025	161.975 and 162.025
Gain (dBi)	2-5	2-5
System loss (dB)	~ 3.6	~ 3.6

2.2.2   Coastal radar

Coastal radar or (Civil) marine navigation radar is one of the largest markets when it comes to radar usage. Estimates suggest that around 3 million vessels worldwide are equipped with such a radar. For large ships, carrying such a radar is obligatory. As for AIS, every passenger ship and every ship above 300 gross tonnage needs to have at least one marine navigation radar, according to IMO regulations [13], which comes down to around 50 thousand ships worldwide [1].

As its name suggest, the majority of these radars are used for navigation at sea or in waterways; it provides skippers with information about their surroundings which could either be other ships or a land mass and its structures. Yet it can also be used by coastal authorities for surveillance purposes. Although techniques are the same as for navigation purposes, the latter group is known as a Vessel Tracking Services (VTS) radar [1]. For the specific purposes studied in this thesis, namely, target detection by coastal authorities, the name "coastal radar" or, in general, "radar" is used. (When "radar" is used for a specific system, one can assume that coastal radar is referred to, unless an other radar system is specifically specified.)

Other than AIS, general coastal radar systems are not depending on others to determine their locations. The radar system sends a radio signal which is (partially) received back after reflection. Where for AIS the reception of the signal suffices, radar is much more depending on the actually received signal itself. Based on the time between transmission and reception, the location of the object (and possible the object itself) is determined. To this extent, it is essential for radar to have directional reception and transmission, meaning that both reception and transmission can be steered in a specific direction. This is done by producing a narrow horizontal beam [17]. To provide this narrow horizontal beam on the one hand and to cover the complete surroundings of a ship on the other hand, radar antennae are rotational antennae which have a characteristic horizontal cuboid-like shape (see figure 2.1). Because of this, and because of other techniques involved in optimising detection, many more describing parameters are involved than for AIS.

In the next section, coastal radar is described up to its corresponding parameters, yet only the parameters that are included directly in the RRE or related to the discussed above will be specified. Other parameters that are used for calculations later on in this thesis will be stated in appendix A. More background on different radar techniques and accompanied parameters can be found in books such as [1] and [12].

Coastal radar parameters

Coastal radar operator frequencies vary between S-band which ranges from 2.9 to 3.1 GHz and X-band which ranges from 9.3 to 9.5 GHz [1, 17]. Although both are used, the obligation for all passenger ships and ships above 300 gross tonnage, is to carry at least one X-band radar [1, 13].

Figure 2.1: The Eierland lighthouse on Texel with on top a characteristic coastal radar antenna and on the left at the second ring an AIS antenna.[6]

The transmitter power of coastal radar is much higher than for AIS. Peak powers for an S-band transmitter lay between 30 and 75 kW, whereas for an X-band transmitter they lay between 5 and 50 kW [18].

Because radar is a more directional system than AIS for both reception and transmission, the gain is much higher. For S-band systems, transmitter and receiver gain vary between 26 and 28 dBi and for X-band systems between 27 and 32 dBi. At the same time, more specific beam widths and a rotation rate are involved. For both S-band and X-band, the rotation rate is between 20 and 60 rounds per minute (rpm). The horizontal and vertical beam width are between 1 and 4 degrees, and 24 to 30 degrees for S-band respectively and between 0.75 and 2.3 degrees, and 20 and 26 degrees for X-band respectively [18].

System losses can be determined in a similar fashion as for AIS, only now both reception and transmission have to be taken into account as well as a higher frequency.[7] As the frequency

---

[7]The calculations to do so are made for X-band here, but can, based on the cited literature, also be applied for S-band.

Table 2.2: General coastal radar parameter values for both bandwidths.

Characteristic	S-band		X-band	
	Minimum	Maximum	Minimum	Maximum
Peak power (kW)	30	75	5	50
Frequency (GHz)	2.9	3.1	9.3	9.5
Gain (dBi)	26	28	27	32
Rotation rate (rpm)	20	60	20	60
Beamwidth (deg)				
Horizontal	1	4	0.75	2.3
Vertical	24	30	20	26
System loss (dB)	3.5	8.5	3	8.5

rises, so do the transmission line losses. Around 10 GHz, a one-way loss of around 2 dB can be considered for a cable length of approximately 30 m. Poor connections and cable bends together with a duplexer can be consider to lead to another 2 dB loss. Also the rotary-joint of the antenna can cause an additional plumbing loss of around 0.4 dB. For non-ideal equipment a 2 dB loss can be added as an indication value. For an X-band equipment system consisting of a rotating navigation antenna with 15 m of cable (one-way) and a duplexer between the transmitter/receiver and the antenna, 6.4 dB is a rough estimate of the total system loss [4]. This value corresponds to the characteristic values describe by the IMO, stating a system loss of between 3.5 and 8.5 dB for X-band systems (and between 3 and 8.5 dB for S-band systems) [18].

An overview of all coastal radar parameters can be found in table 2.2.

2.3   Subconclusion

The radar range equation solely includes most of the physical parameters that are involved in any form of application that uses radar or radio waves. Based on the RRE and the parameters stated above for AIS and radar, the detection ranges of both systems can partially be determined, however two essential parameter values are missing: the minimum signal-to-noise ratio (or minimum detectable signal) and the pattern propagation. The pattern propagation that involves the environmental impact on radar and radio wave propagation is extensively discussed in the next chapter. The minimum signal-to-noise ratio will be discussed in chapter 4 and will be determined explicitly in chapter 6.

Chapter 3

Environmental impact on radio wave propagation

In the previous chapter, the physical parameters involved in radar and radio techniques were discussed. Although some parameters were stated precisely the pattern propagation, which contains information about the environmental impact on radio signals, was not. To be able to include pattern propagation in some way, a understanding of the effects that the environment can have on radar and radio wave propagation is needed.

In this chapter, common radar wave propagation mechanisms are discussed. Starting point is the spherical spreading as it is encountered in free-space. Consecutively, more propagation mechanisms which are encountered in the earth's atmosphere are discussed and added to give rise to more realistic propagation conditions that are met within the so called standard atmosphere. Also, important anomalous propagation mechanisms, i.e. propagation mechanisms that lead to an anomaly from standard atmosphere, are described. Since this study focuses on detection over sea, anomalous propagation effects due to surface height changes, vegetation, or infrastructure are mainly left out.[1]

3.1   Standard propagation

Spherical spreading

Spherical spreading is the basic radar wave propagation mechanism. Due to an increasing surface area of the sphere centered around the transmitter and the outward signal propagation, the signal strength on a single point of the surface of the sphere will decrease whilst the distance from the transmitter increases by a factor that is proportional to the square of this distance. Eq. (2.1), the basis of the radar range equation, illustrates this. Spherical spreading is also the only propagation mechanism in a free-space atmosphere.

Refraction

For real earth atmospheric conditions, spherical spreading is not representative due to numerous other effects influencing the radar wave propagation when it comes to signal strength and direction. The most important of those effects is refraction. Refraction is the bending of the propagation path due to changes in the refractivity index alongside its propagation path

---

[1]Inland, AIS coverage of river traffic is studied by Rijkswaterstaat and needs to model and analyse such line-of-sight factors.

and is caused by molecular air particles such as nitrogen, oxygen, carbon dioxide, and water vapour [19]. Refraction effects can be described using Snell's law which gives the relation between the angles of incidence and refraction of the boundary layer between two mediums. When one of these mediums is either vacuum or air, the refractivity index is given by:

$$n = \frac{c}{v} \tag{3.1}$$

with c being the propagation velocity in a vacuum and v the propagation velocity in the other medium [19]. Since the refractivity index is usually close to one when it comes to radar applications, a related more practical value termed refractivity, N, is used. Refractivity is defined by:

$$N = (n - 1) \times 10^6 \tag{3.2}$$

and is dimensionless, although often referred to as measured in N-units.

By using the Debye formula [20] for the polarisability of polar and nonpolar molecules, N can be specified as:

$$N = c_1 \frac{p}{T} + c_2 \frac{e}{T^2} \tag{3.3}$$

with T the air temperature in Kelvin, p the pressure in millibars, e the partial pressure[2] of water vapour in millibars, and c_1 and c_2 both constants [19]. The used values for c_1 and c_2 are determined empirically in an experiment by Smith and Weintraub in 1953 [21] and complete the formula:

$$N = 77.6 \frac{p}{T} + 3.73 \times 10^5 \frac{e}{T^2}. \tag{3.4}$$

Finally, the most common way to describe refractivity is in terms of the *modified* refractivty, M. The relation between M and N, when the altitude, z, is in m and r_{earth} is the earth's radius in m, is given by

$$M = N + \frac{z}{10^{-6} r_{\text{earth}}} \approx N + 0.157z. \tag{3.5}$$

The advantage of the modified refractivity is that it takes into account the curvature of the earth in such a way that in a standard atmosphere, as described later-on in section 3.1.1, the difference in M-units, dM, divided by the difference in altitude, dz, increases linearly, whereas the same fraction is negative, and therefore decreases, for trapping layers (section 3.2.3). As a result, M-units are ideal to visualise ducting effects in relation to altitude [2, 22].

Diffraction

In a same manner as light is diffracted by a straight edge, radar waves tend to diffract over the earth following the curvature of its surface [2, 4]. This phenomenon that is called diffraction causes the direction of the radar wave propagation path to bend over the earth's surface so that the radar waves spread into the area of the atmosphere that is out of the geometric line-of-sight, the so called geometric shadow zone, and thereby extending the radar detection range beyond the line-of-sight. Diffraction can also be caused by height differences or infrastructure, which is usually referred to as knife-edging, as is described in [7, Chap. 8].

---

[2]Partial pressure of a gas is defined as the hypothetical pressure of the gas when it alone occupied the volume of the mixture at the same temperature.

Reflection

Due to reflection of radar waves on the earth's surface or on atmospheric refractivity layers multipath interference can occur. Multipath interference is the interference, i.e. the coming together of two or more waves following different paths, between direct and reflected waves [5, 2]. As a wave hits a surface, a portion of the energy of the wave is reflected, leading to a continuation of the propagation of the wave in another direction. On large, smooth surfaces such as the sea, a large portion of the waves energy is reflected and the propagation path will continue under an angle to the surface that is equal to the angle of the incident wave. This way, a second reflected path from the transmitter to the target can arise alongside the original direct path. If the reflected and direct path, which are both waves, arrive at a point together whilst they are in phase they are said to constructively interfere, increasing the energy of the resulting wave to a level higher than that of either of the waves alone. If they arrive at a point together whilst they are out of phase they destructively interfere and the resulting waves energy will be lower than that of either of the waves alone [2]. On the other hand, part of the energy can also be reflected back in the direction of the transmitter. This backwards reflection, that is called (sea) clutter, can cause noise reception - reception that is not from the target - which makes the target detection more difficult. This effect is stronger when the reflecting surface is less smooth, for instance a rough sea [2].

Scattering

When a radar wave hits the surface, not all the energy is reflected in one direction. Some of the energy is reflected in directions other than the main direction. This mechanism is called scatter. Scattering can not only be caused by the earth's surface, but also by irregularities in refractivity or hydrometeors such as rain, fog, clouds, snow, and hail [23]. And even ionospheric layers, meteor trails, and lightning can cause possible interference due to scattering [8].

Attenuation

Atmospheric gases such as water vapour and oxygen can cause attenuation of radar wave energy. Molecules of the gases absorb part of the energy of the radar wave as heat, so that the radar wave loses this energy. Besides atmospheric gases, attenuation can also be caused by precipitation such as rain, snow, and hail in which the hydrometeors absorb the energy of the incident waves [24].

3.1.1 Standard atmosphere

Straight line propagation is representative in the free-space, however not within the earth's atmosphere. To be able to relate anomalous propagation to "standard" propagation another standard is set, named the "standard atmosphere". Standard atmosphere is a *hypothetical* atmosphere in which certain average conditions for the earth's atmosphere are met, including standard conditions for the previously mentioned propagation mechanisms [5, 23]. When it comes to refractivity, standard atmosphere is associate with a average linear gradient of $dN/dz = -39\text{N/km}$, [19, 25, 26] which is an approximation - valid in the first height kilometre of the atmosphere - of the exponential decrease of N under an increase of height [25]. As a result, "standard" wave propagation paths do not follow a straight line, but bend a little towards the earth. The curvature of the path is described by the effective earth's radius r_{eff}, being the radius of the circle that is followed by the propagation path. The effective earth's radius is

usually expressed as a factor k of the real earth's radius, r_{earth}. For a standard atmosphere it follows that

$$k = \frac{1}{1 - 10^6 r_{\text{earth}} \frac{dN}{dz}} \approx \frac{4}{3}, \tag{3.6}$$

so that the effective earth's radius is $4/3$ times as big as the real earth's radius [25, 27].

Because of its average conditions, lack of anomalous propagation, and its frequent usage standard atmosphere is used as a reference throughout this thesis. It is however important to note that standard atmosphere is not at all representative for every location at every moment. Standard atmosphere is, as said before, a hypothetical atmosphere that is computationally friendly and corresponds to long-time averages, but at the same time it is not the atmosphere that is encountered at regular basis all around the world [5].

3.2   Anomalous propagation

As the opposite to standard propagation - the propagation found during standard atmospheric conditions -, other atmospheric conditions can lead to non-standard or anomalous propagation. Anomalous propagation is, when smooth terrain is considered, characterised by a vertical refractivity profile that differs significantly from the vertical refractivity profile associated with standard atmosphere. Those differences, stated in table 3.1 and visualised in figure 3.1, can be split into three types of anomalous propagation mechanisms: superrefraction, subrefraction, and trapping. Those three mechanisms are described in the subsections below, including different types of atmospheric ducts that are related to trapping.

Table 3.1: Refractivity gradients under different conditions [2, 5].

Condition	N-gradient (N/km)	M-gradient (M/km)
Subrefraction	$0 < dN/dz$	$157 < dM/dz$
Normal	$-79 < dN/dz \leq 0$	$79 < dM/dz \leq 157$
Standard	$dN/dz = -39$	$dM/dz = 118$
Superrefraction	$-157 < dN/dz \leq -79$	$0 < dM/dz \leq 79$
Trapping	$dN/dz < -157$	$dM/dz < 0$

3.2.1   Subrefraction

Under normal atmospheric conditions radar waves tend to bend downwards towards the earth. However, under certain conditions the distribution of temperature and humidity can lead to increasing refractivity values with height. In that case, radar waves bend upwards away from the earth. This phenomenon is known as subrefraction. Subrefraction does not occur often in general. However, its resulting detection range decrease can be severe [25].

3.2.2   Superrefraction

Under some conditions, radar waves tend to bend downwards to the earth more than normal. This is the case when the refractivity gradient is less steep than in normal conditions due to increasing temperature with height and/or rapidly decreasing water vapour content with height.
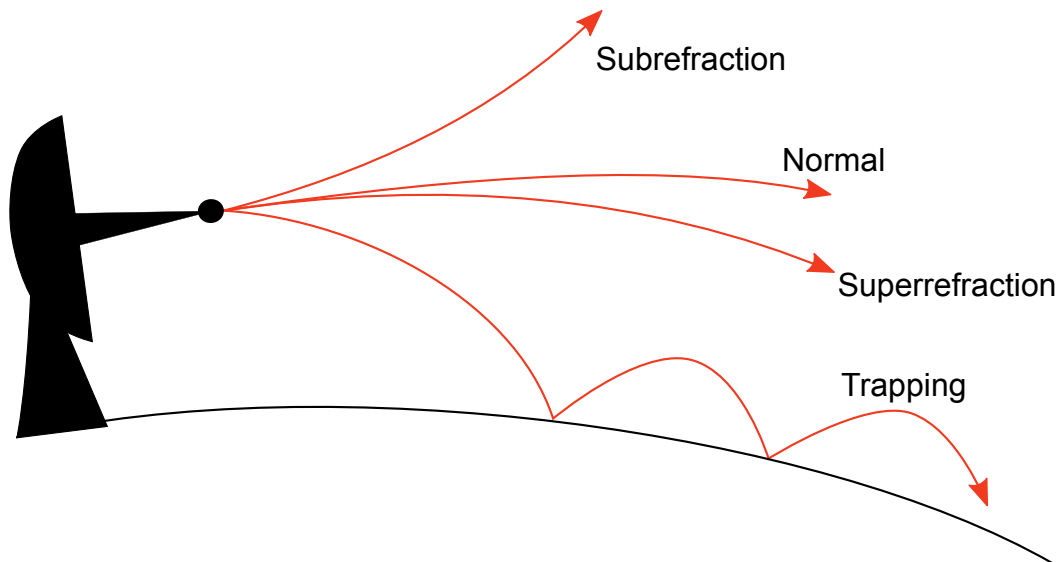
Figure 3.1: Visualisation of different refractivity conditions [1].

As long as radar waves bend downwards this way, but the curvature of their paths is less than the curvature of the earth the refraction is called superrefraction. Superrefraction is strongly related to near earth variations in humidity and temperature and its effects on radar systems are therefore directly related to their heights above the earth's surface. However, superrefraction can potentially lead to extended detection ranges [25].

3.2.3 Trapping

If a propagation path is bent downwards to such extent that it exceeds the curvature of the earth, it is revered to as trapping. Essentially, trapping is an extended, more extreme, version of superrefraction. Therefore, the conditions under which trapping occurs are similar. The phenomenon is called trapping, because the radar waves are confined within a certain region of the atmosphere. From above, the radar waves are bent downwards and below the radar waves can either be reflected on the surface of the earth or refracted back upwards. The region in which the radar wave is confined is termed a tropospheric duct. Multiple types of ducts can distinguished and are treated separately below [25].

3.2.4 Tropospheric ducts

Evaporation duct

Nearly everywhere above oceans and other large bodies of water, evaporation ducts occur, caused by rapid change in relative humidity and temperature with height. The air layer directly in contact with the surface of the water is saturated with water vapour, whilst the layer a few metres above is usually not saturated. Therefore, the relative humidity decreases from the surface upwards. At a certain height, an ambient value related to the general meteorological conditions is met and the humidity decrease will come to a halt. The height at which this equilibrium is met is the evaporation duct height which can be seen as a measure of strength of the evaporation duct. The air layer below - from the surface to the evaporation duct height - is the evaporation duct. The modified refractivity profile associated with an evaporation duct,
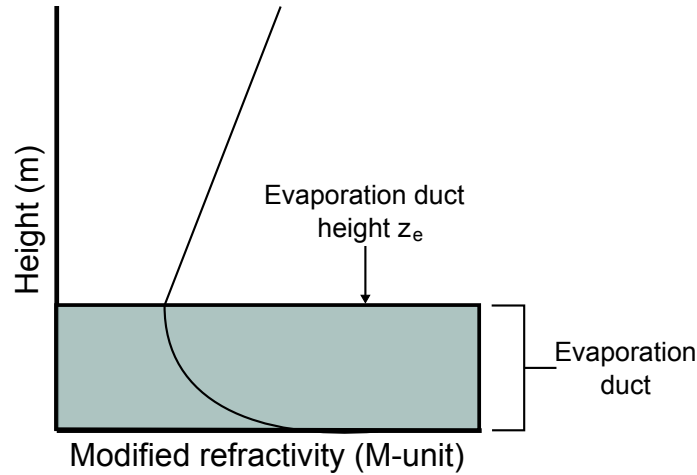
Figure 3.2: Modified refractivity profile of an evaporation duct with evaporation duct height z_e [2].

as is shown in figure 3.2, shows a gradually slowing decrease (of M-units) with height until the evaporation duct height, z_e, is reached and an increase afterwards [5, 2].

Evaporation ducts exist nearly always and nearly everywhere above oceans and other large bodies of water, however heights can vary severely with general heights between 0 to 40 m [1]. On a world scale, the average evaporation duct height is around 13 m, but the averages vary between 5 m at northern latitudes to 18 m at tropical latitudes [5].

The ability of evaporation ducts to trap radar waves is frequency related; the lower the frequency, the higher the evaporation duct height needs to be to cause trapping. An indication of this relation is given by the cut-off-frequency (GHz), CoF:

$$\text{CoF} = 360 \times z_e^{-\frac{3}{2}}, \tag{3.7}$$

with z_e the evaporation duct height in m. The CoF gives a rough estimate of the minimum frequency trapped by the duct [28]. Although trapping is related to the evaporation duct, this does not mean that enhanced detection ranges can only be found for transmitters and receivers both underneath the evaporation duct height. The evaporation duct height is more related to the duct's strength and its ability to trap radar waves [2].

Surface duct

Less common than the evaporation duct, but with more dramatic consequences is the surface duct. A surface duct occurs when atmospheric conditions cause a trapping layer of which the resulting duct has its surface at the earth's surface. Surface ducts occur when higher air layers are exceptionally warm and dry compared to the air directly above the surface. Such conditions can occur when warm, dry continental air flows over a cooler water surface, causing a temperature inversion at the surface. Also, the trapping layer can be strengthened by a moisture gradient caused by evaporation. As a result, surface ducts are more common during warmer months and latitudes close to the equator and can in some areas occur up to 50% of the time [2, 5]. In Northern Europe, surface ducts are found at a yearly average of 5% of the time [19].

Surface ducts can be split into two types based on the relation between the trapping layer and the surface. If the trapping layer in the duct lays at the earth's surface, the duct is referred
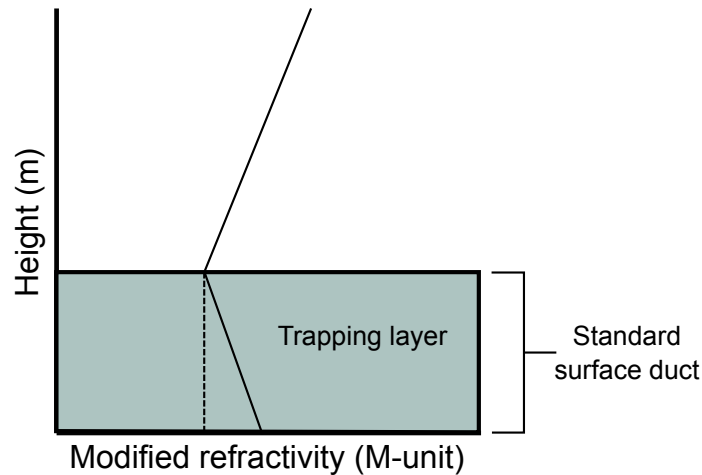
Figure 3.3: Modified refractivity profile of a standard surface duct [2].
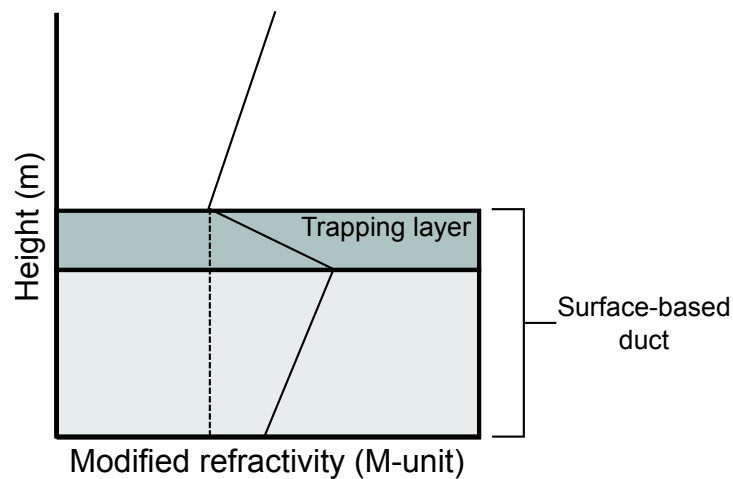
Figure 3.4: Modified refractivity profile of a surface-based duct [2].

to as an attached surface duct or standard surface duct (see figure 3.3). On the other hand, if the duct is created by an elevated trapping layer - yet the duct itself still has its surface on the surface of the earth, the duct is referred to as an detached surface duct or surface-based duct [25] (see figure 3.4).

Unlike evaporation ducts, surfaced ducts are not particularly sensitive to frequency. Increasing detection ranges can already be experienced at about 100 MHz. Also, these types of ducts are responsible for most of the extremely long distance detections, as surface ducts can extend over the ocean for several hundreds of kilometres and last for multiple days with trapping layer heights at several hundred metres and duct thickness of at most a few hundred metres [5].

Elevated duct

When the altitude of a trapping layer is high and the superrefraction is not strong enough, radar waves will, possibly, not bend completely towards to the earth's surface, as it is the case for surface ducts. In that case, a ducting layer occurs that does not extend downwards to the earth's surface, but instead is elevated above the surface. Such ducting effect is called an elevated duct [26] and is displayed in figure 3.5.
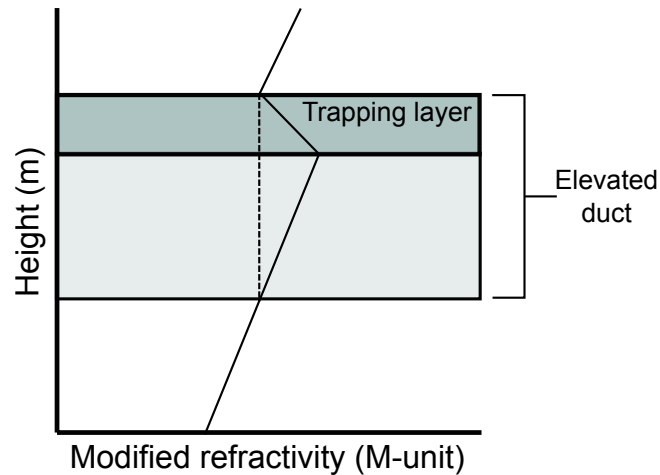
Figure 3.5: Modified refractivity profile of an elevated duct [2].

Since elevated ducts are comparable to surface ducts, the atmospheric conditions under which they arise are similar. In fact, surface ducts may result into elevated duct and vice versa. As upper warm, dry continental air flows over cool, moist marine air, a surface duct can rise and become an elevated duct. However, as the resulting temperature inversion gets stronger elevated ducts can turn into surface ducts [25].

Similar to surface ducts, elevated ducts are frequency independent. Impact on detection can already be found at 100 MHz. Extended detection ranges are found when both target and radar are within the duct or around the altitude of the duct [4]. However, above the duct, the signal strength can be less than the signal strength at the same position during standard atmosphere, due to what is often called a radar hole [5].

The altitude of an elevated duct can be as high as 6 km, but they are more common below 3 km in altitude. Also, they are not uncommon to occur at several hundred metres in altitude. Thickness varies between several hundred to close to zero metres [26, 5]. As for surface ducts, elevated ducts are more common in warmer areas around tropical latitudes. In Northern Europe occurrences are measured as often as 5 to 10% of the time on a yearly average [2, 19].

3.3   Sub-conclusion

In this chapter, five general propagation conditions were discussed, namely, standard atmosphere, and four anomalous conditions, namely, an evaporation duct, a standard surface duct, a surface-based duct, and an elevated duct. Standard atmosphere contains all regular radar wave propagation mechanisms, but no ducts. The other conditions contain, besides the regular propagation mechanisms, one of the atmospheric ducts that can be encountered in the earth's atmosphere. Therefore, by studying standard atmosphere as well as anomalous propagation conditions, all weather influences that are important for radar wave propagation can be dealt with. What remains is the ability to convert an atmospheric situation into refractivity profiles that can be linked to one of the propagation conditions and to specific radar and radio wave propagation information.

Chapter 4

Modelling the maritime atmosphere

The backbone of this thesis is formed by the ability to asses the impact of actual atmospheric conditions or a weather forecast on the propagation of radio signals so that the coverage of the total system can be determined. The modelling of this process, that relates weather to propagation (and coverage), is done extensively throughout this thesis. This chapter will be a guide through the process that is used to show how radar coverage can be computed using atmospheric data, derived from literature.

The breakdown of this chapter is given in figure 4.1: each component of the diagram corresponds to a section of this chapter. The first section will discuss a decomposition of the overall modelling process.
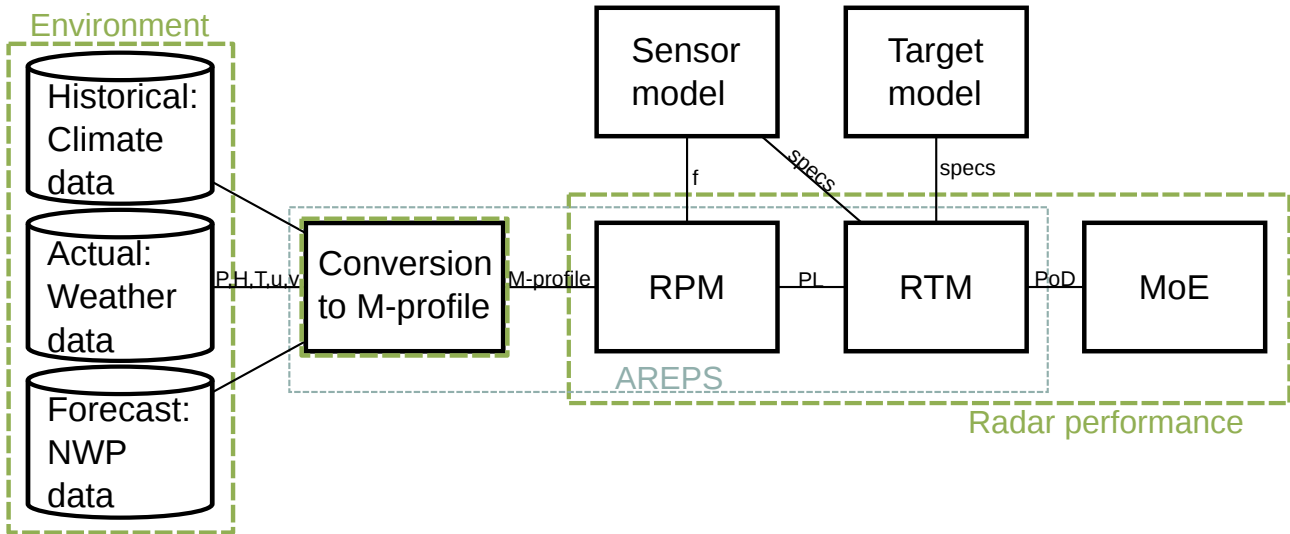
Figure 4.1: Schematic representation of the modelling of the atmospheric conditions for AIS and radar performance purposes.

4.1   Decomposition of the modelling process

The process starts with obtaining relevant environmental information. "Relevant" is in this case defined by what is necessary to obtain refractivity profiles of the area of interest in the second step of this process. In general, the information will consist of atmospheric information such as the wind speed in two directions u, v (m/s), humidity H (mass of the water vapour, divided

by the volume of the air and water vapour mixture), temperature T (K), and air pressure P (Pa), but can also consist of refractivity information directly. The first section will focus on obtaining this environmental information in three time related ways:

- Based on numerous measurements performed in the past, databases exist that contain climate data which can be used to extract relevant information.

- Actual weather information can be obtained for the present situation using different sensing techniques that can either measure weather parameters or refractive profiles directly.

- Future and location dependent information can be obtained from Numerical Weather Prediction (NWP) which are used to model atmospheric conditions and predict future (and location dependent) environmental information based on current input.

The second step in this process is to convert environmental information into what is called tropospheric modified refractivity profiles or M-profiles. The M-profiles are there to define the relation between air layers and the refractive effect they have on electromagnetic signals, i.e., radio signals. This section describes how an M-profile can be determined based on environmental information and the difficulties hereby encountered, which involve: defining lower air profiles accurately using Monin-Obukhov Similarity Theory (MOST) and combining lower and higher air profiles, either for atmospheric parameters or for M-profiles, by what is called "blending".

The third step involves the combination of one or more M-profiles and the wavelength of the transmitted signal into a statement on radar and radio wave propagation, for instance propagation loss (PL). When the signal is transmitted, the M-profiles which are determined to be in the path of the signal will one after the other provide information on the refraction of the signal. The refraction, and therefore of course the impact of a certain M-profile on the signal, is wavelength specific. In total, this process can be used to calculate the total propagation of a certain area by means of a Radar Propagation Model (RPM). Focus will be on a specific implementation of the model used for this, the Advanced Propagation Model (APM), which involves multiple sub-models.

In the fourth step, propagation loss of a signal is converted into whether or not a target is detected. A threshold has to be found to determine what propagation loss is still acceptable in order to detect (a specific) target. Not only does this depend on whether or not an antenna is strong enough to still receive something, but also on whether it is still possible to separate target signals from noise. The way this is done is introduced as the Radar Threshold Model (RTM) which can provide information such as the Probability of Detection (PoD or P_d) at a certain location.

Finally, the Measure of Effectiveness (MoE) is described which focuses on possible output interpretation. This area depends strongly on the user requirements and preferences, but will give some insight in the final steps taken in practice.

At the end of the chapter, the Advanced Refractive Effects Prediction System (AREPS) is introduced. AREPS is a software tooling package that can cover large parts of the process described above (as is indicated in figure 4.1) and that is used throughout this thesis.

What is not included in this chapter are the two external input models containing information about the sensor and target. General information about the studied systems is given in chapter 2 and target information as well as more specific sensor information, including the involved parameters, is given in chapter 6 where the actual cases that are studied are described.

4.2 Environmental data

Single location environmental data can be obtained directly by performing measurements at that specific location. (Simple) weather measurement stations available at every naval surface vessel already collect usable information, i.e. wind speed, temperature, air pressure, and humidity, for radar and radio wave propagation assessment purposes. Yet single location data does not suffice for general non-homogeneous atmospheric conditions. The need for three-dimensional and time-varying data is established many times [29]. To determine refractivity profiles (section 4.3), gradients and heights of different refractivity layers urge the collection of data at multiple heights. Spatial changes in air layer heights, in turn, urge the collection of data at multiple locations.

Radiosondes, i.e. a direct sensing technique in which air-balloons with attached measurement equipment are released, are commonly used for multiple height measurements. Their general availability and low price make them ideal to be used by many. Downside is that their flight path is (often) non-vertical and that their measurement density is too low at low altitudes, i.e. measurements are often missing or unreliable below approximately 150 m. Also their ability to cover multiple heights does not apply for covering multiple horizontal positions. To this extent, multiple remote sensing techniques can be thought of as well. Nowadays radar, lidar[1], and other techniques can be used to determine atmospheric profiles remotely, i.e. without direct measurements at specific locations [30]. Despite this benefit, their need for (sophisticated) equipment often still makes them impractical for day-to-day usage.

In case applications do not directly rely on the current atmospheric conditions, climate data can be used. Over the years numerous measurements as described above have been performed and the results of many of them have been stored and combined by weather and climate institutes like the Royal Netherlands Meteorological Institute (KNMI). This information is often (freely) accessible online.[2] Also, AREPS contains its own database with climate based ducting information.

Although sensing techniques are numerous and none of them alone provide accurate and adequate information to obtain refractivity profiles continuously and reliably, or are expected to do so in the future [30]. The same can be said about climate data, which is useful as long as averages are concerned, yet not applicable to obtain direct and specific results. Implementing the Numerical Weather Prediction (NWP) model can limit this shortcoming.

4.2.1 Numerical Weather Prediction (NWP)

NWP models compute future weather conditions given initial input weather states. The models are based on the Newtonian equations of motion applied to a parcel of air (also known as the Navier-Stokes equation), the first law of thermodynamics, the principles of conservation of mass and momentum, and the equation of state of a gas. In addition, the equation describing the behaviour of water vapour is usually assumed to complete the set of six equations which are known as the primitive equations [31, 32]. The primitive equations are used to compute future values for wind speed and direction, air pressure, humidity, and temperature for positions in a pre-specified three-dimensional grid representing a certain area of the atmosphere discretely [32]. Initial conditions are determined using data observed with previously described sensing techniques assimilated to the given grid, possibly combined with smaller (time) scale NWP model output data. For local, lower scale models, also boundary conditions can be defined

---

[1]Lidar is a technique that is equivalent to radar, but uses laser instead of radio waves.
[2]KNMI data can be found at data.knmi.nl.

based on the outcome of global, higher scale NWP models [33]. Since the set of equations used consists of non-linear partial differential equations no analytical method can be used to find exact solutions. Instead solutions are found numerically. The resolution and scale on which the NWP models operate can differ based on their purpose. For radar and radio wave propagation assessment applications, resolutions with a grid size of at most 5 km in the horizontal plane and an average of 60 m or better in the lowest 1 km of the atmosphere in the vertical direction suffice [34].

Around the world, different NWP implementations are being used by meteorological institutions and other parties. In the Netherlands, the KNMI is the main user of NWP models. At global level, the KNMI relies on the high resolution ECMWF (European Centre for Medium-Range Weather Forecasts) model which has a spatial resolution approximately corresponding to a grid size of 14 km in the horizontal plane [35] and the ability to make forecast up to 10 days. At national scale, HARMONIE (Hirlam Aladin Regional Mesoscale Operational NWP In Europe) is run, with ECMWF input. HARMONIE, in turn, has a spatial resolution corresponding to a grid size of 2.5 km in the horizontal plane, a vertical resolution corresponding to a grid size of 65.6 m in the first kilometre, and a temporal resolution of 1 hour up to 48 hours ahead [29].

4.3   Conversion to M-profile

As environmental data is obtained, refractivity profiles, or M-profiles, can be determined with Eq. (3.4) from section 3.1. In general, this leads to the relation: the more representative the data, the more representative the refractivity profile.

In the near-surface air layer known as the boundary layer, reaching up to 500-3000m, interaction between the air and the earth's surface takes place. The energy and moisture of the surface can substantially influence the air above. These influences are the strongest in the bottom 10% of the boundary layer known as the surface layer. Factors such as ground temperature and soil moisture - or above seawater, water temperature and sea state - have effect on radar and radio wave propagation in the air layers above [36]. Above sea, the most important of those effects is known as an evaporation duct which is described in section 3.2.4.

In order to model radar and radio wave propagation accurately, different air layers ask for different approaches to extract refractivity profiles. For the upper-air layers, the atmospheric data acquired by direct or remote sensing technique or NWP's can be used as input for Eq. (3.4) directly.

To model evaporation ducts accurately the obtained weather data is often not sufficient in the lower air layers. To that extent, Monin-Obukhov similarity theory (MOST) is often used to enhance lower air atmospheric data, meaning that humidity, air pressure, and temperature profiles are adapted to the real situation based on limited observations, before conversion to the M-profile takes place.

Although MOST is broadly used and assumed to be very helpful when it comes to obtaining accurate refractivity profiles, its downside is that it can lead to inconsistencies at the transition from lower to higher air profiles both in the atmospheric parameters and in M-space. To limit unwanted results induced by these inconsistencies, another technique known as blending is used which connects lower and higher air profiles. As is shown in figure 4.2, blending can be applied in M-space or before the conversion from atmospheric parameters to the M-profile. Blending is described shortly in section 4.3.2.
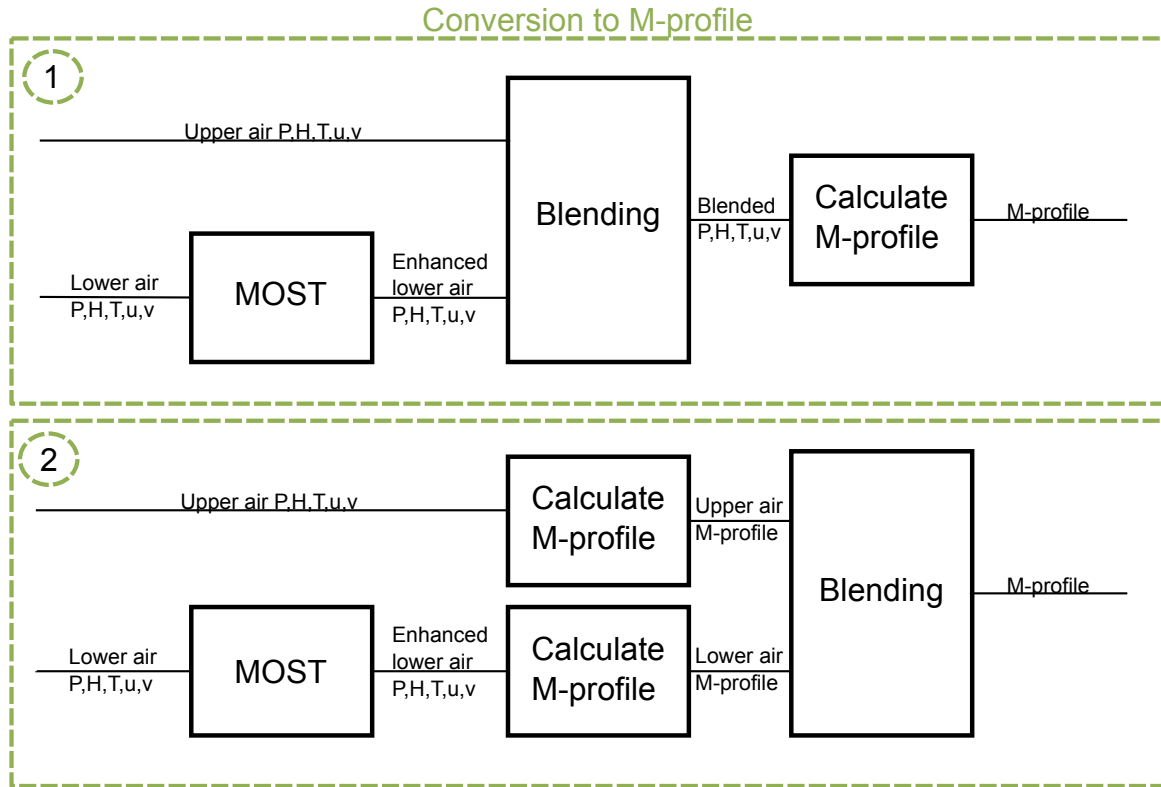
Figure 4.2: Schematic representation of conversion from atmospheric data into an M-profile, including MOST, blending, and the calculations of the M-profile itself. In (1), blending is performed before the calculation of the M-profile and, in (2), blending is performed after the calculation of the M-profile.

4.3.1   Monin-Obukhov Similarity Theory

In similarity theory, variables are combined into dimensionless groups. Each variable in the group is then obtained experimentally. After that, the dimensionless group, as a whole, is fitted, with an empirical equation, using a function of some parameter. The experiment and the fitting to obtain the equations are repeated. In general, the equations obtained based on the different experiments are similar. The method of obtaining an empirical equation for a dimensionless group is therefore called similarity theory, the accompanied equation is called a similarity relation, and the function a similarity function. When this method is applied to surface layers it is usually referred to as Monin-Obukhov similarity theory (MOST), named after the two researchers first describing this approach [7].

When MOST is applied, one is interested in the atmospheric profiles of four parameters to be able to derive the M-profiles, namely wind speed, humidity, temperature, and air pressure. The last-named of those four, air pressure, is not obtained using similarity theory, but follows from the barometric height formula, which shows an exponential decrease in the air pressure with an increase in height [37]. To derive the other parameters, three new, related variables are introduced on which MOST is applied, namely, the wind velocity u, the potential temperature Θ[3], and the specific humidity q[4].

---

[3]The potential temperature Θ is the temperature of an unsaturated air parcel, when the pressure is brought to 1000 hPa. In general, the potential temperature can be related to the air pressure by $\Theta = T \left(\frac{1000}{p} \right)^{0.286}$ [36].

[4]The specific humidity q is the ratio of the mass of water vapour in the air per mass moist in the air [36],

In MOST, two similarity relations can be defined containing the time averages of the vertical gradient of the wind velocity u and the potential temperature Θ together with the similarity functions ψ_u and ψ_h respectively, in which both similarity functions depend on the dimensionless parameter $\zeta = z/L$, with L the Monin-Obuhkov length described below. The similarity equations are stated as follows:

$$\frac{\psi_u(\zeta)}{k} = \frac{z}{u_*}\frac{\partial u}{\partial z} \tag{4.1}$$

and

$$\frac{\psi_h(\zeta)}{k} = \frac{z}{\Theta_*}\frac{\partial \Theta}{\partial z}, \tag{4.2}$$

in which k is the Von Kármán constant and u_* and Θ_* are scales of the wind velocity and temperature, respectively. The value of k is defined experimentally multiple times and can depend on the similarity functions, but here $k = 0.4$ is used [37, 36].

The Monin-Obukhov length L, in m, can both be seen as a scale parameter as well as a stability parameter. Positive values of L represent the thickness of the surface turbulent layer under a stable atmospheric stratification, whereas negative values of L correspond to an unstable atmospheric stratification [37]. L is defined as:

$$L = \frac{u_*^2\Theta}{kg\Theta_*}, \tag{4.3}$$

with k again the Von Kármán constant and g the acceleration of gravity [36].

Together (4.1), (4.2), and (4.3) form a system of three equations which can be solved for its three unknown variables L, u_*, and Θ_*. In addition, the similarity equation relating the time average of the vertical humidity gradient, q_*, to the similarity function ψ_q can be stated analogously to the equation of Θ_*:

$$\frac{\psi_q(\zeta)}{k} = \frac{z}{q_*}\frac{\partial q}{\partial z} \tag{4.4}$$

in which $\psi_q \approx \psi_h$ can be substituted [36]. Considering this equation, q_* can also be derived.

The initial aim was to derive (vertical profiles for) the wind speed, humidity, and temperature. Related parameter values for u, Θ, and q respectively, can be extracted by considering the integration of the equations (4.1), (4.2), and (4.4) from z_0^α to z (with α being either u, Θ, or q). The height values z_0^α are taken to be the so called roughness heights. At these heights, the values of u, Θ, and q are equal to the values at sea level, respectively. At sea level, the wind speed is zero, the temperature is equal to the water temperature, and the humidity is equal to the humidity of saturated water vapour [37]. (Determining the roughness heights is not completely straightforward and is discussed in both [37] and [36].)

For all three similarity equations, the integration as well as additional derivations are similar. Therefore, it is illustrated here only for equation (4.1), containing the wind speed. For reasons that will become clear later, Eq. (4.1) is rewritten to

$$\frac{\partial u}{\partial z} = \frac{u_*}{kz}\psi_u(\zeta) = \frac{u_*}{kz}(1 - 1 + \psi_u(\zeta)). \tag{4.5}$$

---

and it can be related to the partial pressure of water vapour e and the air pressure p by $e = \frac{qp}{\epsilon+(1-\epsilon)q}$ with ϵ the ratio of the individual gas constant for dry air to that for water vapour [38].

Also an additional function Ψ_α is defined as

$$\Psi_\alpha\left(\zeta^\alpha\right) = \int_{z_0^\alpha}^{z^\alpha} \left(1 - \psi_\alpha\left(\zeta\right)\right) \frac{dz}{z}, \tag{4.6}$$

which is referred to as the integral representation of the similarity function of α with $\zeta^\alpha = z^\alpha/L$ following from $\zeta = z/L$ and α being either u, h, or q. By integration, the following equation can then be obtained:

$$u(z^u) - u(z_0^u) = \frac{u_*}{k} \int_{z_0^u}^{z^u} \left(1 - 1 + \psi_u\left(\zeta\right)\right) \frac{dz}{z} \tag{4.7}$$

or, since $u(z_0^u) = u(0) = 0$

$$u(z^u) = \frac{u_*}{k} \left(\ln \frac{z^u}{z_0^u} - \Psi_u(\zeta^u) \right). \tag{4.8}$$

If a neutral stratification of the atmosphere is reached approximately, i.e. when z/L tends to zero, $\psi_u(\zeta)$ will tend to one and therefore $\Psi_u(\zeta^u)$ will tend to zero. As a result, the equation will be

$$u(z^u) = \frac{u_*}{k} \ln \frac{z^u}{z_0^u}, \tag{4.9}$$

which means that $\Psi_u(\zeta^u)$ characterises to what extent $u(z^u)$ differs from a logarithmic profile and therefore to what extent the surface layer of the atmosphere differs from a neutral stratification [37].

Similarity functions

To apply MOST, the similarity functions $\psi_\alpha(\zeta)$ or their integral representations $\Psi_\alpha(\zeta^\alpha)$ (for α being u or h) were derived experimentally. At first, the results were based on experiments over land, which were not representative for maritime purposes. The similarity functions based on experiments over the ocean, and therefore applicable for maritime purposes, were first developed by Liu, Katsaros, and Businger (LKB) in 1979 [38]. In the LKB model, the wind similarity function $\psi_u(\zeta)$ for unstable ($\zeta < 0$) and stable ($\zeta > 0$) conditions is defined as:

$$\psi_u(\zeta) = \begin{cases} (1 - \beta\zeta)^{-1/4} & \text{if } \zeta \leq 0 \\ 1 + \gamma\zeta & \text{if } \zeta > 0 \end{cases} \tag{4.10}$$

and the similarity function for humidity and temperature $\psi_h(\zeta)$ is defined as:

$$\psi_h(\zeta) = \begin{cases} (1 - \beta\zeta)^{-1/2} & \text{if } \zeta \leq 0 \\ 1 + \gamma\zeta & \text{if } \zeta > 0 \end{cases}. \tag{4.11}$$

The numerical constants β and γ were determined experimentally and set equal to 16 and 5, respectively [37].

After that, multiple other similarity functions were derived from over ocean experiments. Most of these functions will not be discussed here, but can be found in literature, e.g., [37] and [38]. The one model that is discussed below is the COARE (Coupled Ocean-Atmosphere Response Experiment) model developed as a part of the TOGA (Tropical Ocean-Global Atmosphere) program [39]. This model forms the basis for the model that is used in AREPS [40]. The COARE model - other than most models - does not state any of the similarity functions $\psi_\alpha(\zeta)$ explicitly, but states $\Psi_\alpha(\zeta^\alpha)$ directly [37].

In the COARE model, the wind similarity function integral representation $\Psi_u(\zeta)$ for unstable ($\zeta < 0$) and stable ($\zeta > 0$) conditions (in which for convenience reasons ζ^u is denoted as ζ) is defined as:

$$\Psi_u(\zeta) = \begin{cases} \frac{1}{1+\zeta^2}\left(2\ln\left(\frac{1+x_2}{2}\right) + \ln\left(\frac{1+x_2^2}{2}\right) - 2\arctan(x_2) + \frac{\pi}{2}\right) \\ + \left(1 - \frac{1}{1+\zeta^2}\right)\left(\frac{3}{2}\ln\left(\frac{1+y_2+y_2^2}{3}\right) - \sqrt{3}\arctan\left(\frac{2y_2+1}{\sqrt{3}}\right) + \frac{\pi}{\sqrt{3}}\right) & \text{for } \zeta < 0 \\ -a\zeta - b\left(\zeta - \frac{c}{d}\right)e^{-d\zeta} - \frac{bc}{d} & \text{for } \zeta \geq 0 \end{cases} \quad (4.12)$$

and the integral representation of the similarity function for humidity and temperature $\Psi_h(\zeta)$ is defined as:

$$\Psi_h(\zeta) = \begin{cases} \frac{1}{1+\zeta^2}2\ln\left(\frac{1+x_2}{2}\right) + \left(1 - \frac{1}{1+\zeta^2}\right) \\ + \left(\frac{3}{2}\ln\left(\frac{1+y_2+y_2^2}{3}\right) - \sqrt{3}\arctan\left(\frac{2y_2+1}{\sqrt{3}}\right) + \frac{\pi}{\sqrt{3}}\right) & \text{for } \zeta < 0 \\ 1 - \left(1 + \frac{2a}{3}\zeta\right)^{3/2} - b\left(\zeta - \frac{c}{d}\right)e^{-d\zeta} - \frac{bc}{d} & \text{for } \zeta \geq 0 \end{cases} \quad (4.13)$$

in which the auxiliary variables $x_2 = (1 - 16\zeta)^{1/4}$ and $y_2 = (1 - 10\zeta)^{1/3}$ are introduced, and the constants, again determined base on experiments, are $a = 1$, $b = 2/3$, $c = 5$, and $d = 0.35$ [37].

4.3.2   Blending of upper- and lower-air (refractivity) profiles

By techniques such as MOST, it is possible to accurately determine the atmospheric parameters related to an evaporation duct that only occur in the lower-air layer. For upper-air layers, the atmospheric data, e.g. NWP data, is used directly. As a result, two profiles arises: the lower-air profile and the upper-air profile. Since lower-air evaporation ducts can influence propagation in the air layers above and upper-air surface and elevated ducts can influence propagation at the surface, these profiles need to be combined to make accurate radar and radio wave propagation calculations. At the same time, simply connecting the lowest point of the upper-air profile with the lower air profile can lead to inconsistency in the combined profile with unrealistic propagation side-effects as a consequence. Therefore, the profiles need to be somehow blended in a way that avoids inconsistencies, yet also accurately reflects each two individual profiles [29]. The technique used for this is called "blending" and can be applied either in the modified refractivity domain (or M-space), as is shown in (1) of figure 4.2, or in the physical domain, as is shown in (2) of the same figure.

Blending is a relatively new topic and no ideal applications currently exist, therefore it is not treated in detail here. Two earlier sources by Derksen [29] and Fredrickson [41] can be found addressing this topping and extensive information on blending can be found there. However the essence of blending is, as is stated by Derksen, that the upper and lower profile are blended in such a way that the resulting profile satisfies the following conditions:

- the transition is continuous;

- the transition is smooth;

- no strong inconsistencies in the profile, such as strong gradients, as a result of blending are introduced;

- no essential characteristics of both profiles, such as evaporation duct height, are disrupted.

4.4 Radar Propagation Modelling (RPM)

The (modified) refractivity profiles determined in the previous step must be converted into propagation statements, i.e. pattern propagation, F, or propagation loss, PL, to be able to determine the strength of radio signals at a certain point. In order to do so, several methods are developed over the years each with their own advantages and disadvantages. Two of those methods, the ray-tracing method and the parabolic equation method, will be discussed in this section as they are used extensively and are within the scope of this research.

The methods, on their account, can be integrated into a Radar Propagation Model (RPM) to be applied in real propagation calculations. Again several of those models exist. One of them, the Advanced Propagation Model (APM) is discussed at the end of this section. This model is included in AREPS and uses both the ray-tracing method and the parabolic equation method to optimise computational performances as well as output accuracy.

Ray-tracing method

The ray-tracing or geometrical optics method can be used to model anomalous propagation in a relatively simple way based on ray theory. In ray theory, one supposes that "the energy *radiates* outwards in rays along the radial lines from the source" [23, p. 122]. Within the earth's atmosphere, gradients in the refractivity profile can cause the paths of these rays to bend. By consecutively looking at the refractivity profiles along the path of the ray and by taking into account the fact that the ray can reflect on the surface of the earth, the total path of the ray, the ray-trace, can be constructed. By considering multiple rays transmitted at different angles, a ray-trace pattern can be composed [29].

Advantages of the ray-tracing method are that it is computationally fast and applicable to inhomogeneous atmospheric conditions with range-varying refractivity profiles. However, the ray-tracing method also experiences some clear disadvantages. As the interference of the rays is not taken into account, the field strength is hard to determine under ducting conditions. The positive as well as negative impact waves have on each others strength - earlier discussed as "multipath interference" - is ignored.

More extensive information on ray-tracing and a corresponding implementation can be found at [29].

Parabolic equation method

An ideal method to determine radar and radio wave propagation would consist of solving the Maxwell equations exactly. However, for meaningful problems fully solving the equations is intractable due to the computational complexity of the calculations and the size of accurate input data [42]. Therefore, the parabolic equation is based on a reduction of one of the Maxwell equations: the Helmholtz equation.

To state the two-dimensional Helmholtz equation in Cartesian coordinates, two assumptions for the propagation problem are made: the earth is approximated to be flat and propagation takes place in a cone, with its apex at the origin of the signal, centered around a preferred direction, the paraxial direction [42]. Based on these assumption the Helmholtz equation is given by:

$$\frac{\partial^2 \phi}{\partial x^2} + \frac{\partial^2 \phi}{\partial z^2} + k_0^2 n^2 \phi = 0 \tag{4.14}$$

where x is the paraxial direction (or the range) and z is the height, $k_0 = 2\pi/\lambda$ is the free-space wavenumber, $n = n(x, z)$ is the height and range dependent refractive index, and $\phi =$

$\phi(x, z)$ is the height and range dependent electric or magnetic field in the horizontal or vertical polarization, respectively [43].

To derive the parabolic equation a reduced function associated with the paraxial direction x is introduced, such that:

$$\phi(x, z) = \frac{u(x, z)}{e^{ik_0 x}}. \tag{4.15}$$

This reduced function is slowly varying in range for waves propagating at angles close to the paraxial direction, which gives it properties that are numerically convenient [43]. Substituting u into the Helmholtz equation, Eq. (4.14), gives:

$$\frac{\partial^2 u}{\partial x^2} + 2ik_0 \frac{\partial u}{\partial x} + \frac{\partial^2 u}{\partial z^2} + k_0^2(n^2 - 1)u = 0. \tag{4.16}$$

This can be factorised into:

$$\left(\frac{\partial}{\partial x} + ik_0(1 - Q) \right) \left(\frac{\partial}{\partial x} + ik_0(1 + Q) \right) u = 0 \tag{4.17}$$

where

$$Q = \sqrt{1 + q} \text{ and } q = \frac{1}{k_0^2} \frac{\partial^2}{\partial z^2} + (n^2 - 1). \tag{4.18}$$

Based on Eq. (4.17), u has two linearly independent solutions [42], which satisfy the pseudo-differential equations:

$$\frac{\partial u}{\partial x} = -ik_0(1 - Q)u \tag{4.19}$$

and

$$\frac{\partial u}{\partial x} = -ik_0(1 + Q)u \tag{4.20}$$

which correspond to the forward and backward propagating waves along the paraxial direction, respectively. Together these pseudo-differential equations that are of first order in x are the outgoing and incoming 'parabolic' equations [43].

In practice, backwards propagation is often ignored and the corresponding incoming parabolic equation, Eq. (4.20), is neglected. The remaining forward propagation waves can be modelled by finding an (exact) solution for the outgoing parabolic equation, Eq. (4.19), which is:

$$u(x + \Delta x, z) = e^{ik_0 \Delta x(-1 + Q)} u(x, z) \tag{4.21}$$

where Δx is the incremental range step [44, 43].

In case the standard parabolic equation (SPE) is considered, Q is approximated by a first-order Taylor expansion, i.e. $\sqrt{1 + q} \approx 1 + q/2$. The resulting SPE - again ignoring backwards propagation - will then be:

$$\left(\frac{\partial}{\partial z^2} + 2ik_0 \frac{\partial}{\partial x} + k_0^2(n^2 - 1) \right) u = 0. \tag{4.22}$$

Based on the formal solution, one can conclude that determining all numerical solutions is an iterative process. This idea is used in the algorithm that is widely-used to compute these solutions which is known as the 'Fourier split-step method', which is elaborated in [43]. This algorithm starts at a reference range and iteratively - with increasing range - computes the solutions such that the vertical profile at a given range x_i is based on the vertical profile at

the previous range $x_{i-1} = x_i - \Delta x$, whilst the upper and lower boundaries of the domain have appropriate boundary conditions. The split-step solution of the SPE that arises, is given by:

$$u(x + \Delta x, z) = \exp\left(ik_0(n^2 - 1)\frac{\Delta x}{2}\right)\mathbf{F}^{-1}\left(\exp\left(-ip^2\frac{\Delta x}{2k_0}\right)\mathbf{F}(u(x, z))\right) \tag{4.23}$$

where $\mathbf{F}$ and $\mathbf{F}^{-1}$ represent the forward and inverse Fourier transforms respectively, and p is defined as $p = k_0 \sin\theta$ with θ being the propagation angle referenced from the paraxial direction [44].

Important to note is that the original u was defined to be functional for waves propagating at angles close to the paraxial direction. This remains valid for the solution of u. To remain accurate, propagation angles should be less than $10° - 15°$ [44]. Therefore, the SPE is often also called the narrow-angle parabolic equation. Some more wide-angle PE's can be derived using various other methods.

4.4.1 Advanced Propagation Model

Above, two methods to model radar and radio wave propagation were introduced, each with their own advantages and disadvantages; the ray-tracing method was fast, but inaccurate and the parabolic equation was more accurate, but slow. Ideally, the best of both, the speed and the accuracy, would be combined. The Advanced Propagation Model (APM) does exactly that.

The APM is a hybrid RPM that uses four basic submodels. These models are Flat Earth (FE), Ray Optics (RO), Extended Optics (XO), and the (split-step Fourier) Parabolic Equation algorithm (PE) and they all make use of the methods described above. Together, these models cover the complete atmospheric propagation [45]. In figure 4.3, the regions on which each submodel is applied are displayed.

The PE model is the most suitable model of all four to compute propagation loss with varying refractivity and terrain along the propagation path. Therefore the PE model is the primary model around which the other three submodels are built. On the other hand, the region to which the PE model is applied is deliberately kept small in order to limit the size of the Fast Fourier Transform (FFT) which makes this method less efficient than the other models [45]. In the upcoming four subsections, the main principles of all submodels are described starting from the PE model. More extensive information on the APM and the submodels, including the derivation of the pattern propagation or propagation loss, can be found in [45] and [46].

Parabolic Equation (PE) model

The PE model used in APM is comparable to the general PE method described above. However, it uses a slightly altered PE formula, that is more suitable to make calculations at a wider angle:

$$u(x + \Delta x, z) = \exp\left(ik_0\Delta x 10^{-6}M(z)\right)\mathbf{F}^{-1}\left(\exp\left(i\Delta x\sqrt{k_0^2 - p^2} - k_0\right)\mathbf{F}(u(x, z))\right) \tag{4.24}$$

where x and z are the range and height coordinates, k_0 is the free space wavenumber $2\pi/\lambda$, Δx is the incremental range step over which the field solution is propagated, $M(z)$ is the modified refractivity profile varying with height (which is of course related to n), and $\mathbf{F}$ and $\mathbf{F}^{-1}$ represent the forward and inverse Fourier transforms respectively. The variable $p = k_0 \sin\theta$ with θ being the propagation angle referenced from the horizontal direction.[5]

---

[5]A derivation of the wide-angle PE formula, Eq. (4.24), similar to the narrow-angle PE formula, Eq. (4.23), can be found in [47].
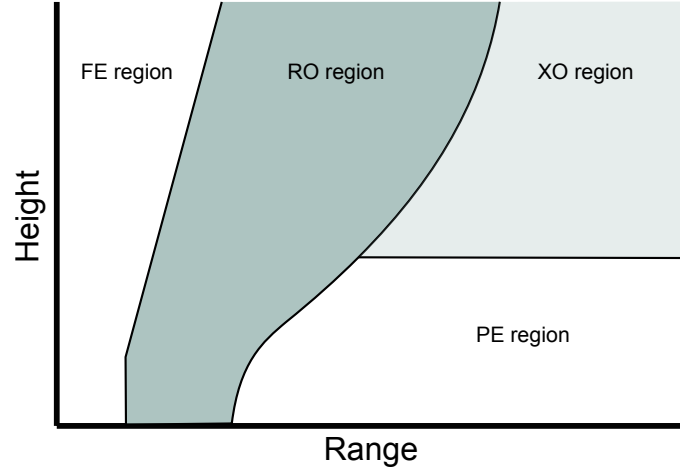
Figure 4.3: An overview of the complete APM model, showing all regions in which the different submodels are applied [3].

The PE model is applied to the lower area of the atmosphere, beyond the RO region (see lower right of figure 4.3) up to a maximum altitude z_e. The value of z_e is selected to limit the size of the PE region, and as a result the size of the FFT, yet still incorporates all important terrain and refractivity effects. In general, z_e is selected to be either the height of the highest trapping layer specified in the refractivity profile(s) or 120% of the maximum terrain height along the propagation path, depending on which is the highest.

Extended Optics (XO) model

The XO model is applied in the region beyond the RO region and above the maximum height, z, of the PE region (see upper right of figure 4.3). Given the definition of z this region does not contain atmospheric ducts and therefore the refractivity profiles consist solely of positive linear gradients. The XO model is based on the assumption that all rays - direct and reflected - are parallel within this region. That way the field computed by the parabolic equation model at height z can be "extended" into the XO region using geometric optics.

Ray Optics (RO) model

Key to the APM is the maximisation of efficiency without significant reduction of the accuracy. In order to do so, the region in which the PE model is used should be kept minimal by maximising the RO region on its left (see the center of figure 4.3) [46]. The maximum range and altitude which the RO model can be applied to are defined by a limiting grazing angle for reflected rays, ψ, that is determined by:

$$\psi = \psi_0 + \delta\psi, \tag{4.25}$$

with

$$\psi_0 = \max\left(0.002, \frac{0.0443}{\sqrt[3]{f}}\right) \text{ and } \delta\psi = \sqrt{2 \cdot 10^{-6}|M(0) - M_{min}|} \tag{4.26}$$

where f is the frequency in MHz, $M(0)$ is the modified refractivity at the surface, and M_{min} is the minimum modified refractivity over all heights, in general. In case of range-dependent refractivity profiles, the value of ψ is doubled [45]. The function ψ_0 is selected in such a way that

its value is 2.5 times the limit earlier established by Reed and Russell [23], which guarantees that the errors in the RO solution are less than 0.1 dB and $\delta\psi$ is used to account for ducting [46].

The RO model itself is based on ray-tracing (section 4.3) of a series of direct and reflected waves through selected control points. In between those point, the phase angles and magnitudes of these rays can be interpolated at each desired point. The phase angle of each ray is determined from the optical path length difference from the ground range and the magnitude of each ray is computed based on a spreading term relative to free-space spreading [46].

Flat Earth (FE) model

The FE model uses simple ray-tracing as described in subsection 4.4. The model - as its name suggests - assumes propagation over a flat earth with straight line paths for all rays. However, in order to still take into account the earth's curvature and refractive effects, the effective earth's radius, r_{eff}, introduced in subsection 3.1.1, is used. The model is used at all heights and ranges up to 2.5 km from the source (antenna) and is used at all grazing angles exceeding 5° (see figure 4.3) [45].

4.5 Radar Threshold Modelling (RTM)

Although propagation loss as described in the previous section provides valuable information, the essential question is how a system or its operator decides whether or not something is a detection, or in other words, how it is attempted to separate target signals from noise signals. The most evident, and broadly applied, way to do this is by setting a detection threshold. Every signal exceeding the threshold is marked as a detection and every signal below the threshold is not.[6] The question remaining is how to determine an appropriate threshold, which is seldom exceeded by noise signals, yet also seldom not exceeded by target signals.

A measure to determine how often a threshold is exceeded by noise is the probability of false alarm, P_{fa}. The probability of false alarm is defined as the conditional probability that the threshold is exceeded given that there is no signal present in the receiver, or mathematically:

$$P_{fa} = \mathbb{P}(\text{Received signal} \geq W_T | \text{ No target signal is present}), \tag{4.27}$$

where W_T is the threshold in W. The value of P_{fa} can be determined when the probability distribution of the noise is known. Thermal noise is encountered most within the receiver and is described as Gaussian white noise with mean zero and variance ϕ^2, or the mean-squared value of the noise voltage [4]. Before the signal inside the receiver gets to the detector it is filtered to a signal having a non-negative distribution fluctuating around a mean, ψ, which is the root mean-squared (rms) value of the original white noise power. The simplest distribution satisfying this condition is the exponential distribution with parameter $1/\psi$. It follows that

$$P_{fa} = \mathbb{P}(x \geq W_T) = \int_{W_T}^{\infty} \frac{1}{\psi} e^{-\frac{x}{\psi}} dx = \left[-e^{-\frac{x}{\psi}} \right]_{W_T}^{\infty} = e^{-\frac{W_T}{\psi}}, \tag{4.28}$$

where x is the power peak of a noise signal. Since ψ is defined as the rms value of the white noise in the receiver, W_T/ψ is a threshold-to-noise ratio, W_T/N. When the maximum probability of false alarm accepted is set at 10^{-4}, it follows that

$$\frac{W_T}{N} = -\ln(P_{fa}) = -\ln\left(10^{-4}\right) = 9.21 \approx 9.6 \text{ dB}, \tag{4.29}$$

---

[6]The threshold can be set in Wattage, Voltage or decibel.

which means that the threshold lays 9.6 dB higher than the rms decibel value of the noise [48].[7]

So far, the threshold only depends on the probability of false alarm and therefore the signal itself is not taken into account in any way. Setting a threshold value is however a trade off between the probability of false alarm and the probability of detection (PoD or P_d), i.e. the probability that a target signal will be detected. When the threshold is set to high, targets will be missed, however when the threshold is set to low, false detections will occur too often. To that extent, consider a sinusoidal waveform target signal with amplitude A to be present together with the white noise earlier described. Also, consider the detection threshold to be now given in V as V_T. The probability of detection, which is equal to the probability that a peak voltage value y exceeds V_T, is according to a derivation by Rice [50, 4] given by

$$P_d = \int_{V_T}^{\infty} \frac{y}{\phi^2} \exp\left(-\frac{y^2 + A^2}{2\phi^2}\right) I_0\left(\frac{yA}{\phi^2}\right) dy, \tag{4.30}$$

where $I_0(\omega)$ is the modified Bessel function of zero order with argument ω.[8] If no signal is present, i.e. $A/\phi^2 = 0$, Eq. (4.30) gives rise to a more reasonable probability of false alarm distribution, namely the Rayleigh distribution:

$$P_{fa} = \int_{V_T}^{\infty} \frac{y}{\phi^2} \exp\left(-\frac{y^2}{2\phi^2}\right) dy = \exp\left(-\frac{V_T^2}{2\phi^2}\right) \tag{4.32}$$

On the other hand, if A/ϕ^2 gets very large, Eq. (4.30), the probability density function, becomes a Gaussian density function with mean A and variance ϕ^2, so that:

$$P_d \approx \int_{V_T}^{\infty} \frac{1}{\phi\sqrt{2\pi}} \exp\left(-\frac{(y - A)^2}{2\phi^2}\right) dy \ [52]. \tag{4.33}$$

The threshold is now expressed as a relation between the noise variance ϕ^2 and the signal amplitude A by:

$$V_T = \frac{A}{\phi}. \tag{4.34}$$

In figure 4.4 both density functions related to the probability of detection as well as the probability of false alarm are plotted together with a threshold to show the false alarm and detection areas. Finally, the voltage threshold can be related to the signal-to-noise threshold according to Skolnik [4] by:

$$V_T = \frac{A}{\phi} = \frac{(\text{rms signal voltage})\sqrt{2}}{(\text{rms noise voltage})} = \sqrt{2\frac{(\text{rms signal power})}{(\text{rms noise power})}} = \sqrt{2\frac{S}{N}}, \tag{4.35}$$

when using that for a sine-wave with amplitude A the rms is given by $A/\sqrt{2}$ and that $P = V^2/R$ with R the system's resistance [4].

For a given probability of detection and/or a given probability of false alarm it is now possible to determine the voltage threshold V_T and to relate this to the minimum signal-to-noise ratio using the relation described in Eq. (4.35). Reversely, it is possible to determine the probability of detection when the detection threshold of a system is known.

---

[7]A probability of false alarm of 10^{-4} is use in IMO requirements. [49]

[8]The modified Bessel function of zero order with argument ω is defined by

$$I_0(\omega) = \frac{1}{2\pi} \int_0^{2\pi} \exp(\omega \cos\theta) d\theta \tag{4.31}$$

as is shown by [51, p. 282].
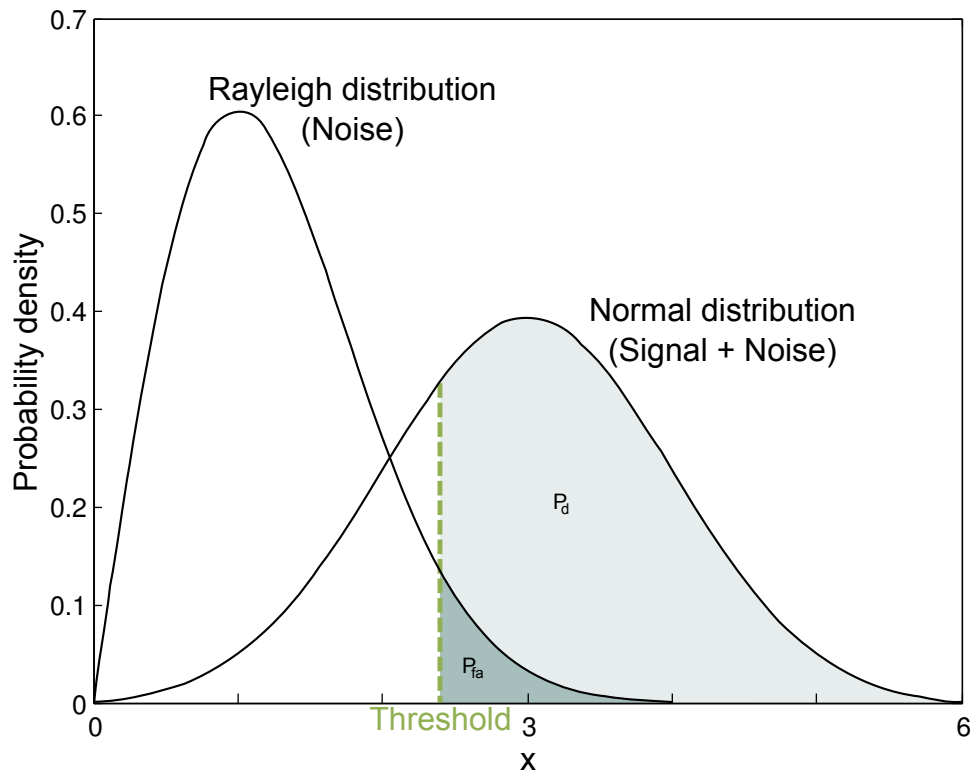
Figure 4.4: Probability density functions of the Rayleigh distribution corresponding to the noise alone and of the normal distribution corresponding to signal and noise together, and a sample threshold value [4].

4.6 Measure of Effectiveness (MoE)

Finally, it is to be determined how well a system performs corresponding to achieving the desired result and accomplishing the mission objectives set by the user. In other words, a measure is needed on how well the system fits the user's exceptions [53]. The measure used for this is the Measure of Effectiveness (MoE).

Because the MoE depends on the perspective of the user, exactly equal system output from the previous step can lead to a total different MoE application. Therefore, it is essential for the usage of an MoE to state the user requirements accurately and extensively beforehand. Based on the user requirements the outcome of the previous step, most likely the probability of detection, can be translated into the desired information. This desired information can be used as the MoE.

Since the MoE is user specific it is not possible to describe the MoE from an overall perspective. Within this thesis focus lays on the coverage area of multiple antennae combined in which targets at a specific height can be detected. Therefore, the Measure of Effectiveness of this thesis is the target detection coverage area. (Based on target characteristics that will be defined later on.) Other examples of the MoE that could be thought of are the exposed area, i.e. the area in which counter detection is possible, the maximum detection range, or the direction in which the probability of detection exceeds the probability of counter detection (or vice versa).

4.7   Advanced Refractive Effects Prediction System (AREPS)

In the previous sections, the complete process of modelling atmospheric conditions to determine (maximum) detection ranges is discussed. To automatise this process, multiple software packages and tools have been developed over the years. One of those software packages is the Advanced Refractive Effects Prediction System (AREPS).

AREPS is developed by the U.S. Space and Naval Warfare Systems Center (SPAWAR) and is currently widely used by the U.S. Department of Defense and other federal governmental agencies. Earlier publicly available versions were and probably still are used by private industries and individuals around the world [2]. When provided with NWP data, and system and target specific information, AREPS is able to performing every step described in the previous section, from defining M-profiles to showing radar wave propagations and radar thresholds.

Previous versions of AREPS were freely available for public use, however the newer and current versions are not. Due to a joint research project between KIXS and SPAWAR on radar wave propagation, to which this study is associated, AREPS is available for this study.[9] Initial versions of AREPS are in use since the late nineties and it is further developed ever since, which makes it one of the most mature software packages, verified and validated during practice and study, available in this field. Because of this, AREPS is used extensively throughout this thesis and is of essential value for its results.

4.8   Subconclusion

Modelling radar and radio wave propagation is an extensive and complex process consisting of many steps. Environmental data needs to be obtained and converted into M-profiles. After that, the propagation of the radar and waves as well as a detection threshold must be modelled, based on sensor and target specifications. Finally, the outcome needs to be interpreted based on the user requirements. The AREPS software package plays an important role in the acceleration and improvement of the central steps of the process, i.e. the conversion to the M-profile, the RPM, and the RTM, and is used where possible throughout this thesis. The remaining improvements to be made on the input and outcome side of the process are emphasised within this thesis. In the previous chapters, environmental conditions and sensor models are discussed in general. In the upcoming chapters, the environmental conditions, and sensor and target models will be made specific to the coastguard's infrastructure and the Dutch continental shelf. Based on that, AREPS calculations will be ran and the outcome will be related to the Measure of Effectiveness of this thesis, namely, the target detection coverage area.

---

[9]Software and output are available for this thesis under a Data Exchange Agreement (DEA 4811).

Chapter 5

Studied North Sea cases and data

The overall goal of this thesis is to make the Netherlands Coastguard aware of what happens to their sensor systems within their situation awareness. To get there, two initial goals and two objectives were stated in the introductory chapter (section 1.2), viz., assess North Sea weather, assess North Sea coverage, identify relevant atmospheric propagation mechanisms, and model AIS (and coastal radar) systems. Each of these inquests relies on its own methods and data. This chapter will walk through the complete process that is followed, emphasising the approach per goal and objective.

The third goal: provide a proof of concept to forecast realistic sensor coverage in the North Sea, is specified in case studies, which, their selves, are also used for the North Sea coverage assessment.

In the beginning of the chapter, more general information on sensors and targets that are used throughout this study are specified. The locations that are assumed to have mounted an AIS and radar system as well as the heights at which the antennae are mounted are set, the specification of the AIS and radar systems that are studied are given exactly, and the studied targets and their parameterisation are stated. Also seven atmospherical conditions that are used as case studies in the thesis are described.

5.1   Existing AIS and coastal radar infrastructure

During this study, the coastguard's AIS and navigation radar infrastructure is examined and discussed. It denotes all fixed locations at which an AIS or, respectively, a radar antenna that is connected to the network of the coastguard is placed at the moment this study started. This location data includes besides geographical locations also the height at which the center of the antenna is mounted (relative to the average ground level (AGL) or mean sea level (MSL)). Since the focus of this study is on the North Sea any further inland or other antenna locations are excluded.

The sensors considered in this study are placed both on onshore and offshore locations. The onshore locations, including locations on the West Frisian Islands ("Waddeneilanden"), consist of lighthouses or other coastal buildings on which the antennae are mounted and are already used to monitor near-coast vessel movement. The offshore locations are mainly oil platforms equipped with such antennae which were originally installed to monitor vessel movement around the platform in order to provide the safety of the platform and its crew.

During this study, real location and height data is used, leading to a realistic expression of the reach of the detection of the coastguard. This information is sensitive and not cleared to be released to the general public. Therefore, it will only be reported in a classified annex. Within

this thesis itself, a realistic, yet simulated data set containing sensor positions and heights will be used to provide unclassified results. This dataset forms a good substitute regarding the scientific goals of this thesis.

For the locations, a spread selection of coordinates is taken, within the studied area, i.e. in and around the Netherlands exclusive economical zone. Five of the locations are on the coast, one of which is on Terschelling, and the other ten are offshore. The representative heights for the antennae are randomly selected between 40 to 60 m for onshore platforms and between 30 to 40 m for offshore platforms (both above mean sea level) which is realistic for coastal infrastructure, i.e. mainly lighthouses, and offshore oil platforms. The simulated dataset itself can be found in appendix B.

5.2 Sensor and target specifications

5.2.1 Sensor

In the begin of this thesis (chapter 2), both AIS and coastal radar were introduced to give an idea of the parameters involved in both systems. In practice, the values of these parameters can vary even for the same type of system. In this thesis, therefore, there is selected one standard set of parameters for AIS as well as for the radar that is used throughout this study. For AIS, this set is associated to a general Class A AIS system. For radar, it is an X-band system that is closely related to the systems currently used by the coastguard. The most general studied parameters for both systems can be found in table 5.1 and a full list can be found in appendix A.

Table 5.1: Representative AIS and radar specs of selected characteristics.

Characteristic	AIS Class A	Radar X-band
(Peak) power (W)	12.5 W	25×10^3
Frequency (MHz)	161	9400
Gain (dBi)	2	35
Rotation rate (rpm)	-	21
Beamwidth (deg)		
Horizontal	-	0.4
Vertical	-	15
System loss (dB)	3.6	6
Probability of false alarm	-	10^{-4}

5.2.2 Target

Within this study, the selected target represents a medium offshore fishing vessel. These types of vessels are common on the North Sea, yet relatively small, which makes them relevant study objects that can be hidden amongst others as well as from radar detection. The corresponding radar cross section is uniformly set at 100 m^2 at a frequency of 10 GHz and 40 m^2 at a frequency of 4 GHz.[1] The representative height related to the given RCS is 5 m above sea level, meaning

---

[1]Characteristic radar cross section values are provided by the commissioners of this research based on their information. Real RCS' vary per angle, a detail which is not further studied within this thesis.

that the source of the reflection is simplified to a point source at a height of 5 m, whilst the real reflection will come from multiple heights that vary between 0 to at least 5 m. For AIS, the height at which the antenna is placed is leading. Therefore, two more heights are selected, namely 10 and 20 m. These heights roughly correspond to the height of the bridge and the height of the mast of a ship both of which can be used to mount an AIS antenna. For radar, the same heights, 10 and 20 m, are used as representative heights, having the same RCS value that was earlier related to (the target at) 5 m. For all three heights, both AIS and radar calculations are made which essentially means that there are three types of targets considered that all have the same RCS, but variable (antenna) height.

5.3 Studying atmospheric propagation mechanisms

As AIS and radar operate at different frequencies, equal atmospheric conditions can lead to different radar wave propagation considering signal strength and direction for both systems. To be able to relate atmospheric or weather conditions to radar coverage, it is therefore essential to know what kind of propagation effects exist and how they influence losses at a certain frequency. To provide for this knowledge, expert sources in literature are studied.

For AIS, only two recent papers were found which focus not only on VHF propagation, but also on AIS specifically. Both a 2012 study by Green et al [8] and a 2007 report [9] of the International Telecommunications Union (ITU) form the basis of this part of this study, accompanied by other additional literature that gives information about general VHF propagation. Based on these papers, a summary is made showing the most eminent propagation mechanisms influencing AIS or related frequency signals. (This study is conducted as part of this thesis and is presented in the next chapter.) For coastal radar a similar approach is pursued. In this case, the results are however not only based on literature focusing on radar in particular, but on more general literature about radar propagation in the X-band spectrum. This information is more broadly available, because of the utilization of radar over many years.

For both AIS and radar, (any form of) ducting is considered to be the most important mechanism on forehand, because of the presence of (some types of) ducts all over the world and their ability to bend radar wave propagation paths. For that reason, different ducting types are studied thoroughly. The impact of five different type of ducts, represented by the cases introduced later on in this chapter, on distinct frequencies is visualised to provide insight in the similarities and diversities that are encountered for propagation at different frequencies due to these ducts. For four frequencies, all representing a common radar system, stated in table 5.2, the propagation loss is plotted related to height and range.

Table 5.2: Studied operator frequencies and accompanied information.

Bandwidth	Frequency (MHz)	Possible usage
VHF	150	AIS communication
L-band	1500	GPS communication[2]
S-band	3000	Marine navigation
X-band	10,000	Marine navigation

5.4   Assessing North Sea weather

Throughout the whole of this thesis, much focus lays on looking at atmospheric conditions that could alter AIS and radar signals. Yet to link this to real atmospheric conditions some notion of the occurrence of relevant atmospheric conditions on the North Sea is necessary. Instead of studying the North Sea weather as a whole, focus will be on specific atmospheric factors known to affect AIS and radar signals, that arose from the study described in the previous section. Without jumping to conclusions, ducting effects are assumed to be amongst the most important factors that influence radar wave propagation. To that extent, the North Sea weather is studied based on the occurrences of the ducts where a distinction is made between two groups of ducts, namely evaporation ducts, and surface and elevated ducts. Evaporation ducts are studied, because of their strong impact, as will be shown in the next chapter, on X-band radar waves. Other ducting effects - both surface and elevated ducts - are studied together because of their impact on both X-band and VHF propagation.

To study the distinct groups of ducting effects, two different approaches are used. On the one hand, the evaporation duct height near the North Sea coast is studied using the internal AREPS database. Although some evaporation duct is always present, heights can vary throughout the year and throughout the day. In this study, the variations on a single representative location close to the Dutch coast are studied based on the monthly average to get an idea of the importance of evaporation ducts per season.

On the other hand, surface and elevated ducts are studied together as anomalous propagation, anoprop. To study anoprop, data from the KNMI atmospheric precipitation radar is used in an alternative way. For every single day between 1-1-2009 and 31-12-2014, figures of the commutative twenty-four hour precipitation collected by the radar plotted on a map of the Netherlands and a part of the North Sea were stored.[3] (Two examples of these plots are displayed in figure 5.2.) Above land, these pictures provide insight in the total amount of rainfall (or other precipitation) on a specific day. Yet over sea, at a certain distance from the coast - normally out of reach of the radar - "precipitation" is shown as well sometimes.[4] As the KNMI explains, this is not coming from precipitation and can therefore be denoted as clutter.[5] To distinguish between clutter and real precipitation, the range of the radar system is not leading. Although some clear circles can be seen on some days showing the boundary between significant precipitation and (almost) no precipitation in an unnatural way (as shown on the right of figure 5.2), the difference between the way real precipitation and non-real precipitation looks on the map is more important. Real precipitation sums evolve fluently over distance, showing no major difference in measured amount (and associated color on the map) on a small scale, yet clutter does. This can be seen on the left of figure 5.2, where color change is gradual, compared to the right of the same figure, where color change is not at all gradual. Also, strong clutter shows up in specific areas; areas that lead directly to the shipping lanes on the North Sea that are shown in figure 5.1. Therefore, the reception that cannot be derived back to precipitation, can be related to reflection from ships. Since the shipping lanes do not show up at a regular daily basis, the fact that a shipping lane does show up together with the fact that the reflected signal comes from outside the regular reach of the radar and the fact that the resulting image

---

[3]The accumulated rain plots are provided by the KNMI at www.knmi.nl/nederland-nu/klimatologie/geografische-overzichten/radar, last accessed on 12 December 2015.

[4]Since evaporation ducts are mainly limited to areas close to the coast, they can be excluded from the anomaly propagation in this case.

[5]KNMI information on the background of the accumulated rain plots can be found at www.knmi.nl/kennis-en-datacentrum/achtergrond/Gecorrigeerde-neerslagbeelden-radar, last accessed on 8 November 2015.
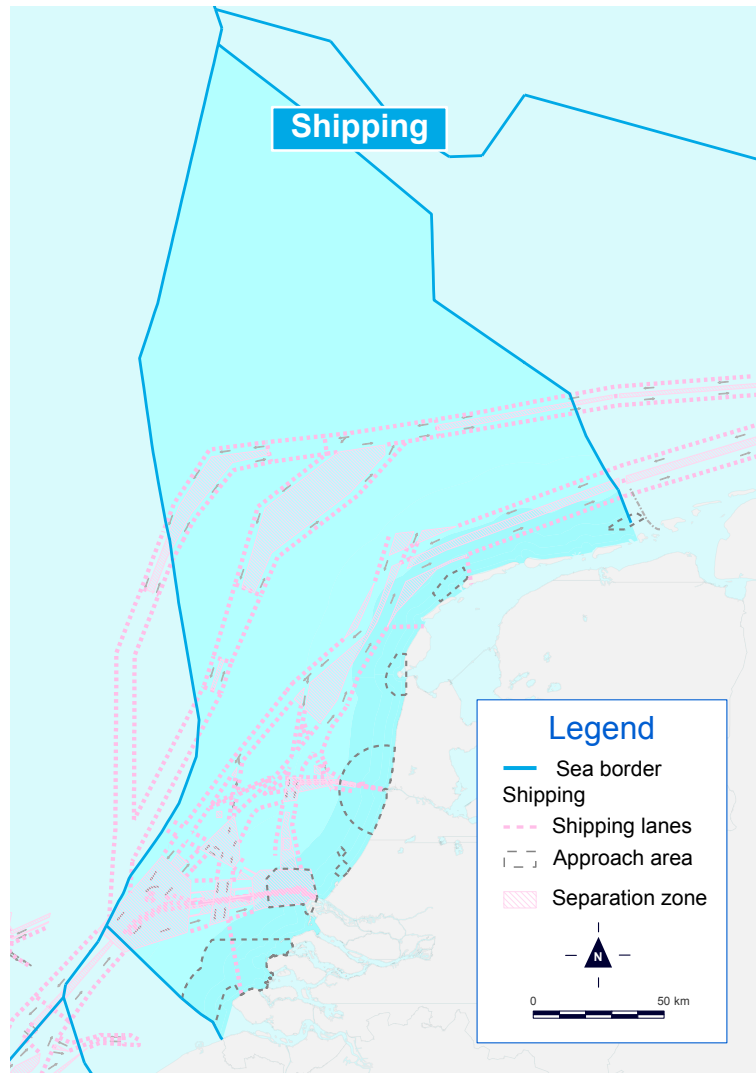
Figure 5.1: North Sea shipping lanes and the sea borders of the exclusive economical zone of the Netherlands and its surrounding countries.[6]

shows non gradual color changes, lead to the conclusion that some anomalous propagation had to be present some time that day. Since the twenty-four hour total precipitation is monitored, the presence of the anoprop could have been limited to a part of the day. On the right of figure 5.2, the image that arises on a day with strong anoprop over multiple parts of the North Sea is shown, including clear sight on the shipping lanes. The left part of the same figure shows the image of a regular rainy data without anoprop.

In this study, all the available pictures - 365 (or respectively 366) per year for a 6 years period - are inspected and all the pictures containing at least one clear part of a shipping line are counted. Those were the days on which there an effect which caused anomalous propagation of radar signals for some time, at some part of the North Sea and therefore an elevated or surface duct was present most likely.

Since the set only contained the pictures for a period of six years, drawing conclusions for the climate as a whole might seem premature, but the results represented in chapter 6 provide a strong indication for the long term expectations.

Figure 5.2: The accumulated rain on a "regular" day, 01-09-2015, (left), showing no shipping lanes or any other signs that could be related to anoprop. The accumulated "rain" corresponding to ship reflection (right), on 19-07-2014, showing 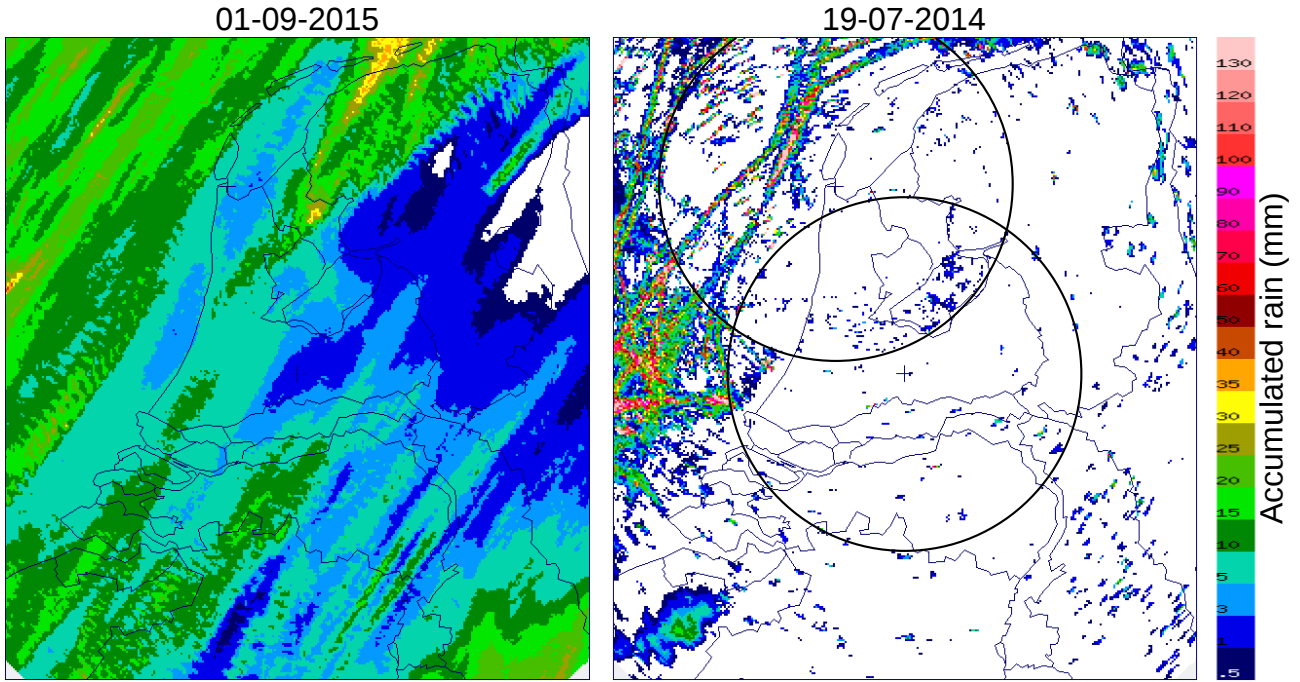clear shipping lanes parallel to the coast and other marine traffic entering the port of Rotterdam. Also two circles are placed to emphasise the maximum detection range of the radar stations, indicated with a +-sign. (Data made available by the KNMI via http://www.knmi.nl/nederland-nu/klimatologie/geografische-overzichten/radar.)

5.5 Determining AIS and radar detection thresholds

In section 4.5, the mathematical approach for determining a radar detection threshold is described. This approach is applicable for any regular radar system in which a signal peak is considered to be a detection. For coastal radar, AREPS is used to determine a threshold - based on the input radar parameters stated above -, expressed as propagation loss in decibel, in a similar fashion. Important to note is that this threshold is not directly equal to the minimum detectable signal, S_{min}, or the minimum signal-to-noise ratio, $\left(\frac{S}{N}\right)_{min}$, but states the maximum propagation loss that is acceptable to receive the minimum detectable signal.

For AIS, it is not up to the receiver to mark a signal as a detection, the message is either received or not, without further reporting on the received signal strength. (For convenience reasons the possibility of receiving half of a message is ignored.) As a result, another method has to be used to determine an AIS detection threshold.

The one-way radar equation, Eq. (2.8), expresses the maximum detection range as a function of (all) other radar parameters. The method used here to determine the AIS detection threshold is based on this. Knowing at which specific point the last message of a target is received together with the propagation loss at that point, gives an indication of the detection threshold which equals the propagation loss at that range. To strengthen this indication, a data analysis study is conducted. The study itself is based on determining a Figure of Merit (FoM). The FoM is used to approximate all the variables that do not involve propagation loss and all variables that

do involve propagation loss together, at the maximum detection range:

$$\text{FoM} \equiv \frac{R_{max}}{F(R_{max})} = \sqrt{\frac{P_t G_t G_r \lambda^2 L_s}{(4\pi)^2 k T_0 B F_n \left(\frac{S}{N}\right)_{min}}}. \tag{5.1}$$

in which $F(R_{max}))$ denotes the pattern propagation factor up to the maximum detection range (and all other variables are as specified in chapter 2). The threshold is now found by determining the FoM, which is by definition equal to the propagation loss at the maximum detection range. (Again this threshold is not equal to the minimum detectable signal, S_{min}, or the minimum signal-to-noise ratio, $\left(\frac{S}{N}\right)_{min}$, but states the maximum propagation loss that is acceptable to receive the minimum detectable signal.) Essential to note is that the FoM is considered to be constant for a specific system, theoretically making it possible to determine the FoM based on a sole data point.

The question that remains is how to obtain values from the FoM. To answer this question, AREPS plays an important role. AREPS can be used to obtain the propagation loss given specific atmospheric conditions and a specific receiver antenna height as well as the wavelength. The propagation loss does however not only depend on the distance, but also on the pattern propagation. To be able to take into account the pattern propagation, the exact signal directions are important. Knowing the distance the signal has traveled is not enough, the exact position (latitude and longitude) and height of the transmitting antenna are essential.

To obtain realistic positions, an actual AIS receiver dataset is used. The dataset is selected from the available datasets based on the fact that it is collected during relative homogeneous weather conditions and corresponding propagation effects during the entire day and over the complete studied area. Thereby allowing the latitude and longitude to be replaced by the distance from the transmitter to the receiver again, leaving it to be the only essential position parameter together with the height of the placement of the target's antenna. Summarising, this means that a pair containing the transmitter antenna height and the maximum detectable range of that target is enough to select FoM values from the propagation loss dataset produced by AREPS.

The mentioned dataset consisted of all - in this case around 16,000 - messages received during a complete day, 09-09-2014, by a single AIS station. The size of the dataset cannot be related directly to the number of ships from which the data is collected. Numerous messages were sent from the same ships at different points in time. After inspecting the database, over two hundred distinct ships were identified, some of which never left port that day. The remaining ships and their tracks are plotted in figure 5.3. Nineteen of those ships were selected based on the fact that they reached maximum detectable range of the AIS antenna during that day. Those ships were studied more thoroughly and the height of their AIS antenna position was obtained. As a result, a dataset of nineteen pairs, X, consisting of the antenna position height and the maximum detectable range, (h, R_{max}), was found.

Based on the AREPS dataset, a numerical curve was computed for every reasonable propagation loss value, which means that all points (h, R_{max}) in the dataset that correspond to a certain propagation loss value are determined. The set containing the pairs that correspond to a certain propagation loss PL are denoted by l_{PL}. Reasonable values for the propagation loss in this case range from 136 to 147 dB with a 0.5 dB step size.

In the next step, the dataset X was fitted to find the "closest" curve l_{PL} for a certain PL using a least square fit [54]. Since l_{PL} is not a continuous curve, the distance to the line and a point $x \in X$ is defined as the minimum Euclidean distance between x and the elements in l_{PL}, i.e.

$$d(x, l_{PL}) = \min_{y \in l_{PL}} \|x - y\| = \min_{y \in l_{PL}} \sqrt{(h^x - h^y)^2 + (R_{max}^x - R_{max}^y)^2}, \tag{5.2}$$

with $y = (h^y, R^y_{max})$ and $x = (h^x, R^x_{max})$. The least square fitting to find the FoM can then be written as the optimisation problem:

$$\text{Minimise: } \sum_{i=1}^{19} d(x_i, l_{PL}) \text{ for } PL \in \{\text{Possible FoM values}\}, \qquad (5.3)$$

with $x_i \in X$. The result of this optimisation is the FoM.

Figure 5.3: All vessel tracks received on 09-09-2014 by a single antenna, plotted with Google Earth. (Tracks over land typically correspond to a ship of which in-between data was absent.)

5.6   Assessing North Sea coverage (cases studies)

The final part of this thesis consists of an analysis of five "theoretical" cases, and two more realistic cases based on Numerical Weather Predictions (NWP) data from the HARMONIE model (subsection 4.2.1). For these cases, atmospheric conditions are specified and the maximum coverage for detecting the targets specified in subsection 5.2.2 is looked at (for both AIS and radar). The theoretical atmospheric conditions of these cases are selected for the most important propagation conditions described in chapter 3 (and determined in chapter 6) and are referred to as standard atmosphere, evaporation duct, standard surface duct, surface-based duct, and elevated duct. (The atmospheric conditions related to the NWP cases are described below.) In general, the important notions of these cases can be found in the same chapters. The specific M-profiles for all cases are stated in figure 5.4. Three of the profiles, viz., standard atmosphere, evaporation duct, and standard surface duct are AREPS sample profiles. The

other profiles, elevated duct and surface-based duct, are selected from the cases used in an earlier study by Derksen in 2015 [29].
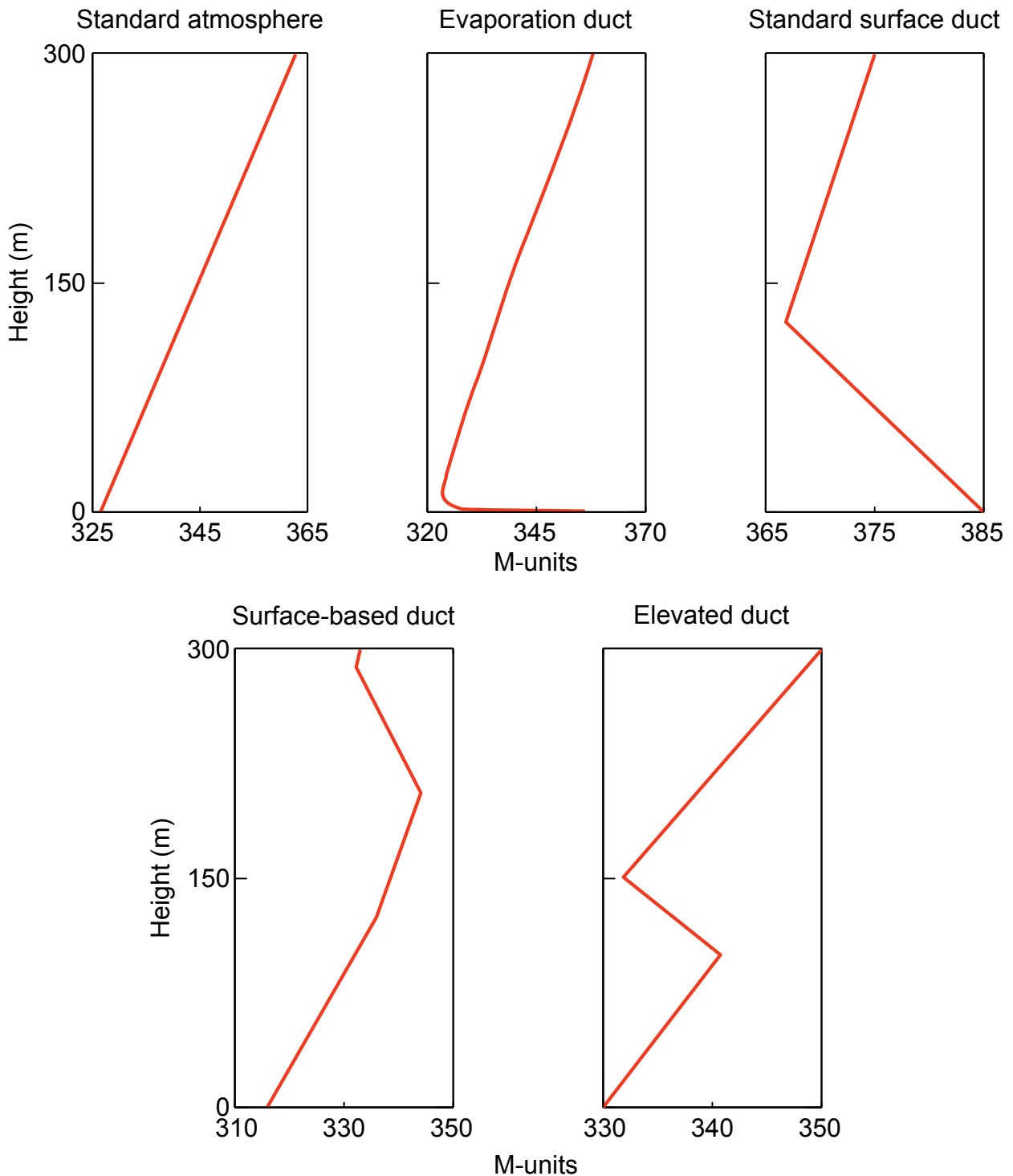
Figure 5.4: M-profiles of the studied theoretical cases.

For all five theoretical cases, one fundamental assumption is made, namely that the M-profiles are uniformly present and, hence, that the atmosphere is a uniformly stratified medium. This means that for every sensor and in every bearing direction the same M-profile is used for the calculations. This approach is beneficial when it comes to comparing the impact of specific propagation conditions (or ducts). Every case corresponds to a single propagation mechanism

(or duct) and no interference between those mechanisms occurs. However this theoretical model is illustrative, it is unrealistic in practice. Duct heights, thicknesses, and presence can differ over distance and, also, different ducting conditions can coexist at the same location at the same time. Although this makes the analysis of the impact of a specific duct more difficult, some notion on how diverse real-life atmospheric conditions are in relation to propagation is valuable. To that extent, two additional more realistic cases are studied. For this study, two atmospheric NWP datasets are used that represent two historical dates and times, namely 13-03-2014 (00:00) and 10-07-2013 (06:00). The dates are again selected out of multiple datasets that were studied earlier by Derksen [29] from a related perspective.

5.6.1   Used tools

AREPS

From every platform, propagation loss calculations are made at thirty-six bearings (or seventy-two bearings for the NWP cases) at equal angles from each other, i.e., 10 degrees (or 5 degrees for the NWP cases), starting straight to the North, so that the complete surroundings from the platform are covered. (In case of a uniformity condition for the M-profiles, a single bearing would suffice. However, to make the followed approach more generally applicable, this is ignored.) The single propagation loss calculations output consisted of the propagation loss for every grid point of a range versus height grid with twenty-one height layers varying from 0 to 100 m with stepsize 5 m and up to 1440 range layers varying from 0.5 to 720 km (0 is not included as beginning range step). All together, this will lead to a collection of fifteen propagation loss sets each containing thirty-six height versus range propagation loss matrices of size 21×1440.

The calculations itself are preformed by AREPS (version 4.1.0.138a). The atmospheric conditions for each theoretical case are imported as M-profiles into AREPS. For the more realistic cases, the NWP data is imported into AREPS after which the M-profile is obtained (by AREPS) for every single direction from every antenna location. Following, the calculations for every single platform are run separately, using the APM described in subsection 4.4.1. After finishing the calculations, the propagation loss information for every bearing of every platform is stored in separate binary format files.

Matlab (theoretical cases)

Binary format files outputted by AREPS are imported into Mathworks Matlab (version R2012a) where the propagation loss can be compared to the threshold earlier established. This way the maximum detection range can be determined. The way this is done differs for AIS and coastal radar. For AIS, the first distance from the antenna which has a higher propagation loss value than the threshold, so from where the target is out of reach of the antenna, is selected and the distance one step, 0.5 km, before that is set as the maximum detection range. For radar, starting away from the antenna, the first distance which has a lower propagation loss value than the threshold, so from where the target is within reach of the antenna, is selected and set as maximum detection range. Those different approaches are selected to ignore small multipath interference gaps for radar. (Radar suffers much more from multipath interference, as is described in section 3.1, than AIS. This can also be observed from figure 6.1 in chapter 6.)

In section 5.2, three target heights are determined. For those three heights, the approach stated in the previous paragraph is applied on every bearing of every single platform to obtain the maximum detection ranges. For all the maximum detection ranges corresponding to all

single bearing of a single platform, the corresponding location coordinates are determined. After that, all coordinates corresponding to bearings originating from the same platform are combined in order of increasing bearing angle, so that a list of thirty-six points denoting the locations of the angles of the coverage polygon arise. In other words, a list of thirty-six points is composed representing the outer border of the detectable area.

The detectable areas of all the antennae are then combined into one overview. This is done by deleting the overlap of the coverage of different antennae, so that only the outer border of the total collective coverage of all the antennae remains, which can be seen as the combined maximum coverage when it comes to detecting a target at a specific height. When the coverage of all platforms is combined, the maximum coverage can be visualized in combination with a North Sea map. This way, locations in which the coverage is inadequate, can directly be related to real earth locations. Beside land borders and shorelines, this map also contains the offshore border of the exclusive economical zone (EEZ) of the Netherlands as being the absolute outer borders of the Netherlands Coastguard responsibility area.[7] (The used Matlab code is included in appendix D.)

Matlab (NWP cases)

For the NWP cases, the approach described above is not sufficient. The atmospheric profiles for the NWP cases, could change rapidly in all directions and different propagation effects could coexist. To partially solve this, the bearing resolution used in AREPS was doubled to seventy-two bearings per platform. Within one bearing direction, the changes in M-profile and the corresponding changes in ducting effects could, more than during uniform conditions, lead to alternating regions with propagation loss above and below the threshold. Because of that, showing the coverage areas based on a single border will either ignore coverage gaps or ignore area in which there is detection.

The approach used for the NWP cases does not aim to computed only a outer border of the detection area. Instead, every entry of each propagation loss matrix, of course at the studied target height, is individually compared to the threshold. In case the threshold was not exceeded, the point is plotted on the North Sea map. This approach is repeated for each platform. Together, all points of the same colour show the total coverage area to detect a target at the corresponding target height. (It could be argued that at some points detection from multiple platforms is encountered and that, as a result, multiple points are displayed at a same/similar location. Since this will not influence the coverage area, this is ignored.) (The used Matlab code is included in appendix D.)

---

[7]To display detailed borders and shorelines as well as other geographical information, the Matlab Mapping toolbox together with GSHHS (Global Self-consistent, Hierarchical, High-resolution Shoreline) data provided by the US National Oceanic and Atmospheric Administration (NOAA) is used. Provided at: www.ngdc.noaa.gov/mgg/shorelines/gshhs.html, last accessed at 23 November 2015. For the EEZ, information provided by the Netherlands Ministry of Defence is used. Provided at: www.defensie.nl/english/topics/hydrography/contents/maritime-zones-and-boundaries/netherlands-boundaries-in-the-north-sea, last accessed at 23 November 2015.

Chapter 6

Propagation and weather assessment results

From an overall perspective, the main goal of this thesis is to provide the coastguard with additional insight into their situation awareness by looking at the performance of sensor systems. This chapter provides the results that are found throughout the first part of this process which focuses on radar wave propagation and weather conditions, from a general perspective.

In the first section, the relation between propagation mechanisms and AIS and navigation radar frequencies are described. Thereby, an overview of nearly every known propagation mechanisms in relation to the studied systems, is created. Although it is not intended to provide extensive details for every mechanism, it contains reasonable insight into the important factors concerning radar wave propagation. Also, it contains some additional notion on the relation between different ducting effects and frequencies by showing propagation losses multiple frequencies during standard atmospheric and anomalous propagation conditions. Together, this section shows the impact of different propagation mechanisms and, as a result, of their qualitative importance.

In the second section, the focus is shifted to the underlying weather conditions that can be related to different ducting types. The North Sea weather conditions are studied to find those that can be related to important ducts. Thereby it adds knowledge on the extent to which specific ducts are encountered in practice and, as a result, on their quantitative importance regarding their impact on AIS and radar.

6.1 Analysis on AIS and coastal radar signal propagation

In chapter 3, different standard and anomalous propagation mechanisms that could influence radar wave propagation paths were described. In practice, not all of those mechanisms are equally effective for all wavelengths. In this section, all propagation mechanisms are considered in relation to the AIS frequency and coastal radar operator frequency, which are approximated by 160 MHz and 9.4 GHz, respectively.

For anomalous propagation mechanisms known as ducting, frequency relations are hard to describe at two single wavelengths. Therefore, in the second subsection, the propagation losses as a result of different ducting conditions are shown for multiple wavelengths. The types of ducts studied and their accompanied M-profile are set equal to the "theoretical" cases introduced in the previous chapter and will be studied more thoroughly in relation to AIS and radar in the next chapter.

6.1.1 Standard propagation mechanisms

Spherical spreading

Under any kind of atmospheric conditions, spherical spreading of radar wave propagation will, at all frequencies, lead to a decay in signal strength; as the signal spreads, its power will decrease independent of its frequency. Spherical spreading therefore needs to be taken into account in any situation for VHF, X-band, or any other type of bandwidth.

Tropospheric refraction

Tropospheric refraction of radar waves is also influencing - to a certain extent - signals at every frequency. In standard atmosphere, the propagation path of a radar wave tends to bend towards the earth at many frequencies, including VHF and X-band. In other atmospheric conditions, refractivity can differ, causing the propagation path to follow a different trajectory. However, refractivity remains at least equally important and should be taken into account in that case. Also tropospheric refraction plays an important role when it comes to ducting described below.

Diffraction

The influence of *diffraction* on radar wave propagation around the earth's curvature depends reversely upon the operator frequency of the studied system; waves at lower frequencies are stronger diffracted compared to waves at higher frequencies. Fundamental reason for this is that diffraction depends on the wavelength compared to the size of the object, in this case the earth. According to Skolnik [4], radar wavelengths, for instance for radar, are too small compared to the size of the earth, leading to little signal diffraction. For AIS, diffraction around the curvature of the earth can lead to extended detection range, according to studies on AIS by Green et al [8] and the ITU [9].

Reflection

Reflection of radar waves can influence propagation in multiple ways. Background reflection, *clutter*, can cause noise which can complicate target detection, when radar applications are considered [2]. As AIS is a one-way system, no clutter is involved there. Furthermore surface layer or refractive layer reflection can result in *multipath interference*. If the frequency increases, the wavelength decreases, according to the relation $f = c/\lambda$. As a result, interference occurs more often for higher frequencies compared to lower frequencies. Looking at AIS and radar this translates to more frequent interference for radar, yet multipath interference can not be ignored for AIS.

Attenuation

Attenuation can be caused either by atmospheric gases, including water vapour, or precipitation, manly rain. Propagation loss due to attenuation by atmospheric gases is very limited for frequencies below 20 GHz and can therefore be excluded both for VHF and X-band frequencies [5]. When it comes to attenuation caused by rain, losses are still limited for VHF frequencies. For X-band - around 10 GHz - rain can cause some attenuation, up to a propagation loss of 0.1 dB/km during a rainfall of 10 mm/h and up to 1.0 dB/km and above during heavy rainfall of 50 mm/h and above [7]. As a result, attenuation can be ignored for AIS applications and only needs to be considered for radar during special circumstances.

Scattering

Scattering, both tropospheric scattering and scattering due to hydrometeors, is considered not to influence AIS signals according to Green et al [8]. In the same study, scattering caused by more rare effects such as ionospheric layers, meteor trails and lightning are concluded to be unlikely to influence AIS signals. For radar applications scattering, especially tropospheric scattering, can be considered to significantly influence propagation, in particular when it comes to over line-of-sight propagation [25].

6.1.2 Anomalous propagation mechanisms

Beside standard propagation, anomalous propagation conditions can influence AIS and radar signals severely. As described in section 3.2, sub- or superrefraction can extend or shorten detection ranges, but, more importantly, trapping layers can arise which create ducts. Although it has been known for a long time that ducting can cause anomalous propagation at multiple wavelengths, not all frequencies are influenced by every type of duct equally. To get an idea of the impact of the four ducting types studied in this thesis, e.g., evaporation ducts, standard surface ducts, surface-based ducts, and elevated ducts, in relation to the wavelength, the propagation loss is plotted in figure 6.1. As a reference, standard atmospheric propagation loss is added. The results given different propagation conditions are discussed in the subsections below.

Standard atmosphere

During standard atmospheric conditions, the propagation loss front (over a flat earth) more or less looks like some power of x with x being the range. However, as the wavelength increases, so does the propagation loss, causing high wavelength signals to lose their power more quickly. Also, as the wavelength increases, "lobing" patterns can be seen at close ranges. This pattern which shows an alternating rise and decline of propagation loss is the result of multipath interference and is, as described in the previous section, stronger at higher wavelengths. (Upper row of figure 6.1; lobing can be seen at frequencies of 1500 MHz and above.)

Evaporation duct

The evaporation duct shows practically no impact at 150 MHz signals. At 1500 MHz, although propagation loss overall decreases a little compared to standard atmosphere, the pattern remains the same. The same can be said about the propagation loss pattern at 3000 MHz; no pattern changes can be seen there either. At 10,000 MHz, the characteristic propagation loss pattern of an evaporation duct arises showing a strong detection peak at low altitudes whilst at high altitudes and close ranges the propagation loss pattern is close to standard. It also shows the potential "danger" of an evaporation duct; just above the detection peak and just below the area where propagation is close to standard, detection can be limited. (Second row of figure 6.1; the typical propagation loss pattern as a result of an evaporation duct can be seen at 10,000 MHz.)

Standard surface duct

The presence of a standard surface duct can be seen in the propagation loss at every wavelength. At 150 MHz, some power-of-x like pattern still exists, but it stretches out much further than during standard atmospheric conditions. At higher wavelengths, starting at 1500 MHz, a

multipath interference pattern develops. Direct waves, surface reflected waves, and waves which are bend downwards by the trapping layer cross each others paths and thereby increase as well as decrease signal strength. (Third row of figure 6.1; multipath interference pattern can be seen at frequencies of 1500 MHz and above.)

Surface-based duct

The surface-based duct propagation loss pattern is in many ways comparable to the standard surface duct pattern. At 1500 MHz and above, the pattern is dominated by multipath interference. Yet at close ranges the propagation is similar to standard atmosphere at all wavelengths as no interference takes place in this region. In general, there is less interference within surface-based ducts then there is within standard surface ducts, because within in surface-base ducts signals reflected by the trapping layer will bend back upwards more often before hitting and being reflected by the surface. (Fourth row of figure 6.1; multipath interference pattern can be seen at frequencies of 1500 MHz and above.)

Elevated duct

The elevated duct propagation pattern is comparable to that of a surface based duct. At close range, the propagation pattern is similar to standard atmosphere and after that reflected waves takes over. In general, the importance of multipath interference decreases as the height of the elevated duct increases. For this relatively low elevated duct with a trapping layer at 150 m, some multipath interference is shown at 1500 MHz and above. However, the characteristic pattern of an elevated duct also appears at those wavelengths. Signals are bend down by the trapping layer and bend upwards again somewhere below alternatingly, to give rise to a sine-wave pattern. (Bottom row of figure 6.1; beginning of the sine-wave can be seen at frequencies of 1500 MHz and above, being the strongest at 10,000 MHz.)
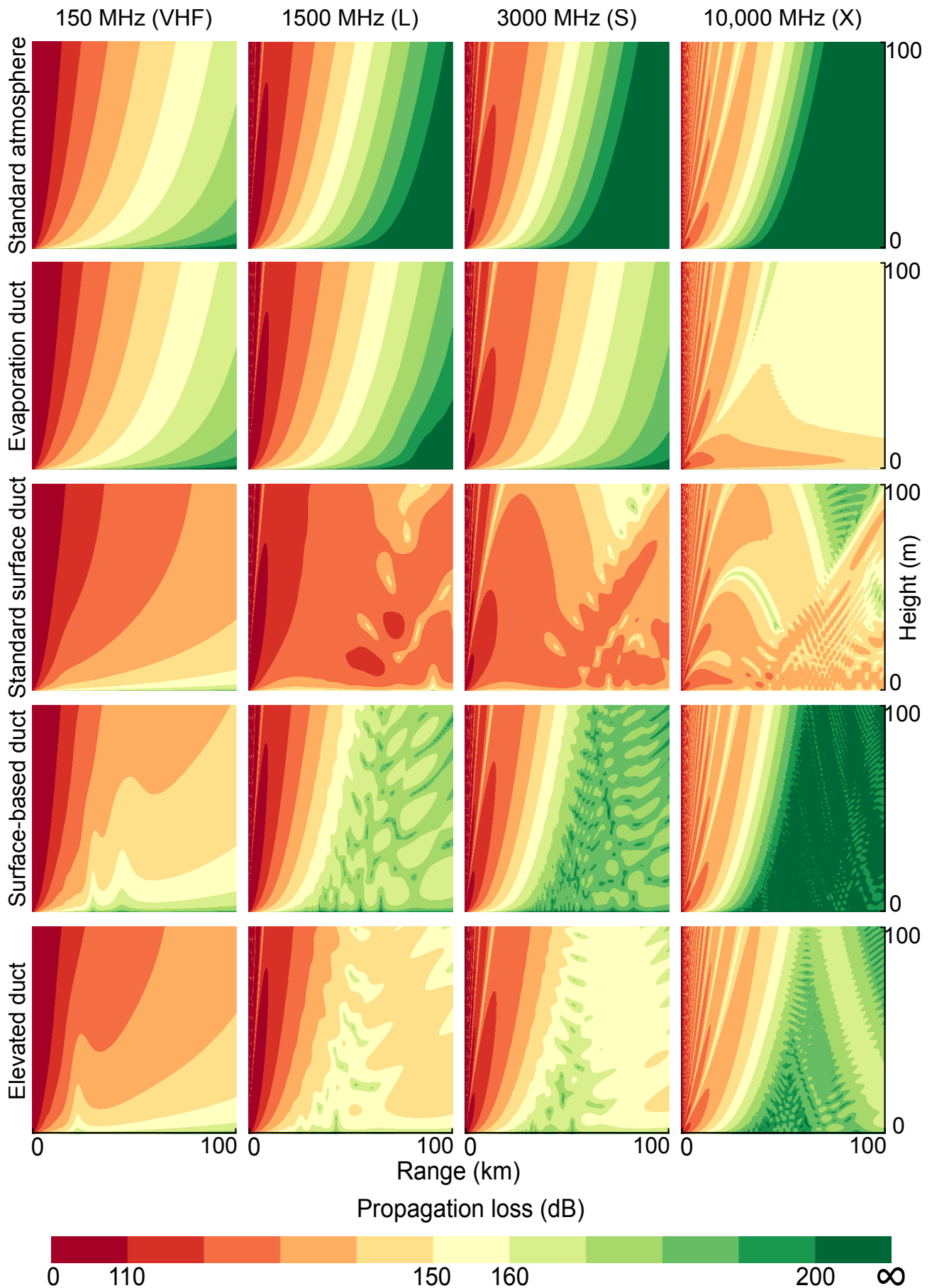
Figure 6.1: Overview of the propagation loss of four different wavelengths under five atmospheric conditions, showing the impact of different anomalous propagation conditions as the wavelength rises. (Antenna height: 25 m above MSL)

6.2 North Sea climate assessment

The impact atmospheric ducts have on radar propagation does not only depend on the extent to which the ducts are able to alternate detection ranges. It is also important to know how often these ducts occur, or, in other words, to know their quantitative impact. Therefore, the North Sea climate is assessed based on the presence of all ducting types. The different ducting types are split into two categories: the evaporation duct and the surface and elevated ducts (or anomaly propagation). The results are shown in figure 6.2.

The black line shows the six year average occurrence of range extending anomaly propagation - in this case: all ducting effects except for the evaporation ducts - is shown for every month. The gray line in the same figure shows the average height (with a basis of four metres) of the near coast evaporation ducts for every month.

During winter - December, January and February - the almost absence of elevated type ducts is very clear. During these three months less than two days with elevated type ducts occur each year. During autumn - September, October and November - those effects are not seen often either. The occurrence of the elevated ducts is less than one out of ten days for October, and November and for September the occurrence is less than one out of six days. How different is this during Spring and Summer - March until August -, then elevated ducts are seen on between one third up to almost half of the days each month. Whilst looking at AIS or radar propagation elevated ducts must therefore be taken into account in general, but especially during spring and summer.

For the evaporation duct height a more gradual curve is present. There is peak around June, and July and the lowest values can again be found during winter, but seasonal differences are not as sharp as for the elevated type ducts. Also the heights that are shown are somewhere between four and fourteen metres, meaning that for radar always some detection range extension at low altitudes will be present around these heights. However, it needs to be noted that this is a single location average. The evaporation duct height has a dynamic presence and is in general higher close to shore than out at sea just as that it is higher during the day than during the night.
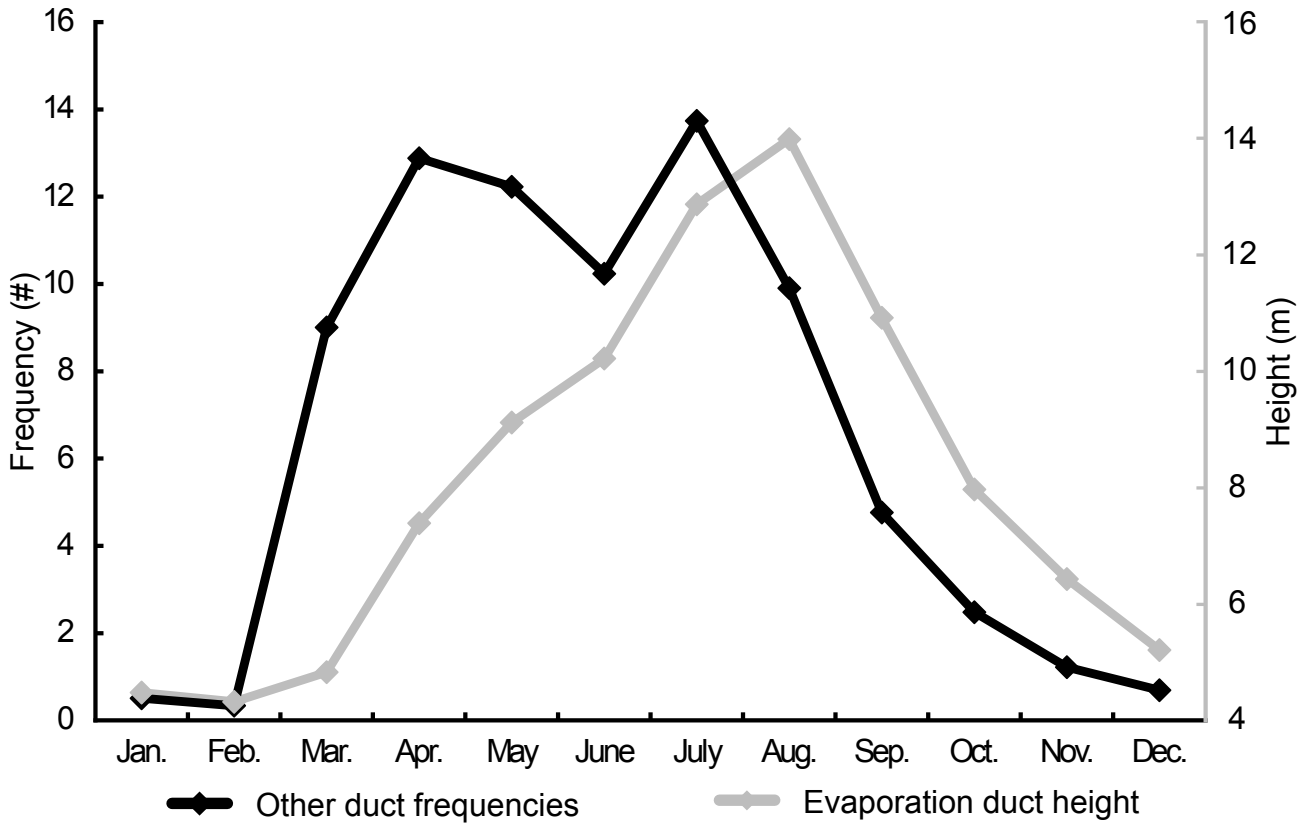
Figure 6.2: Graph showing the average evaporation duct height and the average other duct frequencies throughout the year.

6.3   Subconclusion and discussion

In this chapter, radar wave propagation was investigated for five main atmospheric conditions, namely standard atmosphere, evaporation ducts, standard surface ducts, surface-based ducts, and elevated ducts. For standard atmosphere, it was found that some propagation mechanisms do affect coastal radar signals, whilst they do not have an impact on AIS signals. More interestingly, it was shown that evaporation ducts do influence X-band signals corresponding to radar, whilst VHF propagation related to AIS is unaffected. This result corresponds to a study by Hitney and Vieth in 1990 [55], showing no influence of evaporation ducts on radar frequencies below 2 GHz. (A minor exception to this was seen at 1500 MHz, however this was not significant.) Other ducting effects, elevated and surface ducts, were found to influence both frequencies, which, on its account, corresponded to the information found in [56] and [57]. Together, this can be combined in table 6.1 showing the impact of all propagation mechanisms in AIS and radar.

Evaporation ducts are present to some height always. Although their absolute height shown in figure 6.1 might be misleading - it is based on a single location - the pattern throughout the year is found often. At locations closer to the coast, the measured evaporation duct heights are, on average, greater than further out at sea, but the year-through pattern remains. Looking at the average height throughout the year, throughout the North Sea, evaporation duct heights are close to what is earlier described as a small target. Therefore, evaporation ducts are significantly interesting to analyse in relation to coverage.

Elevated and surface ducts were found to be present up to 10 to 14 times per month during

Table 6.1: Overview of all propagation mechanisms and their relation to AIS and coastal radar. Green denotes all mechanisms that are considered to influence propagation significantly, orange denotes all mechanisms that influence propagation only in exceptional cases and red denotes all mechanisms that are considered not to influence propagation.

	AIS	NavRad
Standard propagation		
Spherical spreading	green	green
Tropospheric refraction	green	green
Diffraction	green	green
Reflection		
Clutter	red	green
Multipath	orange	green
Attenuation		
Atmospheric gases	red	red
Precipitation	red	orange
Scattering		
Hydrometeors	red	orange
Tropospheric	red	green
Anomalous propagation		
Sub/superrefraction	green	green
Ducting		
Evaporation duct	red	green
Surface duct	green	green
Elevated duct	green	green

spring and summer, and almost not at all during autumn and winter. This pattern is in general supported by a 2004 study by Von Engeln and Teixeira [58] on ducting effects all around the world, showing almost no presence of ducts on the North Sea during autumn, and winter and clearly more during summer. Although the results presented here were based on the available data of six years, the results clearly show the importance of these ducts on the North Sea. It also sets the tone for further and longer analysis of this data which (to our knowledge) was never before used to determine the presence of North Sea ducts.

Chapter 7

Case studies results

In the previous chapter, radar wave propagation was studied in general. It contained an analysis of propagation during different atmospheric conditions and showed its importance, yet it did not relate to actual detection. In this chapter, the perspective is shifted from propagation loss to target detection using static antenna platforms throughout the North Sea. To relate propagation loss to target detection, a detection threshold has to be determined. Based on the methods described in section 5.5, the detection thresholds for AIS and coastal radar are determined in the first section of the chapter.

In the resulting part of the chapter, cases that are described before (section 5.6) will be studied. As a start, five theoretical cases, representing standard atmosphere, evaporation ducts, standard surface ducts, surface-based ducts, and elevated ducts, will be discussed and, continuously, two, more realistic cases based on Numerical Weather Predictions (NWP) are studied that correspond to an evaporation duct and an elevated duct in practice, respectively.

7.1   Detection threshold

For a generic coastal radar studied here, the break-even point between detection and no-detection is found at a propagation loss of 143.55 dB. The accepted probability of false alarm was set at 10^{-4} and the probability of detection within this threshold is 95%. This means that, in theory, at every point in space where the propagation loss from the transmitter is lower than this threshold, a target having a radar cross section value as described in section 5.2 will return a signal with enough strength to be detected in 95% of the cases.

For AIS, a threshold is found at a propagation loss of 142 dB based on the calculations described in section 5.5 applied to the data in appendix C combined with the propagation loss data resulting from AREPS calculations, which is also visualised in figure 7.1. Since AIS is a one-way system, every point in space where the propagation loss is lower than this threshold can be interpreted as the point over where sent messages will be received by the receiver at the origin of the propagation loss calculation. This means that, in this case, the probability of detection is aimed to be set at 100%; no margin is incorporated. However, it is notable that the standard deviation of the propagation loss values found for the ships is 2.5 dB, which, under the given conditions, approximately corresponds to a distance of 3 km (for a target at a target height of 10 m).
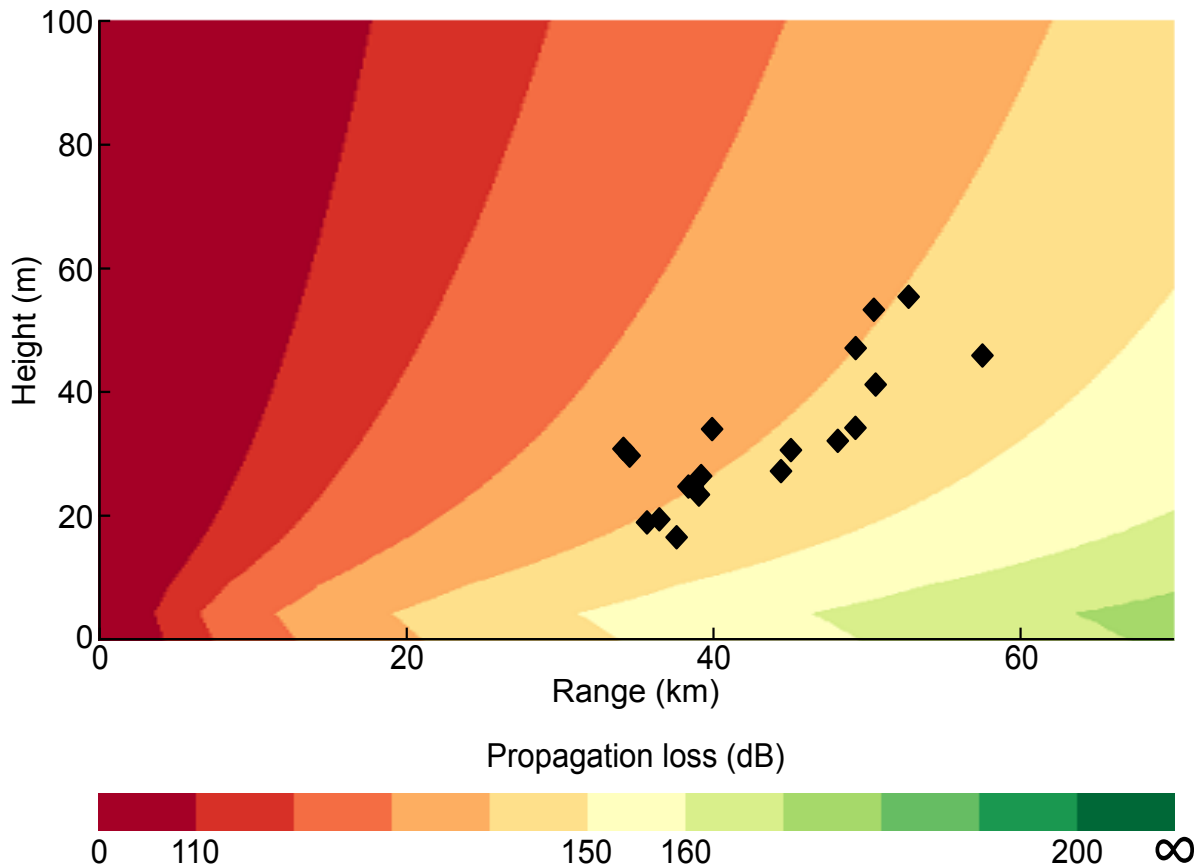
Figure 7.1: Propagation loss plot (AREPS) in combination with the maximum detection range and heights pairs measured for real ships on by an AIS antenna located at the main naval base of the Netherlands at Den Helder.

7.2 Theoretical cases (uniform atmosphere)

Five cases, that are representative for a standard atmosphere, an elevation duct, a surface-based duct, a surface duct, and an evaporation duct are analysed here for both AIS and radar. Standard atmosphere is used as a comparison for the other cases that are of main interest. For each case, the propagation loss in a single direction is displayed in a height versus range plot (assuming the sensor to be at a height of 25 m above mean sea level) to show the influence of the ducting effect on the propagation at both AIS and radar wavelength. Below, the covered area for different targets at different heights is shown as an overlay on a map of the North Sea and its surrounding landmass.[1] Within the North Sea area the outer border of the exclusive economical zone of the Netherlands is shown as a black line. The area between the coastline and this line is assumed to be the area in which coverage is preferred and can therefore be also used as a comparison in case real antenna locations are evaluated. (Magnified representations of the maps are included in appendix E.) Also, a table is added to each case study, stating the maximum detection ranges and the coverage area of a single antenna. The coverage area is always compared to the coverage area of standard atmosphere under the same conditions, regarding target height, antenna height, and system (except for standard atmosphere itself). An overall detection range table can be found in appendix G.

---

[1]The IJsselmeer and Markermeer are shown as sea area on the map, however, they are not considered to be of interest here. On the other hand, the Wadden Sea is taken into account.

For all cases, it needs to be noted that an equal refractivity profile is assumed for every platform in every direction, or, in other words, that the atmosphere is assumed to be homogeneous. In real life, the profile can change severely over the North Sea area and different types of ducts can occur at the same time.

For every case, AIS and radar are shown together in order to compare the performance of both systems. A major advantage of this approach is that it is immediately clear which system outperforms the other in each situation. To that extent, it is important to bear in mind that AIS is expected to be unaffected by the evaporation duct whilst this is not to be expected of radar. For all other cases, both AIS and radar are expected to be influenced. Also, important to note again is that the coverage of radar is based on a specific target having an accompanied RCS. For other targets, the results considering radar and thereby its comparison to AIS can differ severely. (However, in the previous chapter, parameters were chosen to be related to a representative target.) Finally, it needs to be remarked that the heights for which coverage is shown should be interpreted differently for AIS and radar. For AIS, the transmitting antenna needs to be at (or around) the indicated height, independent of the ship's proportions. For radar, the indicated heights are the heights at which the representative RCS value is placed at. In practice, reflection will come from the surface of the complete ship, so reflection will occur at multiple heights.

In addition, it needs to be emphasized again that the results shown here are not representative for the real North Sea situation when it comes to the systems positions and as a result: coverage. To indicate this all images showing a North Sea map are marked with the statement "Simulated position" and may in no case be displayed to any without this statement. Results obtained by using real positions will be made available as a classified annex to the commissioners of this research.

7.2.1 Standard atmosphere

In standard atmosphere, the M-profile shows a relatively stable decrease with height. As a result, the propagation losses shown in upper part of figure 7.2 are also relatively stable for both AIS and radar. In the near earth area, the propagation loss increases sharply with range. As height increases, propagation loss gradually increases less sharply yet still considerably with range. For radar, also lobing effects (which are ignored when it comes to the detection range) are present as a result of multipath interference.

Considering coverage, a similar increase with height can be seen. The area of detection increases gradually as the height increases. For antennae at an average height, the increase in detection range is presented in table 7.1.

When comparing AIS and radar it is clear that the detection area of AIS is larger than the detection area of radar, especially as the target height increases. For a single platform, the area covered by an AIS antenna can be compared to the covered area of a radar antenna by looking at table 7.1.

Table 7.1: Standard atmosphere single antenna performance for an average height antenna at sea and an average height antenna above land including its detection range and coverage for multiple target heights.

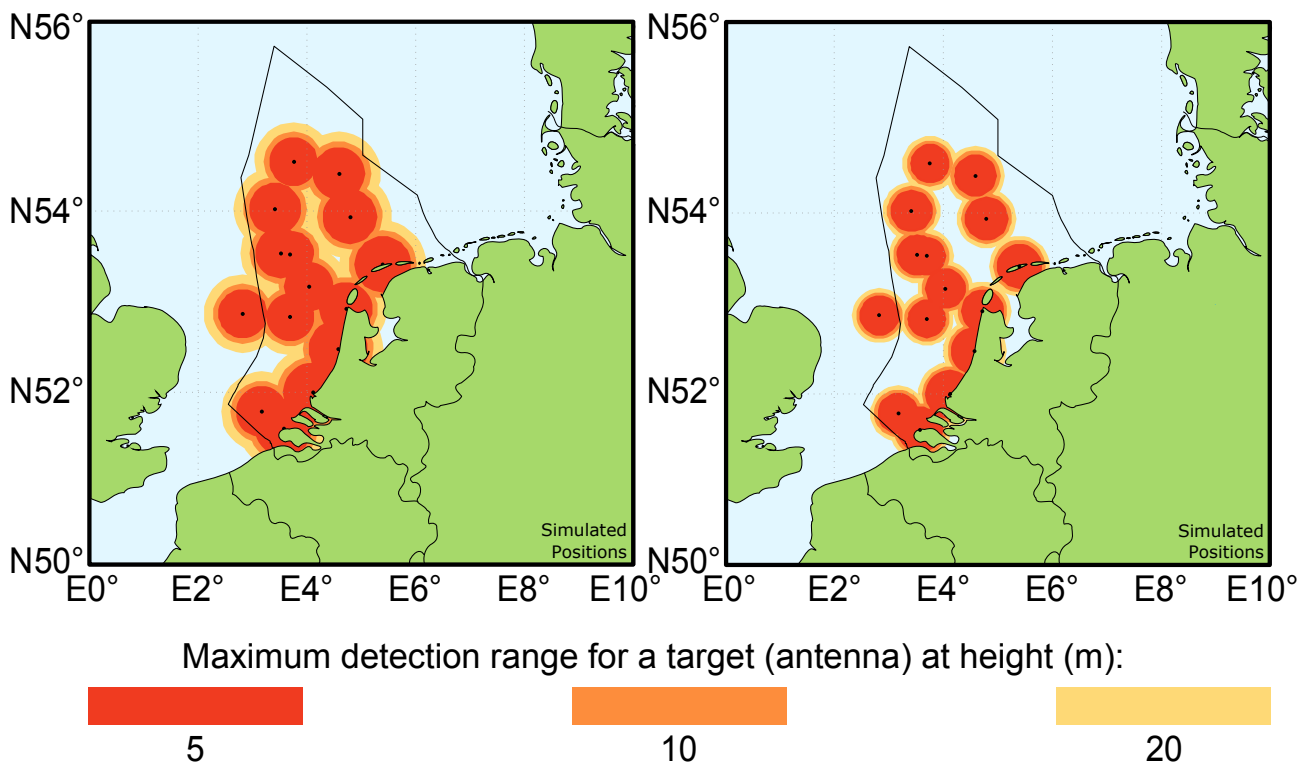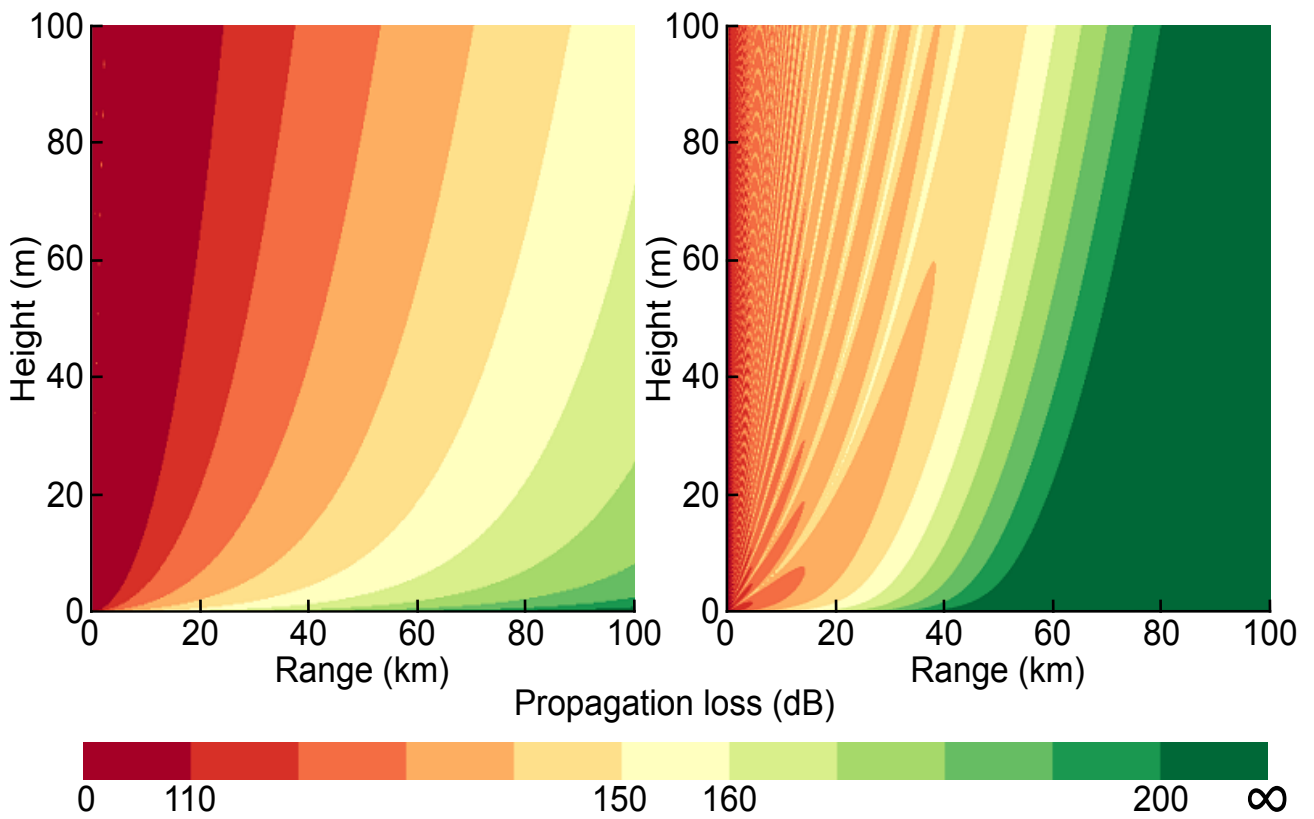|	Automatic Identification System					
	Av. height at sea 39.8 m (MSL)			Av. height above land 50 m (MSL)		
	Range		Coverage area	Range		Coverage area
Target height	(km)	(NM)	(km^2)	(km)	(NM)	(km^2)
5 m	31.5	17.0	3117	34.5	18.6	3739
10 m	37	20.0	4301	40.5	21.9	5153
20 m	49.5	26.7	7698	53.5	28.9	8992
	Coastal radar					
5 m	23.5	12.7	1735	26	14.0	2124
10 m	27	14.6	2290	31	16.7	3019
20 m	32.5	17.5	3318	36.5	19.7	4185

Figure 7.2: Coverage and propagation loss in standard atmosphere for both AIS and coastal radar.

7.2.2 Evaporation duct

Evaporation ducts can cause extended detection ranges in near earth surface air layers. In general, higher air layers remain untouched. This is clearly shown within the M-profile of the evaporation duct case studied here. From the surface upwards until the evaporation duct height a gradually slowing decline in M-units with height is shown. Above the evaporation duct height a "standard" M-profile - as found in standard atmosphere - follows. Looking at the propagation loss of radar, upper right of figure 7.3, a similar effect can be seen. Around the evaporation duct height, a strong peak can been seen in which propagation loss over range is limited (and as a result, detection range increased) compared to standard atmosphere. As height increases, the propagation loss pattern more and more compares to the propagation loss pattern that was shown for standard atmosphere (upper right of figure 7.2). Although the evaporation duct height is a specific height, the propagation loss pattern changes gradually, leading to a combination of "evaporation duct propagation" and "standard propagation" at some heights around the evaporation duct heights.

For AIS, no sign of the presence of an evaporation duct can been seen in the propagation loss (upper left of figure 7.3). The propagation loss pattern is the same as for standard atmosphere, which corresponds to the results of the previous chapter, stating that frequencies below 2 GHz remain uninfluenced by evaporation ducts. Therefore, the limited propagation loss that is found for radar is not found for AIS.

When it is assumed that evaporation ducts are the only ducting effects present in an atmosphere that is, besides that duct, "standard", no difference is experienced in AIS coverage. At all heights, both considered here as well as shown in the propagation loss plot in the upper left of figure 7.3, the coverage is constant. For radar, the major difference is found at heights around the evaporation duct height - in this case 5 m. The presence of the given evaporation duct leads to a significant coverage increase at a height of 5 m which sometimes even exceeds the coverage at 10 m, whereas in standard atmosphere the coverage increases with height. Especially, for lower placed antennae, the coverage can even exceed the coverage found at a detection height of 20 m. This is clearly shown in the lower right of figure 7.3 in which the red coloured layer corresponding to 5 m is placed below the other layers. When the layer is shown - as for instance is the case at the most Northern platform - the coverage at five meters exceeds the coverage at 20 m. In table 7.2, the coverage of the studied evaporation duct situation is compared to standard atmosphere studied earlier, especially showing the increase in covered area for a target at 5 m.

Table 7.2: Evaporation duct single antenna performance for an average height antenna at
sea and an average height antenna above land including its detection range and coverage area
compared to standard atmospheric coverage area under the same conditions for multiple targets.

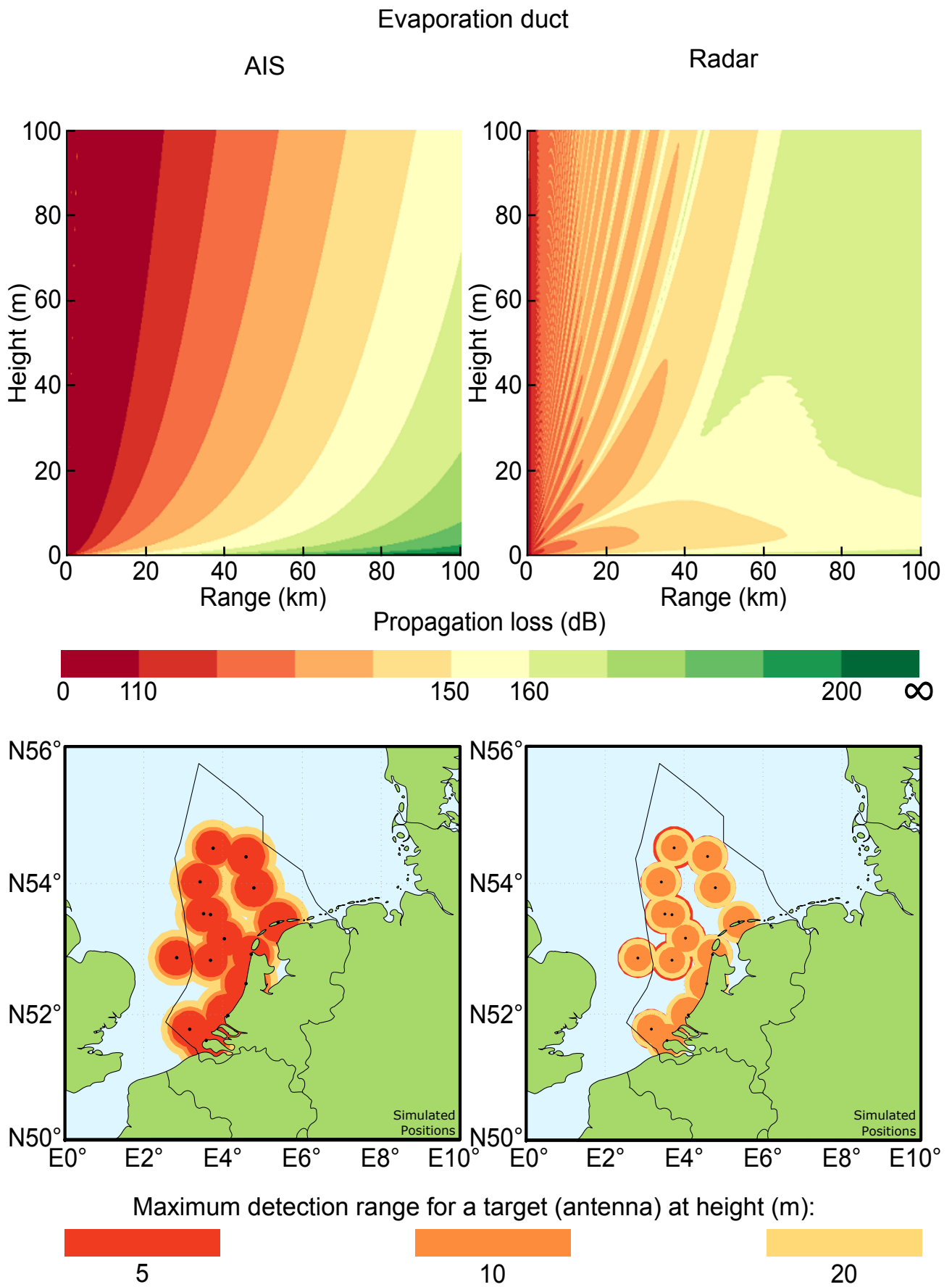|	Automatic Identification System					
	Av. height at sea 39.8 m (MSL)			Av. height above land 50 m (MSL)		
	Range		Coverage area	Range		Coverage area
Target height	(km)	(NM)	(%)	(km)	(NM)	(%)
5 m	31.5	17.0	100	34.5	18.6	100
10 m	37.5	20.2	103	40.5	21.9	100
20 m	50	27	102	53.5	28.9	100
	Radar					
5 m	33	17.8	197	34	18.4	171
10 m	22	11.9	66	25	13.5	65
20 m	33.5	18.1	106	36.5	19.7	100

Figure 7.3: Coverage and propagation loss during an evaporation duct for both AIS and coastal radar.

7.2.3   Standard surface duct

During a standard surface duct, coverage can be extended in air layers directly attached to the surface. In general, this will include the targets at height of 5, 10 or 20 m studied here. For AIS, the resulting coverage region is enhanced gradually with height, meaning that there is no specific height at which detection ranges stick out, yet at all heights coverage will be extended. For radar, a different outcome arises. Although the coverage plot on the bottom right side of figure 7.4 shows an increase at every height, it is not at all gradual with height. At 20 m, coverage is broader than at 5 or 10 m in general, but differences arise from different antennae. Also, at some points coverage at a height of 5 m exceeds coverage at 10 m. Since atmospheric conditions are the same for every antenna location, this indicates that antenna height is of major influence. Looking at the upper right plot of figure 7.4, this conjecture is strengthened by the fact that the complete studied area is filled with multipath interference; the direct path(s), surface reflected path(s), and the path(s) reflected by the trapping layer cross multiple times leading to a scattered propagation loss pattern in which propagation loss can differ over 30 dB within 5 km both positive and negative. Specific conclusion would therefore depend strongly on the accuracy of the target and antenna height. However, the fact that the coverage is extended at every height, together with the fact that radar receives reflection of the target at different heights, could be used to indicated the importance of standard surface ducting effects.

For AIS, coverage can be compared to standard atmosphere per height, which is done in table 7.3. For radar, this could be misleading given the enormous differences in propagation loss with relatively small differences in height. Therefore, the average increase over 1 to 5, 1 to 10, and 1 to 20 m compared to standard atmosphere is shown in table 7.3 to indicated the strength of this standard surface duct, in general.

Table 7.3: Standard surface duct single antenna performance for an average height antenna at sea and an average height antenna above land including its detection range and coverage area compared to standard atmospheric coverage area under the same conditions for multiple targets.

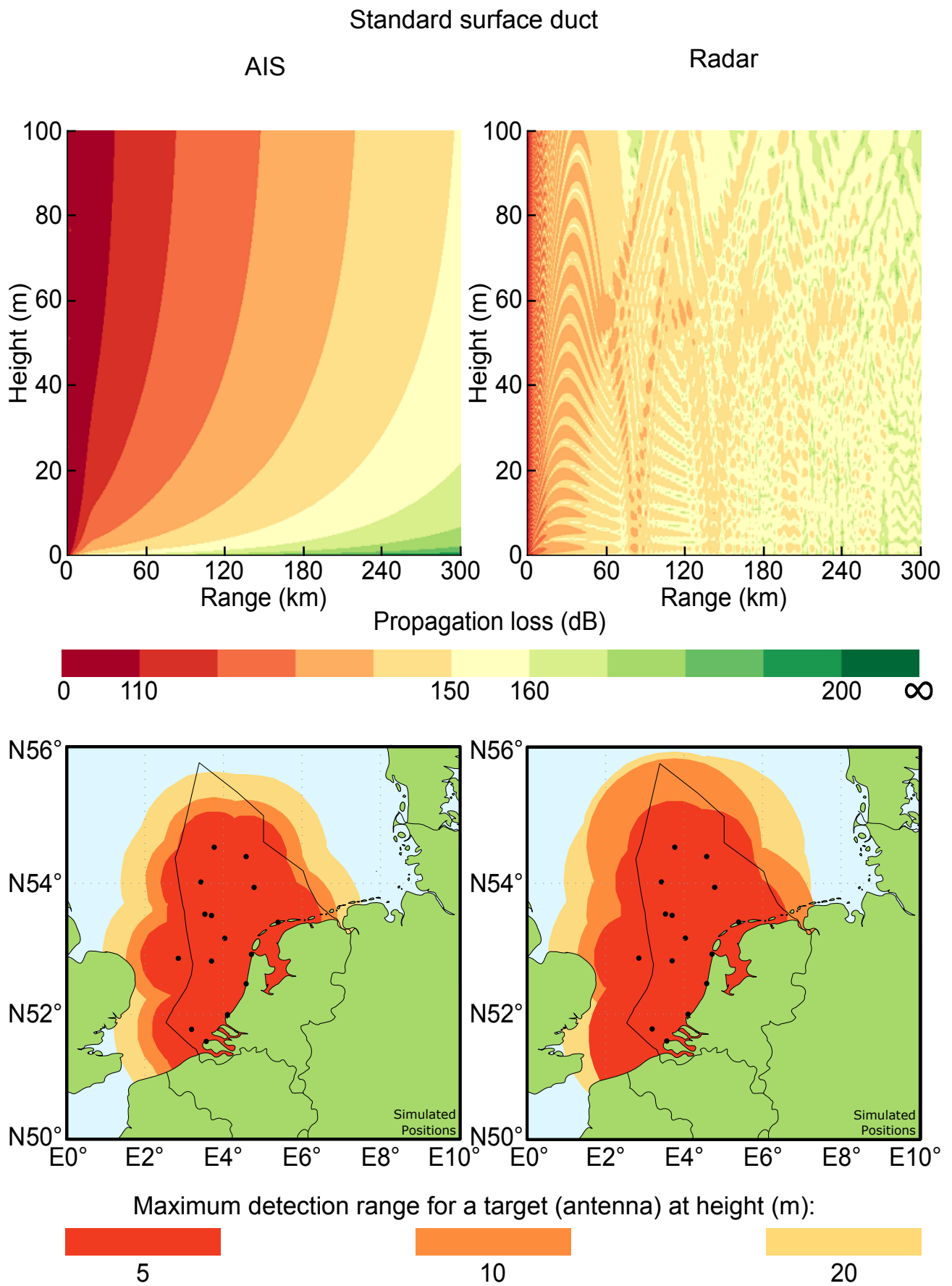|	Automatic Identification System					
	Av. height at sea 39.8 m (MSL)			Av. height above land 50 m (MSL)		
	Range		Coverage area	Range		Coverage area
Target height	(km)	(NM)	(%)	(km)	(NM)	(%)
5 m	69.5	37.5	487	77.5	41.8	505
10 m	91	49.1	605	101	54.5	622
20 m	136.5	73.7	760	147	79.4	755
	Radar					
5 m	101.5	54.8	1865	73.5	39.7	799
10 m	111.65	60.3	1710	93.35	50.4	907
20 m	124.95	67.5	1478	104.53	56.4	820

Figure 7.4: Coverage and propagation loss during a standard surface duct for both AIS and coastal radar.

7.2.4   Surface-based duct

Surface-based duct differ from standard surface ducts when it comes to the bottom of the ducting layer. For standard surface ducts, the bottom of the duct is formed by a refractive layer, which, besides direct waves, also refracts waves that are already reflected by the upper trapping layer. For a surface-based duct, this is not always the case. Radar waves reflected by the trapping layer are bent back upwards, partially or completely, before hitting the surface. As a result, less multipath interference is found for radar. What remains is a sine-wave propagation pattern which can also be observed in the propagation loss plots of both AIS and radar in the upper part of figure 7.5.

For radar, the effects are mostly limited to propagation losses that exceed detectable values, as is shown in the upper right of figure 7.5. For that reason, coverage is comparable to standard atmosphere (lower right of figure 7.5). For AIS, the relation between target and antenna height is important. For the somewhat lower antennae found on the North Sea, a decrease in coverage at a target height of 10 m is encountered, whilst for the coastal antennae, which are generally placed higher, the coverage for a target at height 20 m is strongly increased (lower left of figure 7.5). Given the propagation loss of the surface-based duct, this could indicate that some targets and antennae are placed in such a way that they benefit more from the propagation pattern within the duct than others. Also the increase in propagation could be much stronger for target antenna at heights above 20 m, which are not considered here.

Table 7.4: Surface-based duct single antenna performance for an average height antenna at sea and an average height antenna above land including its detection range and coverage area compared to standard atmospheric coverage area under the same conditions for multiple targets.

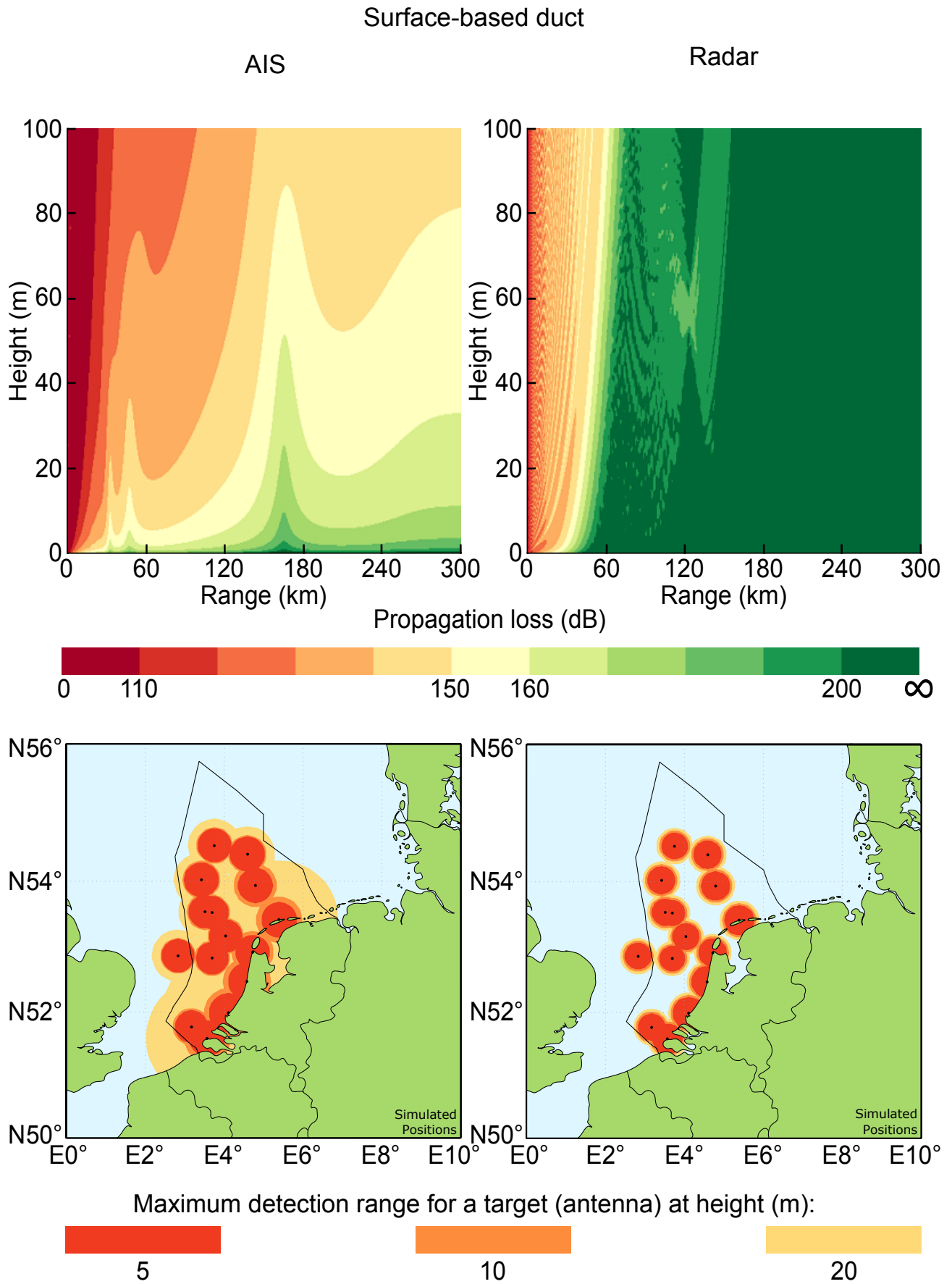|	Automatic Identification System					
	Av. height at sea 39.8 m (MSL)			Av. height above land 50 m (MSL)		
	Range		Coverage area	Range		Coverage area
Target height	(km)	(NM)	(%)	(km)	(NM)	(%)
5 m	28	15.1	79	30	16.2	76
10 m	30.5	16.5	68	38	20.5	88
20 m	45.5	24.6	84	104	56.2	378
	Radar					
5 m	21.5	11.6	84	24	13.0	85
10 m	26	14.0	93	28	15.1	82
20 m	30.5	16.5	88	33	17.8	82

Figure 7.5: Coverage and propagation loss during a surface-based duct for both AIS and coastal radar.

7.2.5 Elevated duct

As for surface-based ducts, elevated ducts are characterised by their sine-wave propagation pattern within the duct, yet for elevated ducts, the bottom of the duct is not attached to the surface. In the upper right of figure 7.6, the propagation pattern for radar clearly shows this. It also shows significant multipath interference either from refractive layers or from the surface which is relatively close, in this case. (As a result of the low altitude of the elevated duct.) Although radar waves are not intended to hit the ground, for AIS, the propagation loss is already affected starting at only a couple metres above the surface (upper left of figure 7.6).

Considering coverage, similar effects are seen in the bottom two maps of figure 7.6. For radar, range extension would have been very reasonable at practically every height above 20 m, but up to that height the decrease in propagation loss will not result in the target signal being above the detection threshold. As a result, coverage is similar to standard atmosphere, as is shown in table 7.5. How different that is for AIS, at all three studied heights coverage is extended severely.

Table 7.5: Elevated duct single antenna performance for an average height antenna at sea and an average height antenna above land including its detection range and coverage area compared to standard atmospheric coverage area under the same conditions for multiple targets.

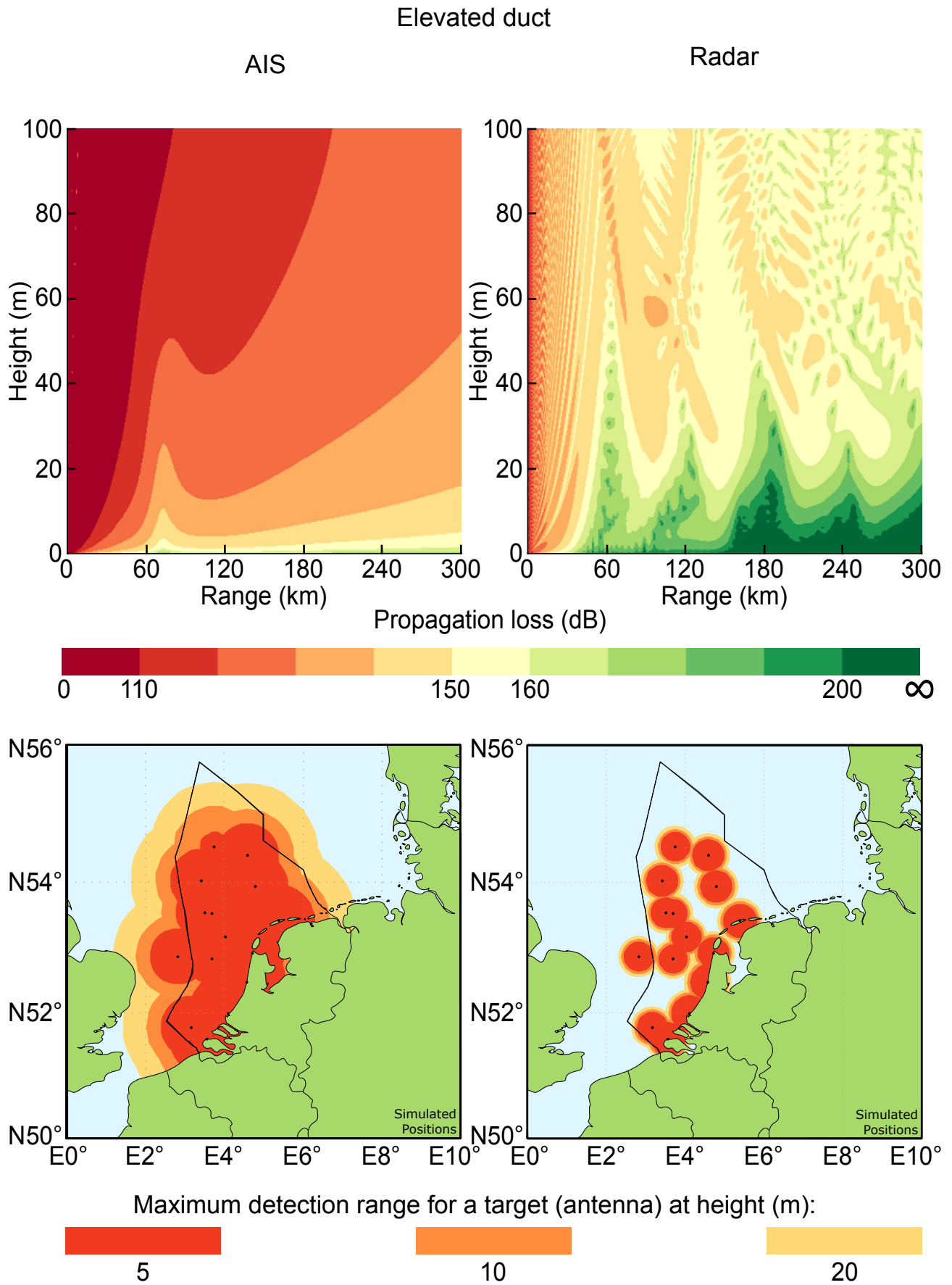|	Automatic Identification System					
	Av. height at sea 39.8 m (MSL)			Av. height above land 50 m (MSL)		
	Range		Coverage area	Range		Coverage area
Target height	(km)	(NM)	(%)	(km)	(NM)	(%)
5 m	55	29.7	305	64.5	34.8	350
10 m	75.5	40.8	416	86	46.4	451
20 m	120	64.8	588	132	71.3	609
	Radar					
5 m	24.5	13.2	109	27	14.6	108
10 m	29.5	15.9	119	32	17.3	107
20 m	35	18.9	116	38	20.5	108

Figure 7.6: Coverage and propagation loss during an elevated duct for both AIS and coastal radar.

7.3   NWP data cases (non-uniform atmosphere)

As found above, theoretical differences between AIS and radar are severe. Both AIS and radar often experience anomalous propagation, and as a result maximum detection ranges are found, that are much different than for standard atmosphere. What remains is the question how the above cases relate to real conditions. In real circumstances the atmospheric conditions are everything but equal over the area and over time. As a result, M-profiles can and will differ per platform and even per direction within a single platform. To give some insight in the real situation, two more cases (section 5.6) are analysed using HARMONIE NWP data. Those NWP datasets are related to real cases in which respectively an evaporation and an elevated duct is experienced (without excluding the other).

For the previous cases M-profiles were set equal over all bearings of all platforms, which made it possible to show a representative height-range plot. For the real cases, M-profiles differ and no such single plot can be made. Instead the upper parts of the figures are used to display the elevated and evaporation duct heights for that specific case spread out over the North Sea which are obtained by using AREPS. The lower part of the figures is again used to display the coverage at the North Sea for targets at three heights. (Magnified representations of the maps are included in appendix E.) Important to emphasise is that evaporation ducts are of no influence to AIS signals, however the opposite cannot be said of the relation between radar and elevated ducts. Therefore, the elevated duct in the upper left plot can be related to the AIS plot in the lower left directly, but for the lower right radar plot both of the upper plots need to be taken into account.

For both cases the coverage results that are found will be compared to standard atmosphere as before. Although hardly any real atmospheric conditions will ever occur that correspond to standard atmosphere, it is again used as a reference.

The remarks that are made for the previous theoretical cases about the specific RCS that is used for radar, the difference between AIS and radar when it comes to interpreting the target height, and especially the simulated positions are again valid. Although, realistic NWP atmospheric data is used for these cases, positions are still simulated (which is denoted by "Simulated positions").

7.3.1 Impact of a real evaporation duct

In the complete North Sea, area elevated ducts are absent except for a small area stretching from the coast of the United Kingdom halfway across to the Dutch coast. In this area, which lies between 1° and 3° Eastern longitude and 51.5° and 52° Northern latitude, an elevated duct occurs between 200 and 240 m, as is shown in the upper right part of figure 7.7. When this elevated duct is compared to the theoretical elevated duct case studied earlier, subsection 7.2.5, it can be obtained that this duct lays around 100 m higher.

From the theoretical elevated duct case studied earlier, it is also known that AIS coverage was strongly enhanced, whilst the impact on radar coverage was minimal. Although the propagation loss pattern showed some strong influence in higher altitudes, the lower altitudes studied here were not affected to such extent that coverage was enhanced. Comparing this to the elevated duct studied here will lead to the hypothesis that radar coverage is not enhanced and AIS coverage might be enhanced at that specific location (all compared to standard atmosphere again), since the elevated duct is even higher is this case.

Looking at the lower left of figure 7.7, which is related to AIS, one platform is reasonably close to the elevated duct. For this platform, some major detection range peaks can be found in directions pointing in and around the elevated duct. The effects are the most spread and the strongest for targets at 20 m. For targets at 10 m also a strong increase is found, but in a more specific direction, whereas for targets at 5 m some small additional detection area can be seen.

For radar, the lower right of figure 7.7, a additional coverage area is seen for the same platform in the same direction for targets at all heights, however, this area is reasonable small compared to the detection areas that arose for AIS. This increase could also be related to the elevated duct, yet at the same location the evaporation duct height is higher - with heights varying between 6 to approximately 10 m above mean sea level - than its surrounding area, stretching from the Dutch to the British coast. As the platform is located inside the area with a strong evaporation duct, the detection range peak could also be related to this duct, as well as to a combination between the elevated and evaporation duct.

At the upper North, above 53.5° Northern latitude, the evaporation duct height also varies between 7 and 10 m. Although no large peaks can be seen here, a significant detection range increase at 5 m can be noted. As a result, the detected area at 5 m exceeds the detected area at 10 and 20 m for the more Northern platforms, as it was also found for the platforms - with lower antenna height especially - studied in the theoretical evaporation duct case (subsection 7.2.2).
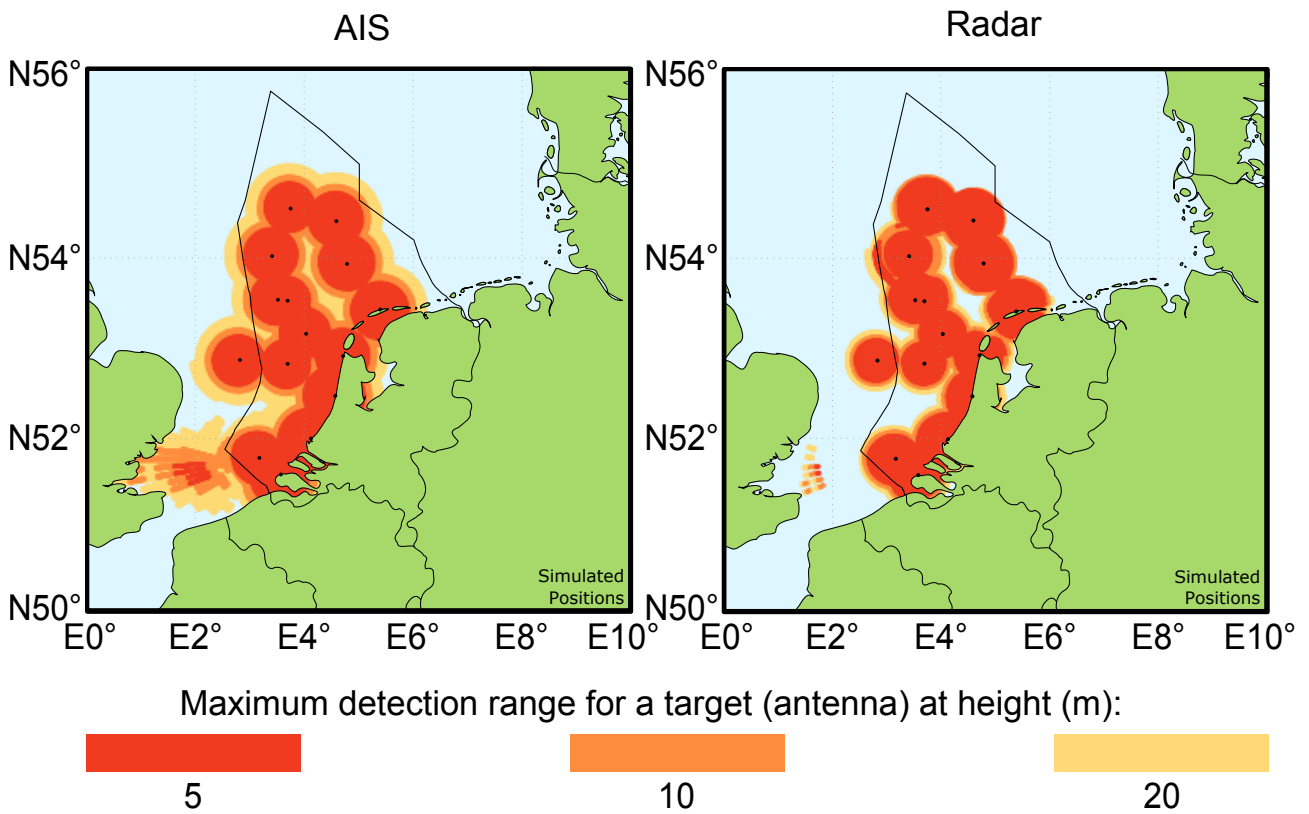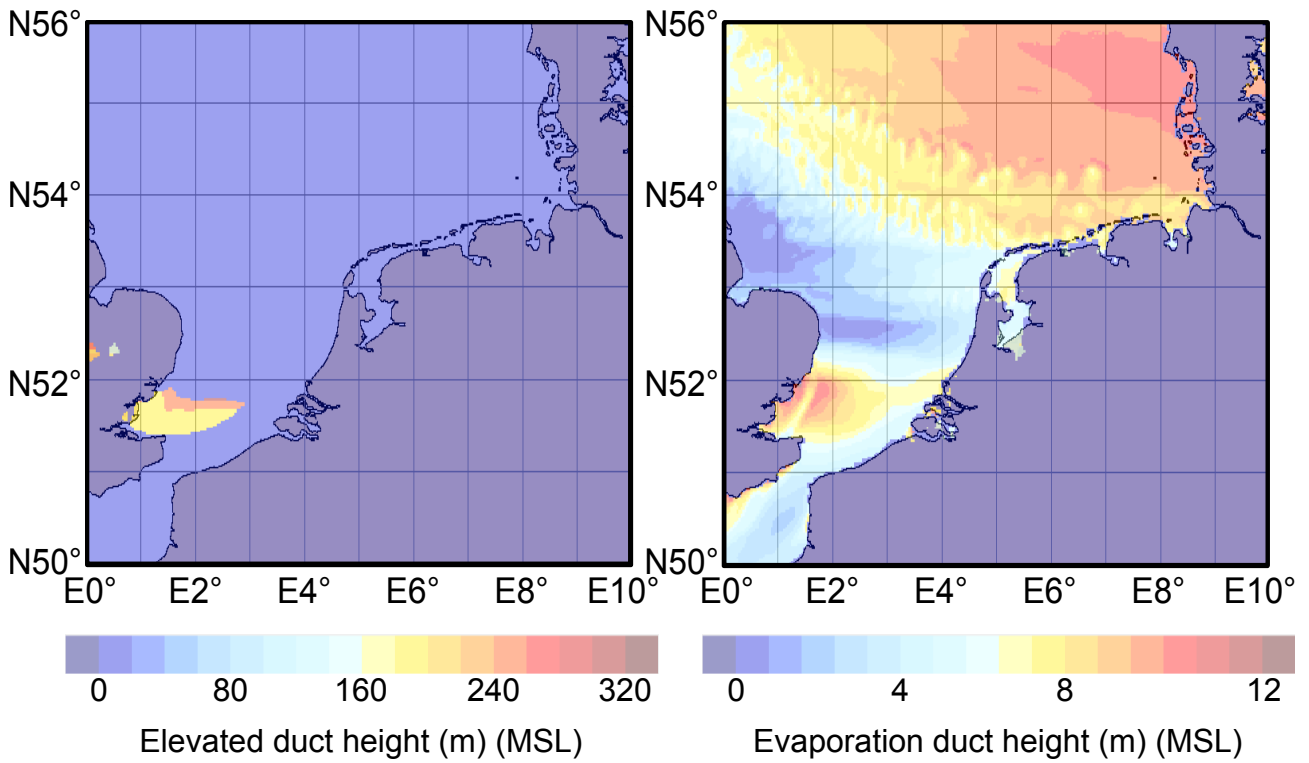
Figure 7.7: Based on real data the elevated duct height and evaporation duct height are shown above (AREPS). Below the corresponding coverage for both AIS and coastal radar are shown for targets at three different heights.

7.3.2 Impact of a real elevated duct

Unlike in the previous studied case, the elevated duct in this case is not restricted to a small area. To the North and North-West of the Netherlands a large elevated duct with heights between 60 and 200 m occurs and in front of the Dutch provinces of Zeeland and Zuid-Holland another elevated duct is found with heights varying from 60 to 100 m. Both elevated ducts can be seen in the upper left of figure 7.8.

At both areas an increase in AIS coverage, as shown in the lower left of figure 7.8, can be found at all heights. The increase is the most spectacular in the more Northern area where at some points detection ranges increase over 150 km for targets with an antenna height of 20 m.

For radar, the coverage increase is again the strongest at a target height of 5 m, although increases at all other heights are also found. For almost all platforms, except for the single platform outside the EEZ to the West, some increase are found, as is shown in the lower right of figure 7.8. Not only does the figure show a steady coverage increase, but, also, there are many coverage peaks and gaps. For some antenna, e.g., the most Northern antenna, there is a coverage gap in multiple directions, leading to a band in which there is no coverage whilst at the same time there is also a band in which there is coverage some further away from the antenna. Also, many "dots" are shown, corresponding to a small area in which there is detection (as can be seen in the lower right of figure 7.8).

In general, the increase in coverage could be related to the elevated ducts, which are present above almost all of those platforms (upper left of figure 7.7), yet given the detection height it is also likely to be influenced by the evaporation ducts. Around the coastline and up to the North, an evaporation duct stretches out with heights varying between 9 and 18 m (upper left of figure 7.8). Therefore, it is likely that the coverage increases are caused by a combination of both ducting effects.
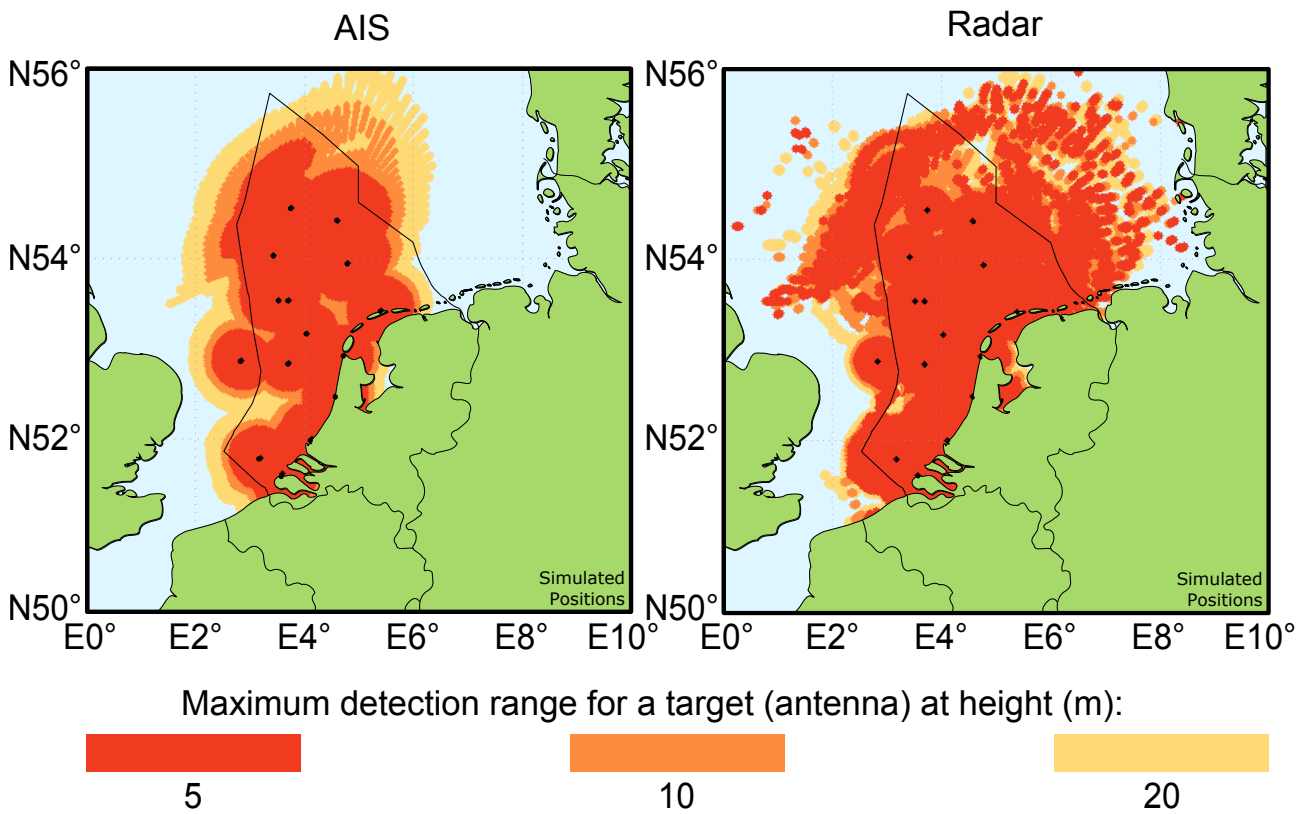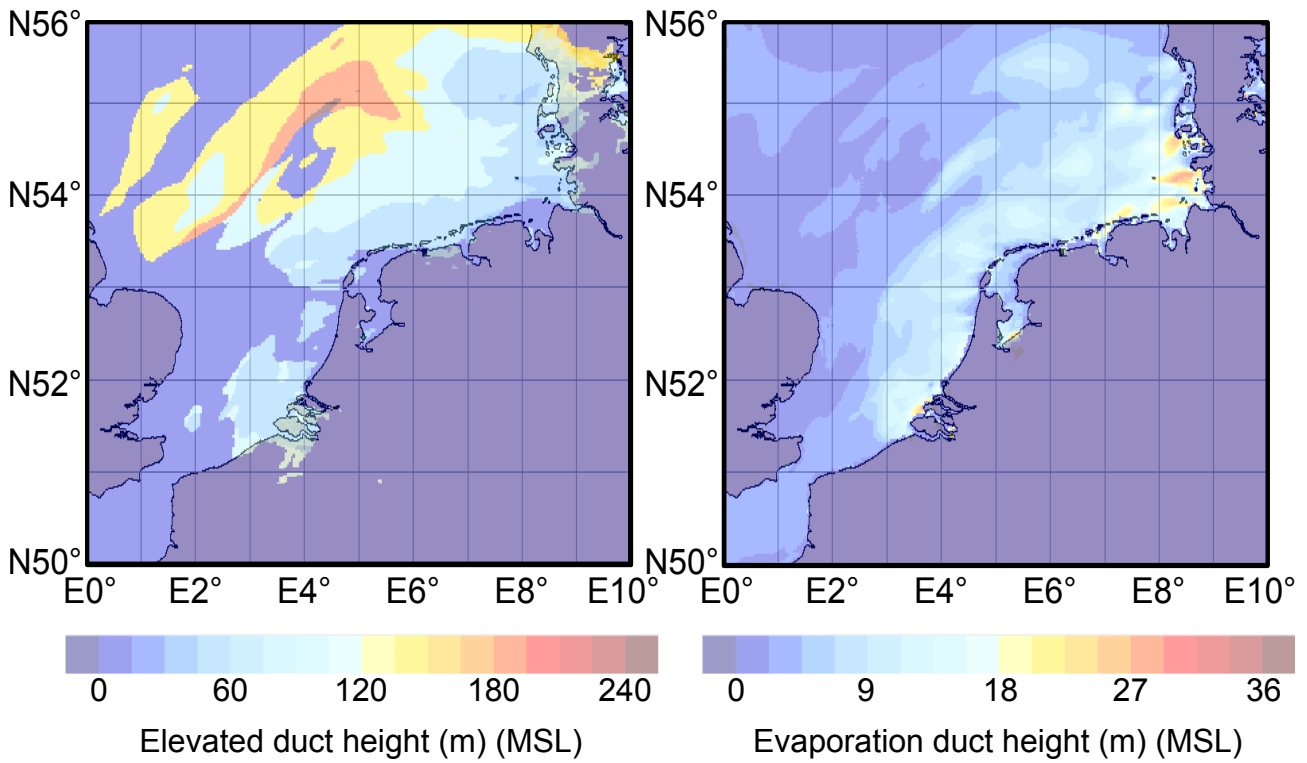
Real elevated duct

Figure 7.8: Based on real data the elevated duct height and evaporation duct height are shown above (AREPS). Below the corresponding coverage for both AIS and coastal radar are shown for targets at three different heights.

7.4 Discussion

At the beginning of this chapter, the detection thresholds were set for both AIS and radar by stating a maximum acceptable propagation loss. Applying these thresholds to standard atmosphere will roughly lead to the detection ranges that are regularly assumed to be encountered. (In appendix F, a comparison to the line of sight detection ranges is given.) However some remarks can be made.

For radar the threshold solely relies on a single calculation which means that the outcome is very depending on a single set of input parameters. Although those parameters where carefully selected during this study, some (minor) differences can be encountered in practice for some of the parameters.

The threshold used for AIS was determined based on linking real maximum detection ranges and heights to propagation loss calculated by AREPS via a least square error estimation on the maximum detection range and target antenna height. Downside of the method is that every range kilometre is taken equally important to every metre in height. In general, this could strongly influence the result, however the fact that the datapoints lay between roughly the same ranges in kilometres (35 to 60) as between the heights in metres (15 to 60) makes up for this. Another possible method: taking the average propagation loss, would take less notion of the height and range, and as a result would not have this problem. On the other hand, it would also not take notion of the fact that a single decibel in propagation loss at higher altitudes lays - in general and also in this case - further apart than at lower altitudes. Furthermore, the average propagation loss also equals 142 dB. Additionally, also the inaccuracy in the detection range and the height of the antennae is not taken into account. All together this makes the AIS detection threshold a volatile parameter. On the other hand, the value provided here gives a rough, but given the data reasonable, estimation to start with; an estimation that was not available before in either literature or in operational tools to model AIS coverage (such as AREPS).

Looking at the case studies, some general notions can be made. (Notions on individual cases are combined with the results of the specific case already.) In the first place, no ducting conditions show coverage that is significantly smaller than the coverage found for standard atmosphere, whilst coverage increase compared to standard atmosphere is often found. For some cases, i.e. the elevated and surface-based duct, impact on the radar signal propagation loss is found, yet coverage hardly changes. Given the target height, a possible explanation for this is that decrease in propagation loss compared to standard atmosphere is not strong enough at low altitudes.

The cases based on real data show that, in practice, coverage patterns are not as smooth as for the theoretical cases. The border of some coverage areas show some sharp angles which reveal the limitations of the methods that were used here. Detection ranges were calculated at a five degree angle from each other centered around a platform. Therefore, the distance between consecutive bearings will rise together with the maximum detection range. Which lead to less accurate detection information further away for the platform.

The real cases also show that multiple ducts can be present at a single locations. In both real cases, radar shows extended coverage that is most likely related to both an evaporation and an elevated duct (or a combination of both), given the fact that detection ranges are extended for 5, 10, and 20 m targets as well as at locations that either show an elevated or an evaporation duct.

Chapter 8

Conclusion

8.1   Resume

The Netherlands Coastguard coordinates and carries out multiple operational tasks on the North Sea regarding both the provision of service and law enforcement. For their maritime situation awareness, the coastguard depends on the Automatic Identification System (AIS) and coastal radar systems. The operators of these sensor systems often experience abnormal effects such as coverage gaps and different detection ranges for AIS and radar. Possible explanations for these effects are technological limitations of the system (including slot management), poor antenna positions, and environmental/atmospheric impact on radar and radio wave propagation.

This thesis studies the environmental impact on radar and radio wave propagation on (Class A) AIS and (X-band) radar at the operational area of the Netherlands Coastguard, i.e., the exclusive economical zone (EEZ) of the Netherlands. Although AIS and coastal radar differ in their way of detection - AIS is a one-way communication system and radar a two-way system -, both rely on radio wave propagation for the transmission of their signals. The propagation path of these signals is influenced by the atmospheric conditions.

Five important categories of atmospheric conditions may be distinguished: standard atmosphere, evaporation ducts, standard surface ducts, surface-based ducts, and elevated ducts, of which standard atmosphere is often used as a reference by manufacturers and others. In this thesis, all five conditions have been combined and represented in an atmospheric refractivity profile. Based on these profiles, the radar and radio wave propagation has been modelled and, as a result, detection ranges and coverage have been determined. The same has been done based on weather data, which is then first translated to atmospheric refractivity profiles.

Together, the ability to model radar and radio wave propagation based on accurate sensor, target, and weather information, and knowledge of the most important atmospheric conditions have been used to answer the research question of this thesis:

> "How do seasonal weather changes above the exclusive economic zone of the Netherlands influence the coverage of existing Automatic Identification System and coastal radar infrastructure?"

To provide an answer to this question, three main goals and two supporting objectives were stated at the beginning of this thesis. Those goals and objectives are the following:

I Identify relevant atmospheric propagation mechanisms.

II Assess North Sea weather.

III Model AIS (and coastal radar) systems.

IV Assess North Sea coverage.

V Provide a proof of concept to forecast realistic sensor coverage in the North Sea.

The answers to these questions will be discussed in the next section.

8.2 Conclusions

For both AIS and coastal radar, no indication has been found of atmospheric conditions that could negatively influence the detection range and the associated coverage area significantly for any of the studied targets. Standard atmosphere, which has been used as a reference, showed minimum detection ranges compared to all anomalous propagation conditions. Conversely, extended detection ranges, compared to standard atmosphere, have been found under multiple anomalous propagation conditions. During surface and elevated ducts, both AIS and radar experienced extended detection ranges. For standard surface ducts, detection ranges exceeding a hundred kilometres have even been encountered. For elevated ducts, it has, however, also been found that heights could rise to several kilometres, diminishing their impact on the ground.

Coverage gaps have not been found within standard atmospheric detection ranges. At further ranges, coastal radar coverage gaps can exist during surface and elevated ducts, caused by the sine-wave propagation pattern that arises during these ducting conditions. For AIS, the sine-wave pattern is less strong and therefore coverage gaps will be limited.

In general, the maximum detection ranges for AIS are significantly higher (by approximately one-third during standard atmospheric conditions) than radar detection ranges. However, evaporation ducts extend radar detection ranges at low altitudes, whilst AIS is not influenced by the same ducts. Also, strong multipath interference during standard surface ducts, could, also at low altitudes, increase radar detection ranges to distances that exceed the AIS detection ranges.

Looking at seasonal weather changes, summer is the most important regarding anomalous propagation. Not only are the evaporation ducts the highest (and, consequently, the strongest) at the end of summer, but, other ducts are also most frequently present during this season. At one-third to a half of the days of each month either a surface or an elevated duct has been found. During spring similar numbers have been detected for surface and elevated ducts, although the evaporation duct height is generally lower. In autumn, evaporation duct heights are comparable to those in spring, but elevated and surface ducts are much less common. In winter, anomalous propagation is, in general, close to absent. Evaporation duct heights are, on average, low and surface and elevated ducts are close to absent.

Based on the above, standard atmosphere - most common during winter - gives the worst propagation conditions. Given the calculations made in the scope of this thesis during standard atmospheric conditions, it can be concluded that the current situation awareness of the Netherlands Coastguard within the exclusive economic zone of the Netherlands is strong for AIS and sufficient for radar. Nevertheless, the conclusions of the present research suggest several specific points at which coverage can be improved.

8.3 Overall discussion

Before ending this thesis by looking ahead to interesting future perspectives following this thesis, this section looks at the methods that are used within this thesis to model radar coverage and

how they could be improved.

First of all: accurate sensor (and target) input data is key. Throughout this thesis, input data for the sensors - both platform information and system characteristics - and the targets are selected to be as close to reality as possible. However, sensor system characteristics can differ per system, whereas target characteristics depend on the nature of the specific target of interest. Moreover, the platform locations and heights are important. A difference in the placement height of the antenna can mean the difference between an antenna being inside or above the duct and can thereby change coverage severely (as has been encountered within this thesis). It is thus recommendable to acquire accurate information about the sensors, platforms, and characteristics of the selected targets.

Obstruction of the signal by landmass, vegetation, or infrastructure may also be of influence. The antenna platforms on land are, in general, high and close to the coast, which makes obstruction unlikely. At sea, most antennae are placed on oil platforms, yet not always on top. During this research, it became clear that some antennae are placed at the side of the platform, creating a blind angle possibly as large as 180 degrees. To determine accurate coverage, either the antennae suffering from a blind angle need to be identified and relocated to improve reception or the coverage absence needs to be incorporated in the system.

Finally, some notes on using AREPS. AREPS offers a great variety of input and output options. It gives the user the opportunity to describe both target and sensor specifically, input large sets of atmospheric data, and it could output both propagation loss and coverage. However, AREPS calculations are limited to a single sensor. Every calculation is made in a specific direction from the antenna location. This makes the combination of coverage areas from different antennae difficult and it causes the maximum detection range locations of neighbouring calculation directions to be further apart as the maximum detection range increases. Ideally, the maps should be made discrete, using a grid related to the latitude and longitude coordinates in which the coverage - or even the probability of detection - is shown for every point of the grid.

8.4   Recommendations

This section contains the recommendations following from this thesis in two parts. The first subsection states recommendations for interesting or important further research. The second subsection given recommendations meant for the Netherlands Coastguard, who initiated this research.

8.4.1   Recommendations for further research

To our knowledge, this study was the first to relate weather radar observations to atmospheric ducting climatology. However, since this study only focused on a period of six years and on the North Sea, reasonable perspective for further research is left. An extension of this study to more years could improve the validity of the results. Although, the results per year were in general stable - there were no extreme outliers from the overall results -, the relation to the North Sea climate can be strengthened and trends can be determined with more certainty. At the same time, the data analysed during this study, together with new North Sea data, can be used to determine a more specific relation between the weather and the given propagation (compared to the seasonal relation given in this thesis). Also, the same method to relate atmospheric ducting trends to weather radar data can be applied internationally. (The North Sea analysis was based

on KNMI data, but in other region similar data might be kept which makes it possible to do a similar analysis.)

The method to visualise coverage based on NWP data is also not restricted to the North Sea. By using ECMWF NWP data - which is also compatible with AREPS - instead of HARMONIE NWP data, the coverage area of multiple sensors to detect a specific target as a whole can be analysed all over the world to assist not only the Netherlands Coastguard, but also other coastguards and navies.

In addition, an important topic that needs to be addressed more extensively is the validation of the coverage results that were and can be obtained with this study, especially for AIS. Although this thesis is based on the available literature about AIS and uses additional radar literature and techniques that are generalised for AIS, the limited amount of studies focusing specifically on AIS could leave practical issues unnoticed.

8.4.2 Recommendations for the Netherlands Coastguard

Throughout this thesis, a method to model North Sea coverage based on weather data is developed and applied on both M-profiles (corresponding to theoretical weather conditions) and more realistic HARMONIE Numerical Weather Prediction (NWP) data. In practice, this method could support the situation awareness of the Netherlands Coastguard by providing propagation and coverage information on a regular basis. Not only could it be used to determine current and past propagation (and coverage) conditions, but it could also be used to forecast future AIS and radar coverage. By using NWP HARMONIE or even ECMWF data coverage forecasts can be made for several days into the future. This may provide significant information about the (lack of) coverage within the EEZ of the Netherlands which may help the coastguard identify locations that require the deployment of mobile sensors, i.e., ships and aircraft, at a specific time.

In table 8.1, four possible cases are discussed that operators may encounter when looking at (part of) a coverage map of the North Sea that under standard conditions has AIS and coastal radar coverage, namely: all combinations of whether or not there is radar coverage combined with whether or not there is AIS coverage. In the same table, the initial reaction of the operator, based on the coverage he/she experiences every day without any knowledge of present anomalous propagation effects at that time, is shown. In the third column of the table, the cause in terms of anomalous propagation resulting from this thesis is added. Furthermore, a rule of thumb about the season in which these propagation conditions are to be expected is added. Important to notice is that other facets that could influence the coverage area such as blockage of the signal for both AIS and coastal radar and slot management specially for AIS are not taken into account in this thesis and as such are not taken into account in this analysis.

Both Both systems have coverage in this area, so there are no problems for the operator either with or without a coverage map. However, the operator now knows to where this area stretches out. He or she also knows that besides the ships shown on his or her screen, there are (most likely) no others that remain undetected.

AIS only Without a coverage map, the signal is easily assumed to be a fake AIS signal - possibly necessitating additional action. With a coverage map it is clear that there is no radar coverage, whilst there is AIS coverage. The possible "fake AIS track" can - if progressing in the right direction - be followed until it is within radar reach to rule out if it is fake (before a call to action is made).

Table 8.1: Possible sensor coverage conditions combined with the operators perspective and related extra information based on this research.

Sensor coverage	Operator's reaction	Weather conditions	Time of the year
Both	-	Standard atmosphere Surface/elevated duct	Year round Spring/Summer
AIS only	Risk of fake AIS	Surface/elevated duct	Spring/Summer
Radar only	Possibly suspicious ship behaviour	Evaporation duct	Year round; strongest in summer
None	Blind spot; ship remains undetected	-	-

Radar only Without a coverage map, the ship detected by the radar is assumed to have switched off its AIS, causing possible suspicion and additional action. With a coverage map it is clear that there is radar coverage, whilst there is no AIS coverage. The ship can - if progressing in the right direction - be followed until it is within AIS reach or an additional analysis (regarding its size, speed, etc) can be made (before a call to action is made).

None Without a coverage map no ships are assumed to be present. With a coverage map it is known that there is no coverage in that area, making it a potential area for additional observations that day, e.g., using coastguard ships or aircraft.

Based on the above, it can be concluded that implementing the described methods into the current system of the Netherlands Coastguard would help to increase reliability of AIS and radar data and to increase efficient usage of manpower and resources.

Apart from implementing this method into the current system, the most important recommendation following this thesis is to improve coverage as a whole. Using the coverage maps that were generated during this study (and provided as a classified annex to this thesis), the points at which coverage is not guaranteed are revealed. Based on this, locations can be selected to place new antennae connected to the existing coastguard network, thereby increasing the coastguard's situation awareness and consequently the safety and security within the area.

Bibliography

[1] M. I. Skolnik, *Radar handbook.* The McGraw-Hill companies, 3th ed., 2008.

[2] W. L. Patterson, "The propagation factor, Fp, in the radar equation," in *Radar handbook* (M. I. Skolnik, ed.), ch. 26, McGraw-Hill, 2008.

[3] A. Barrios and W. Patterson, "Advanced propagation model (APM) ver. 1.3. 1 computer software configuration item (CSCI) documents," tech. rep., DTIC Document, 2002.

[4] M. I. Skolnik, *Introduction to radar systems.* McGraw-Hill book company, 2nd ed., 1981.

[5] H. V. Hitney, "Refractive effects from VHF to EHF. Part A: Propagation mechanisms," in *AGARD, Propagation Modelling and Decision Aids for Communications, Radar and Navigation Systems 13 p (SEE N95-14825 03-32)*, vol. 1, 1994.

[6] United Nations, "United Nations conventions on the laws of the sea: exclusive economical zone." `https://www.un.org/depts/los/convention_agreements/texts/unclos/part5.htm`, 2002. Accessed: 08-10-2015.

[7] L. W. Barclay, *Propagation of radar waves.* London, United Kingdom: The Institution of Engeneering and Technology, 2nd ed., 2003.

[8] D. Green, C. Fowler, D. Power, and J. Tunaley, "VHF propagation study," Contractor report DRDC-ATLANTIC-CR-2011-152, Defence R&D Canada, London Research and Development Corp., C-Core, September 2012.

[9] "Long range detection of automatic identification system (AIS) messages under various tropospheric propagation conditions," Tech. Rep. Rep. ITU-R M.2123, International Telecommunications Union (ITU), 2007.

[10] C. A. Balanis, *Antenna theory, Analysis and design.* John Wiley & Sons, Inc., 3th ed., 2005.

[11] M. I. Skolnik, "An introduction and overview of radar," in *Radar handbook* (M. I. Skolnik, ed.), ch. 26, McGraw-Hill, 2008.

[12] I. Faulconbridge, *Radar fundamentals.* Canberra, Australia: Argos Press, 2002.

[13] SOLAS, "Regulation 19 - carriage requirements for shipborne navigational systems and equipment." `https://mcanet.mcga.gov.uk/public/c4/solas/solas_v/Regulations/regulation19.htm`, July 2002. Accessed: 08-08-2015.

[14] European Commission, "Commission directive 2011/15/EU," *Official Journal of the European Union*, 2011.

[15] "Recommendation, technical characteristics for an automatic identification system using time division multiple access in the VHF maritime mobile band.," Tech. Rep. Rec. ITU-R M.1371-5, International Telecommunications Union (ITU), 2014.

[16] R. Herbert-Burns, S. Bateman, and P. Lehr, *Lloyd's MIU handbook of maritime security.* CRC Press, 2008.

[17] National Imagery and Mapping Agency, Bethesda, Maryland, *Radar navigation and maneuvering board manual*, 7th ed. ed., 2001.

[18] "Technical characteristics of maritime radionavigation radars," Tech. Rep. Rec. ITU-R M.1313, International Telecommunications Union (ITU), 1997.

[19] K. Craig, "Clear-air characteristics of the troposphere," in *Propagation of Radiowaves* (L. W. Barclay, ed.), ch. 7, pp. 103–128, 2003.

[20] P. Debye, "Polar molecules," *Dover Publ. Co.*, pp. 89–90, 1957.

[21] E. Smith and S. Weintraub, "The constants in the equation for atmospheric refractive index at radio frequencies," *Proceedings of the IRE*, vol. 41, pp. 1035–1037, Aug 1953.

[22] "The radio refractive index: its formula and refractivity data," Tech. Rep. Rec. ITU-R P.453-9, International Telecommunications Union (ITU), 2003.

[23] H. R. Reed and C. M. Russell, *Ultra high frequency propagation*, vol. 17. Chapman & Hall, 1966.

[24] M. A. Richards, J. Scheer, W. A. Holm, *et al.*, *Principles of modern radar: basic principles.* SciTech Pub., 2010.

[25] W. L. Patterson, *Advanced Refractive Effects Prediction System (AREPS): User's Manual.* Space and Naval Warfare Systems Center (SPAWAR), San Diego, CA, 1st ed., 1998.

[26] H. V. Hitney, J. H. Richter, R. Pappert, K. D. Anderson, G. B. Baumgartner Jr, *et al.*, "Tropospheric radio propagation assessment," *Proceedings of the IEEE*, vol. 73, no. 2, pp. 265–283, 1985.

[27] A. Adediji, M. Ajewole, and S. Falodun, "Distribution of radio refractivity gradient and effective earth radius factor (k-factor) over akure, south western nigeria," *Journal of Atmospheric and Solar-Terrestrial Physics*, vol. 73, no. 16, pp. 2300–2304, 2011.

[28] K. L. Twigg, "A smart climatology of evaporation duct height and surface radar propagation in the Indian Ocean," Master's thesis, Naval Postgraduate School (NPS), Monterey, California, 2007.

[29] J. Derksen, "Radar propagation modelling," Master's thesis, Delft University of Technology, 2015.

[30] J. Richter, "Sensing of radio refractivity and aerosol extinction," in *Geoscience and Remote Sensing Symposium, 1994. IGARSS '94. Surface and Atmospheric Remote Sensing: Technologies, Data Analysis and Interpretation., International*, vol. 1, pp. 381–385 vol.1, Aug 1994.

[31] A. Baede, "Numerieke afmosfeermodellen," syllabus, KNMI, 1988.

[32] J. Mason, "Numerical Weather Prediction," *Proceedings of the Royal Society of London A: Mathematical, Physical and Engineering Sciences*, vol. 407, no. 1832, pp. 51–60, 1986.

[33] T. T. Warner, *Numerical weather and climate prediction.* Cambridge Press, 2011.

[34] T. Haack, C. Wang, S. Garrett, A. Glazer, J. Mailhot, and R. Marshall, "Mesoscale modeling of boundary layer refractivity and atmospheric ducting," *J. Appl. Meteor. Climatol.*, vol. 49, pp. 2437–2457, July 2010.

[35] ECMWF, "Operational configurations of the ecmwf integrated forecasting system (IFS)." http://www.ecmwf.int/en/forecasts/documentation-and-support, May 2015. Accessed: 01-12-2015.

[36] M. Z. Jacobson, *Fundamentals of Atmospheric Modeling.* Cambridge University Press, 2nd ed., 2005. Cambridge Books Online.

[37] V. Ivanov, V. Shalyapin, and Y. V. Levadnyi, "Determination of the evaporation duct height from standard meteorological data," *Izvestiya, Atmospheric and Oceanic Physics*, vol. 43, no. 1, pp. 36–44, 2007.

[38] S. M. Babin and G. D. Dockery, "LKB-based evaporation duct model comparison with buoy data," *Journal of Applied Meteorology*, vol. 41, no. 4, pp. 434–446, 2002.

[39] P. J. Webster and R. Lukas, "TOGA COARE: The coupled ocean-atmosphere response experiment," *Bulletin of the American Meteorological Society*, vol. 73, no. 9, pp. 1377–1416, 1992.

[40] D. A. Newton, "COAMPS modeled surface layer refractivity in the roughness and evaporation duct experiment 2001," tech. rep., DTIC Document, 2003.

[41] P. Fredrickson, "Improving the characterization of the environment for AREPS electromagnetic performance predictions." Presentation, Department of Meteorology, Naval Postgraduate School (NPS), March 2012.

[42] C. Constantinou, "Numerically intensive propagation prediction methods," in *Propagation of radar waves*, ch. 10, p. 163, Les W. Barclay, 2003.

[43] M. Levy, *Parabolic equation methods for electromagnetic wave propagation.* No. 45, IET, 2000.

[44] O. Ozgun, G. Apaydin, M. Kuzuoglu, and L. Sevgi, "PETOOL: MATLAB-based one-way and two-way split-step parabolic equation tool for radiowave propagation over variable terrain," *Computer Physics Communications*, vol. 182, no. 12, pp. 2638–2654, 2011.

[45] A. E. Barrios, "Considerations in the development of the advanced propagation model (APM) for US Navy applications," tech. rep., DTIC Document, 2005.

[46] H. V. Hitney, "Hybrid ray optics and parabolic equation methods for radar propagation modeling," in *Radar 92. International Conference*, pp. 58–61, IET, 1992.

[47] D. Thomson and N. Chapman, "A wide-angle split-step algorithm for the parabolic equation," *The Journal of the Acoustical Society of America*, vol. 74, no. 6, pp. 1848–1854, 1983.

[48] J. Toomay and P. J. Hannen, *Radar principles for the non-specialist.* Scitech Publishing, Inc., 2004.

[49] "Adoption of the revised performance standards for radar equipment," Tech. Rep. Resolution MSC.192-72, Annex 34, International Maritime Organization (IMO), 2004.

[50] S. O. Rice, "Mathematical analysis of random noise," *Bell System Technical Journal*, vol. 23, no. 3, pp. 282–332, 1944.

[51] C. L. Weber, *Elements of detection and signal design.* Springer Science & Business Media, 2012.

[52] B. R. Mahafza, *Introduction to radar analysis.* CRC Press LLC, 1998.

[53] J. M. Green, "Establishing system measures of effectiveness," tech. rep., DTIC Document, 2001.

[54] J. Rice, *Mathematical statistics and data analysis.* Cengage Learning, 2006.

[55] H. V. Hitney and R. Vieth, "Statistical assessment of evaporation duct propagation," *Antennas and Propagation, IEEE Transactions on*, vol. 38, no. 6, pp. 794–799, 1990.

[56] A. E. Barrios, "Radio frequency propagation effects." Presentation, JIVC/KIXS, 2014.

[57] M. Hall and L. Barclay, "Radiowave propagation and spectrum use," in *Propagation of radar waves*, ch. 1, pp. 22–31, 2 ed., 2003.

[58] A. von Engeln and J. Teixeira, "A ducting climatology derived from the european centre for medium-range weather forecasts global analysis fields," *Journal of Geophysical Research: Atmospheres*, vol. 109, no. D18, 2004. D18104.

Appendix A

Characteristic values

This appendix contains the values for all AIS and radar characteristics that are used within this thesis.

Table A.1: Representative AIS and radar specs of selected characteristics.

Characteristic	AIS Class A	Radar X-band
(Peak) power	12.5 W	25 kW
Frequency (MHz)	161	9400
Pulse length (μs)	-	0.2
Compressed pulse length (μs)	-	0.05
Gain (dBi)	2	35
Rotation rate (rpm)	-	21
Beamwidth (deg)		
Horizontal	-	0.4
Vertical	-	15
Polarisation	vertical	vertical
Antenna type	Omni	$\sin(x)/x$
System loss (dB)	3.6	6
Probability of false alarm	-	10^{-4}
Noise figure	-	2 dB

Appendix B

Platform data

This appendix contains the latitudes and longitudes (in decimal coordinates) of the platform location studied within this thesis, i.e., the locations of the simulated platform positions. It also contains the reference labels for the platforms and the height of the antenna location.

Table B.1: Platform data

Label	Latitude	Longitude	Height (m)
coast1	53.421647	5.394409	45
coast2	52.929438	4.716003	40
coast3	52.481778	4.575928	54
coast4	51.992324	4.114502	59
coast5	51.589701	3.570679	52
sea1	54.532237	3.751790	30
sea2	53.532128	3.692259	30
sea3	54.023876	3.414278	37
sea4	52.876642	2.823871	34
sea5	51.775210	3.165686	39
sea6	53.175672	4.035758	34
sea7	52.839117	3.693944	31
sea8	53.544857	3.515122	35
sea9	53.939974	4.789157	40
sea10	54.404543	4.586751	37

Appendix C

Ship data

This appendix contains of data of the ships that were studied within this thesis to determine the maximum detection range for AIS. The maximum range and height values itself were obtained after an extensive analysis. The propagation loss values were obtained by combining propagation loss data compute by AREPS with the maximum range and height established before that.

Table C.1: Ship data

Maximum range (km)	Height (m)	Propagation loss (dB)
46.0	30.5	143.5
35.0	31.0	136.3
50.5	47.0	141.6
41.0	34.0	139.1
54.0	55.5	142.0
35.5	29.5	137.2
51.5	41.0	143.7
51.5	53.5	141.2
40.0	23.5	142.5
38.5	16.5	145.7
37.5	19.5	143.2
39.5	24.5	141.9
45.5	27.0	144.6
40.0	24.5	142.0
50.5	34.0	144.4
40.5	26.5	141.3
58.5	46.0	146.2
37.0	19.0	143.3
49.0	32.0	144.2

Appendix D

Matlab code

This appendix contains the Matlab code that is used to plot the coverage maps that are shown in this thesis. (Some post-process image editing for visual improvement is not included.)

Listing D.1: Code for homogeneous atmosphere

```matlab
%%%% Visualising coverage %%%%
% This program can be used to translate AREPS output into a visualisation
% of the coverage area at a specific height. The program determines the
% maximum detection ranges of different platforms in multiple directions
% (based on a given threshold). The locations corresponding to the
% locatios of the maximum detection ranges are combined per platform and
% later on for all platforms. This way, the border of the total coverage
% area is determined and plot.
%
% Not included: ReadArepsBinaryFile.m
% (m-file to load the AREPS binary output files into Matlab)


% Load gshhs-data (accurate map data)
world = gshhs('coast line\gshhs_i.b');
border = gshhs('coast line\wdb_borders_i.b');
river = gshhs('coast line\wdb_rivers_i.b');

% Plot North Sea map
figure;
title('Standard atmosphere')
axesm('mercator','MapLatLimit',[50 56],'MapLonLimit',[0 10]);
setm(gca, 'GColor', [0.6 0.6 0.6], 'FFaceColor',[0.866666674613953
    0.964705884456635 1], 'Grid', 'on', 'Frame', 'on')
setm(gca, 'MlabelLocation', 2,'PlabelLocation',2,...
    'MlabelParallel','south','MeridianLabel','on',...
    'ParallelLabel','on','MlineLocation',2,...
    'PlineLocation',2)

% Info on the ran AREPS module (First bearing, stepsize, and number of bearings
    )
first_b = 0;
```

```matlab
31  stepsize_b = 10;
32  num_b = 36;
33
34  % Threshold (142 dB for AIS and 143.55 dB for Radar)
35  f = 143.55;
36
37  % Selected heights  (minus 1, divided by 5, to find the height in metres)
38  heights = [2,3,5];
39  numHeights = length(heights);
40
41  % Colors for different heights
42  clr = [189/255 0 38/255;
43      240/255 59/255 32/255;
44      253/255 141/255 60/255;
45      254/255 178/255 76/255;
46      254/255 217/255 118/255;
47      254/255 255/255 178/255;];
48
49  % Loop over all locations
50  for k = 1:15
51      %Loop over all bearings
52      for i = first_b : stepsize_b : stepsize_b*(num_b-1)
53          % Get the data from AREPS
54          file = ['C:/Program Files/AREPS/Data/Projects/radar' num2str(k,'%i') '/
55              radar' num2str(k,'%i') '_APM_' num2str(i,'%03i') '_00_00.bin'];
55          [A] = ReadArepsBinaryFile(file);
56
57          % Dummy vector to save temporary maximum detection ranges
58          a = zeros(max(heights),1);
59
60          %Loop over all heights to create a coverage 'circle' (for a single
61              height and platform)
61          for j = heights
62              % Find maximum detection range and save in a
63              if isempty(find(A.losses(j,:)>f,1)) == 0
64                  a(j) = distdim(A.ranges(A.numRanges-find(fliplr(A.losses(j,:)
65                      +1)<f,1))/1000,'km','deg'); % Radar
65                  % a(j) = distdim(A.ranges(find(A.losses(j,:)>f,1)-1)/1000,'km
66                      ','deg'); % AIS
66              else
67                  % Stopping criterion if maximum range exceeds input data (range
68                      is set equal to the maximum input range)
68                  a(j) = distdim(A.ranges(A.numRanges)/1000,'km','deg');
69              end
70              index = i/stepsize_b;
71
72              % Calculate location of maximum range (based on the platform's
73                  postion and the maximum detection range) and add to the list
```

```
73                    [latc(index+1,j),lonc(index+1,j)] = reckon('rh',platform_loc(k,1),
                           platform_loc(k,2),a(j),i);
74                end
75            end
76
77        % Set last points to complete the 'circle'
78        latc(num_b+1,:) = latc(1,:);
79        lonc(num_b+1,:) = lonc(1,:);
80
81        % Loop over all heights to combine the coverage areas
82        for j = heights
83            % Set detection area for first AIS station (and change notation)
84            [latc(:,j),lonc(:,j)] = poly2cw(latc(:,j),lonc(:,j));
85
86            % Set beginning coverage area
87            if (k == 1)
88                % Loop over all heights
89                for j = heights
90                    lat_end{j} = latc(:,j);
91                    lon_end{j} = lonc(:,j);
92                end
93            % Combine detection area for multiple AIS stations
94            else
95                [lat_end{j},lon_end{j}] = polybool('union',lat_end{j},lon_end{j},
                       latc(:,j),lonc(:,j));
96            end
97        end
98    end
99
100 % Loop over the heights to plot the coverage areas (per height)
101 for j = heights
102     plotm(lat_end{j},lon_end{j}, 'LineWidth',2, 'Color',clr(j,:))
103 end
104
105 % Plot coast lines and color the land masses
106 geoshow([world.Lat],[world.Lon],'Color', [0 0 0])
107 patchm([world.Lat],[world.Lon], [16/255 196/255 70/255])
108
109 % Plot rivers and, land and sea borders
110 geoshow([border.Lat],[border.Lon],'Color', [0 0 0])
111 geoshow([river.Lat],[river.Lon], 'Color', [0 160/255 1])
112 plotm(sea_border_netherlands(:,2),sea_border_netherlands(:,1),'Color', [0,0,0])
113
114 % Plot platform locations
115 plotm(platform_loc(:,1),platform_loc(:,2),'k.')
```

For non-homogeneous atmosphere, line 49 to 103 of the code above can be replaced by the code below.

Listing D.2: (Partial) code for non-homogeneous atmosphere

```
1  % Dummy variable to index the heights
2  index=ones(max(heights));
3
4  % Loop over all locations
5  for k = 1:15
6      % Loop over all bearings
7      for i = first_b : stepsize_b : stepsize*(num_b−1)
8          % Get the data from AREPS
9          file = ['C:/Program Files/AREPS/Data/Projects/radar' num2str(k,'%i') '/
                radar' num2str(k,'%i') '_APM_' num2str(i,'%03i') '_00_00.bin'];
10         [A] = ReadArepsBinaryFile(file);
11
12         % Loop over all heights
13         for j = heights
14             % Loop over all ranges
15             for l = 1:A.numRanges
16                 % Find all points within detection range, i.e., points at which
                        the propagation loss is lower than the threshold
17                 if A.losses(j,l)<f
18                     % Dummy vector to save temporary maximum detection ranges
19                     a = distdim (A.ranges(l)/1000,'km','deg');
20                     % Calculate coverage location and add to the list
21                     [latc2{j}(index(j)),lonc2{j}(index(j))] = reckon('rh',
                            platform_loc(k,1),platform_loc(k,2),a,i);
22                     index(j)=index(j)+1;
23                 end
24             end
25         end
26     end
27 end
28
29 % Turn around heights and colors (to plot heigher air layers with, in general,
        bigger coverage areas on top)
30 reverse_heights = fliplr(heights);
31 fliplr(clr);
32
33 % Loop over the heights to plot the coverage areas (per height)
34 for j = reverse_heights
35     plotm(latc2{j},lonc2{j}, 'linestyle', 'none', 'Marker', '.', 'Color',clr(j
            ,:))
36 end
```

Appendix E

Figures

This appendix contains magnified views of the coverage maps provided within this thesis.
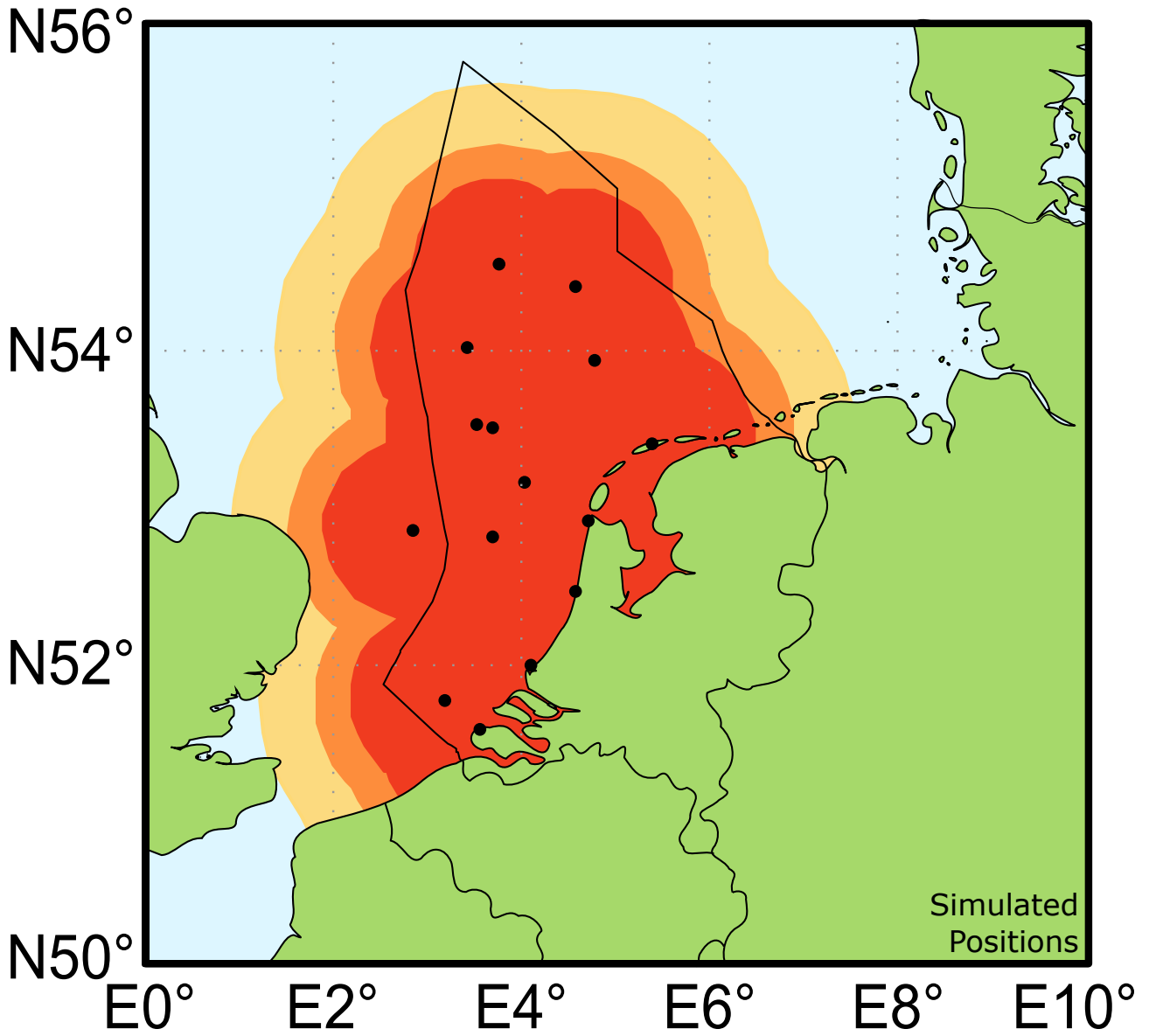
Standard atmosphere

AIS
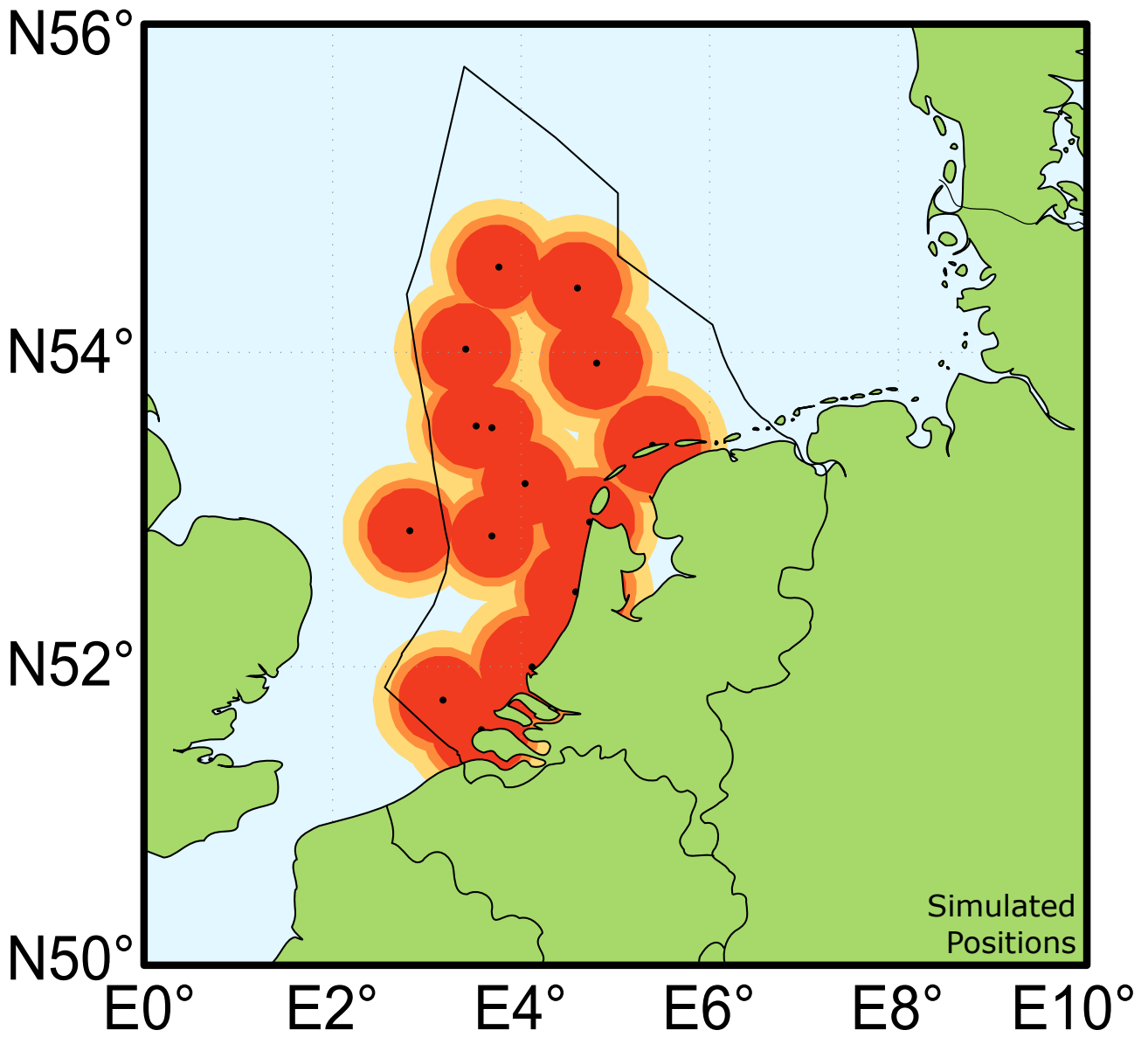
Maximum detection range for a target (antenna) at height (m):

5   10   20

Standard atmosphere

Radar
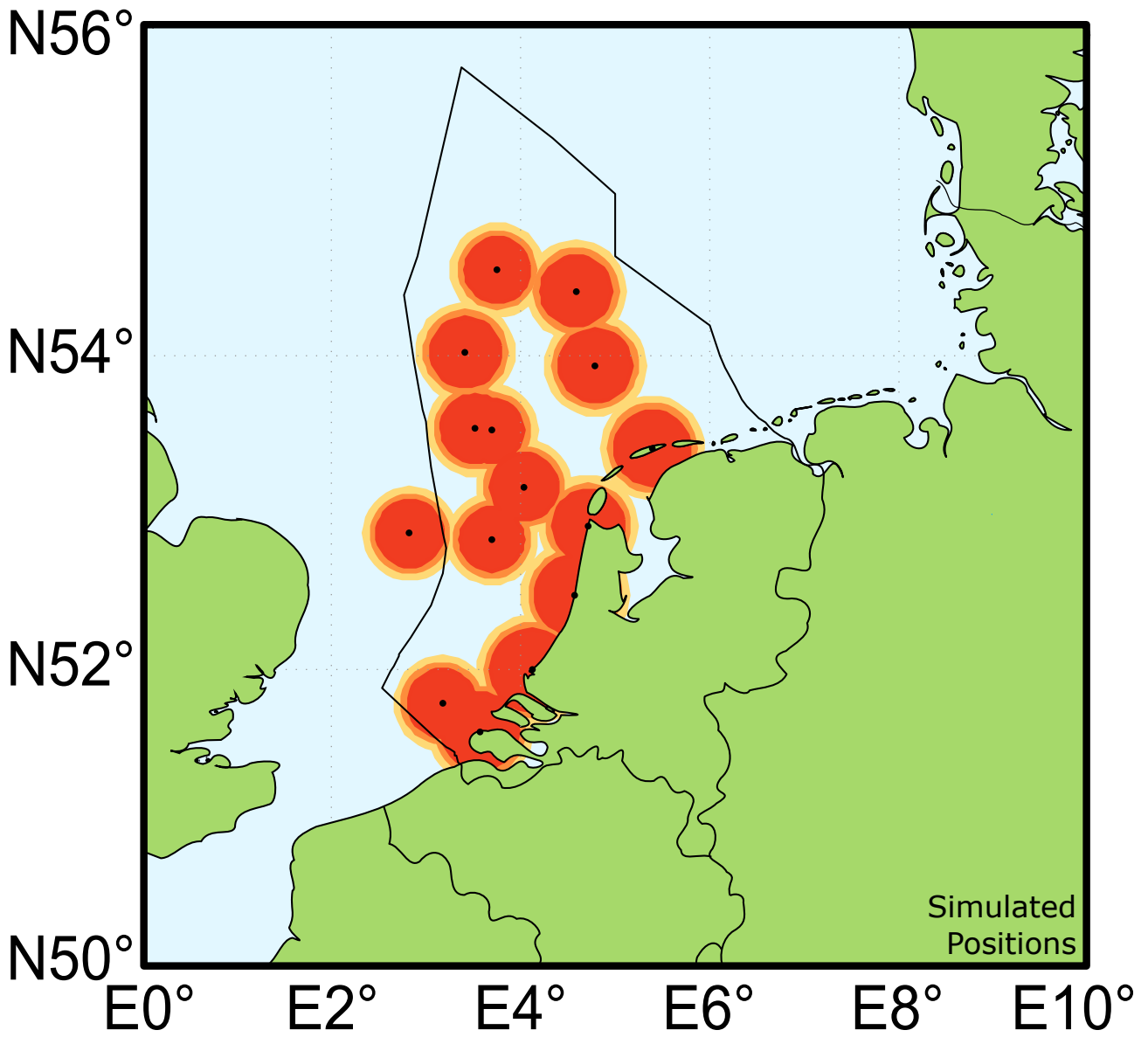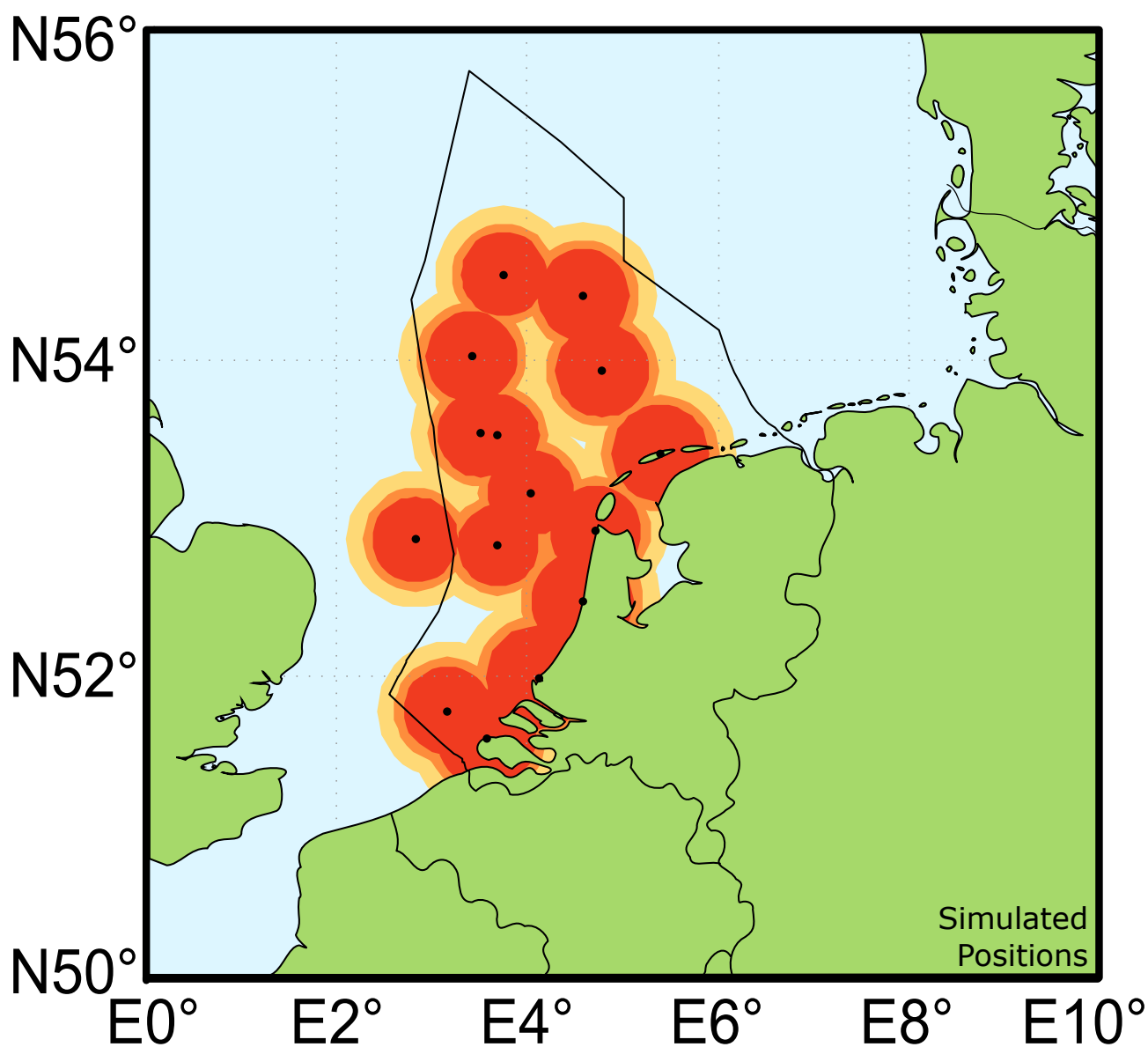
Maximum detection range for a target (antenna) at height (m):

5   10   20

Evaporation duct

AIS

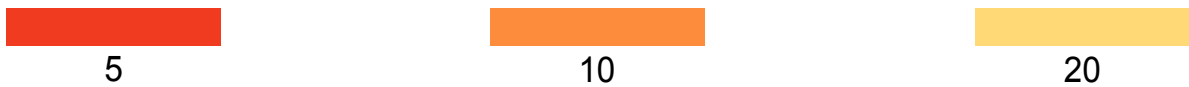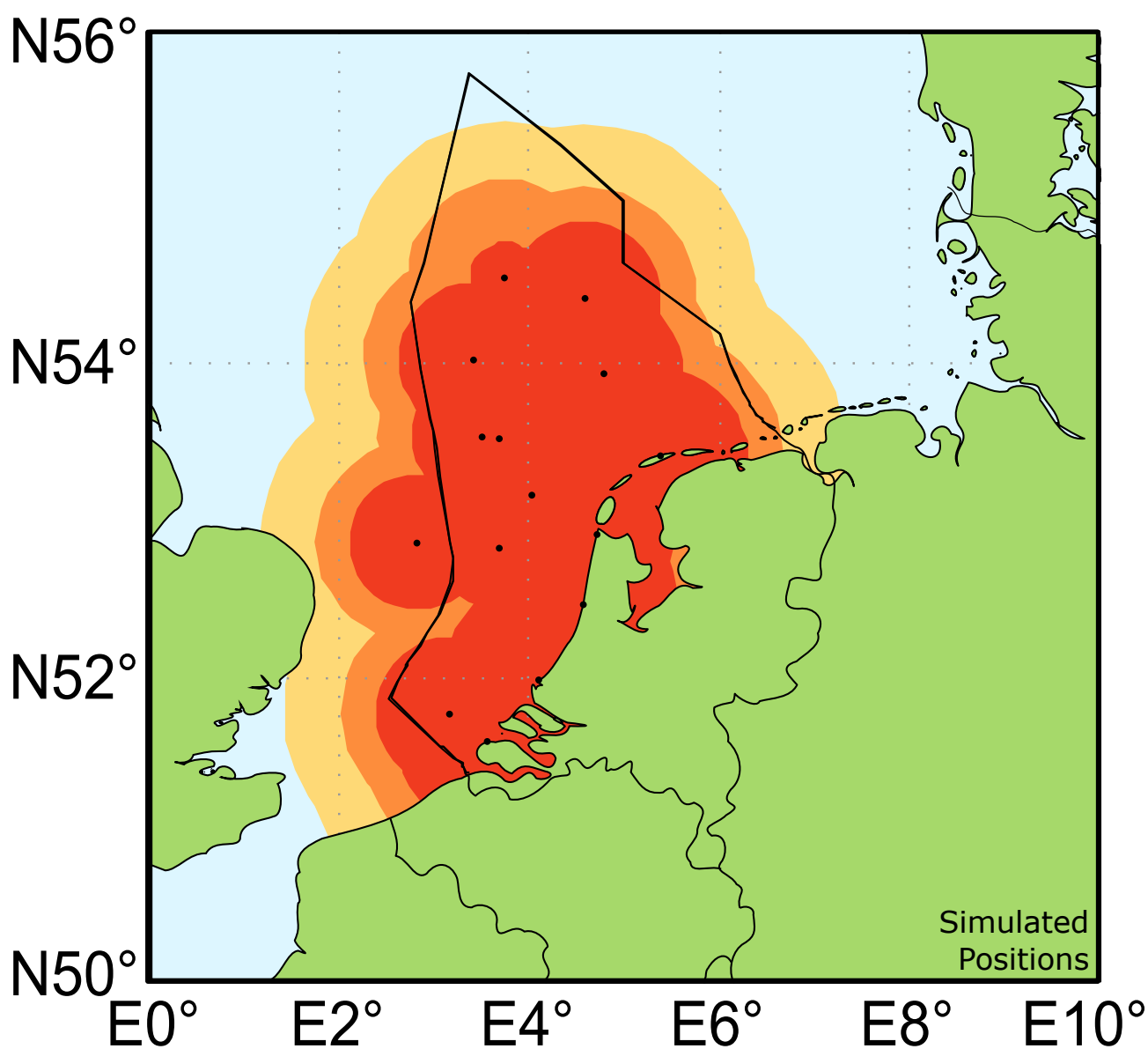Maximum detection range for a target (antenna) at height (m):

| 5 | 10 | 20 |

Evaporation duct
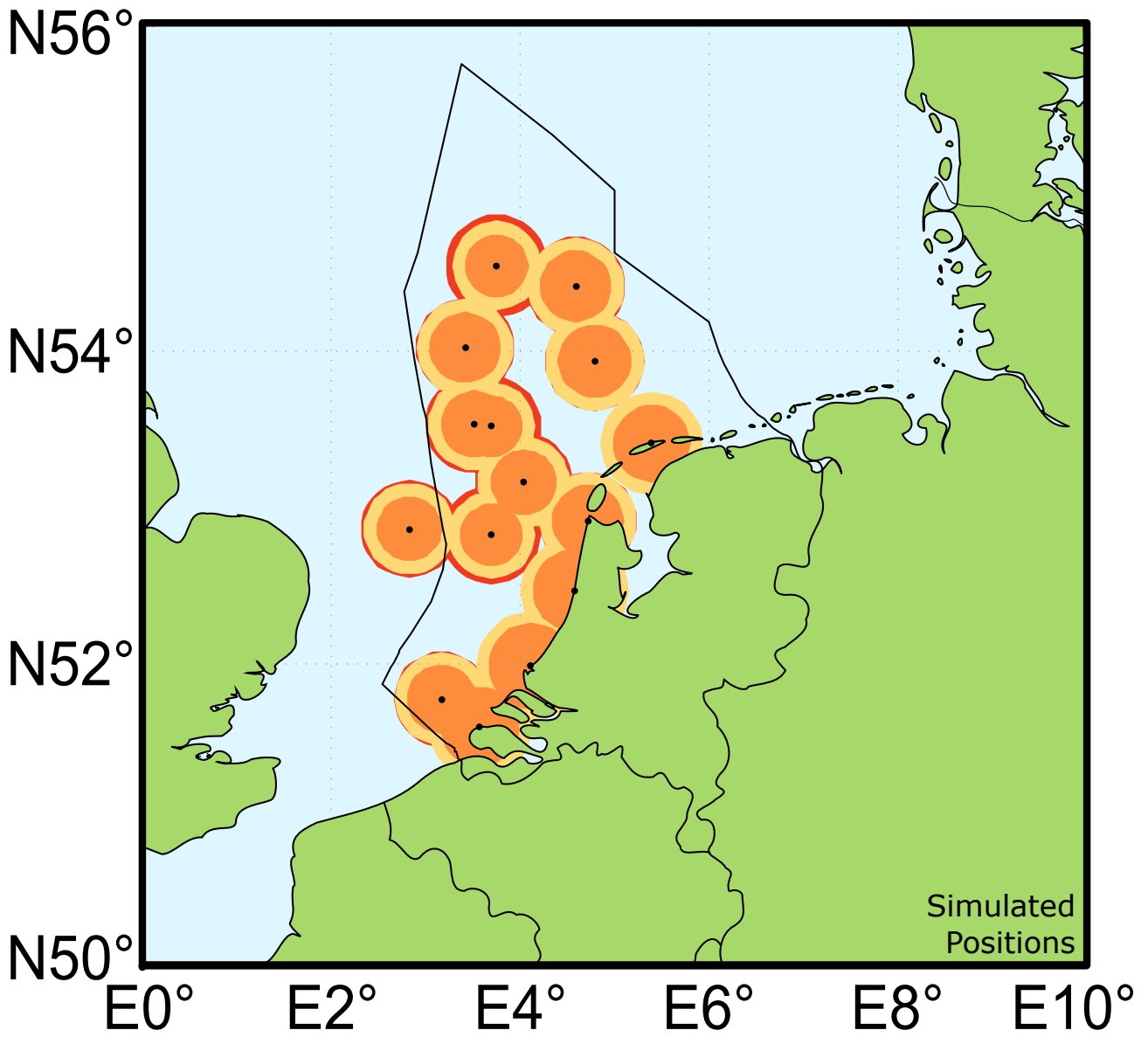
Radar

Maximum detection range for a target (antenna) at height (m):

5 10 20

Standard surface duct

AIS

Maximum detection range for a target (antenna) at height (m):

| 5 | 10 | 20 |

Standard surface duct

Radar

Maximum detection range for a target (antenna) at height (m):
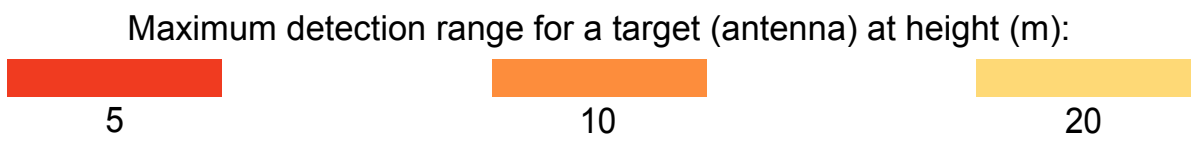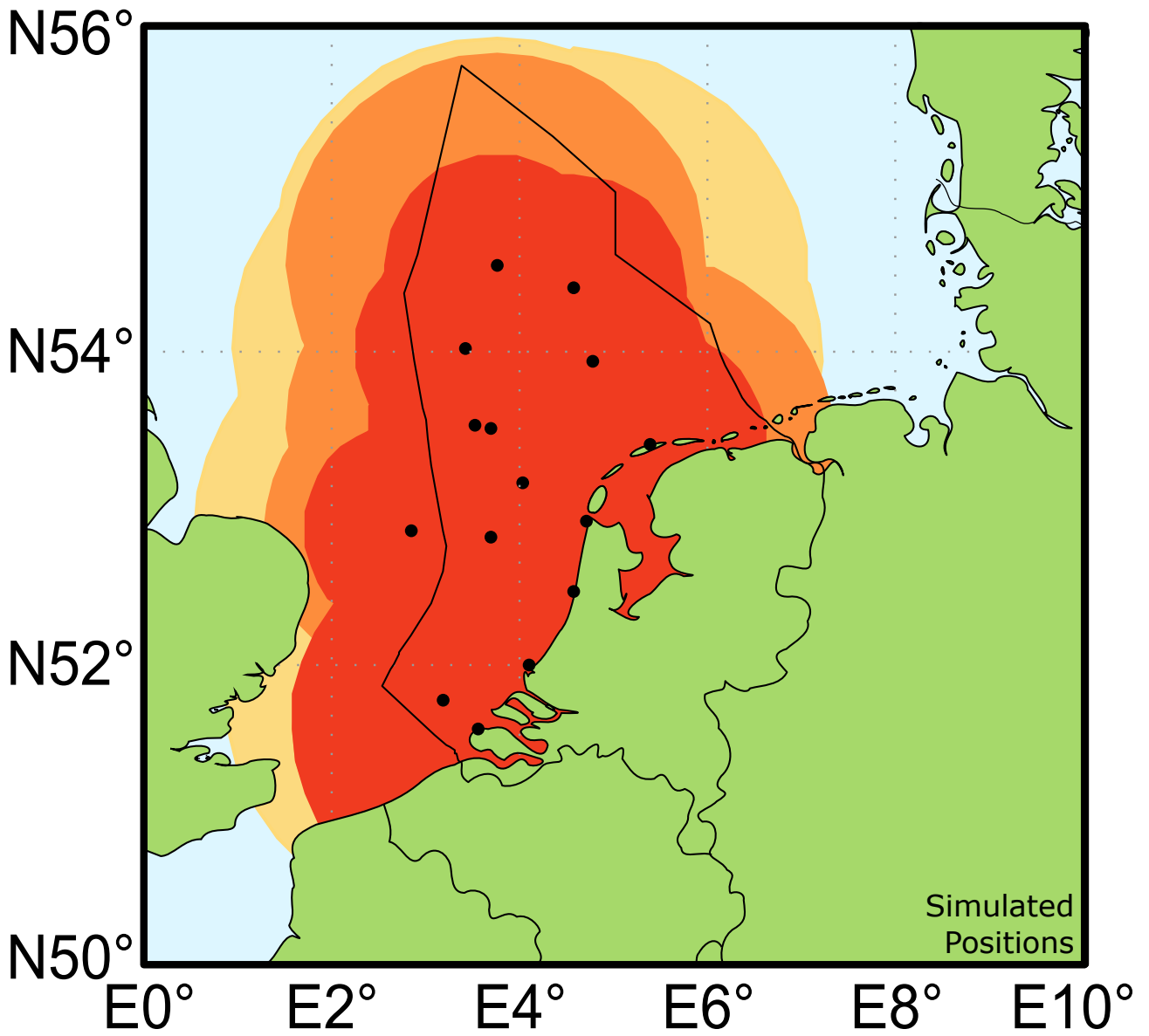
| 5 | 10 | 20 |

Surface-based duct

AIS
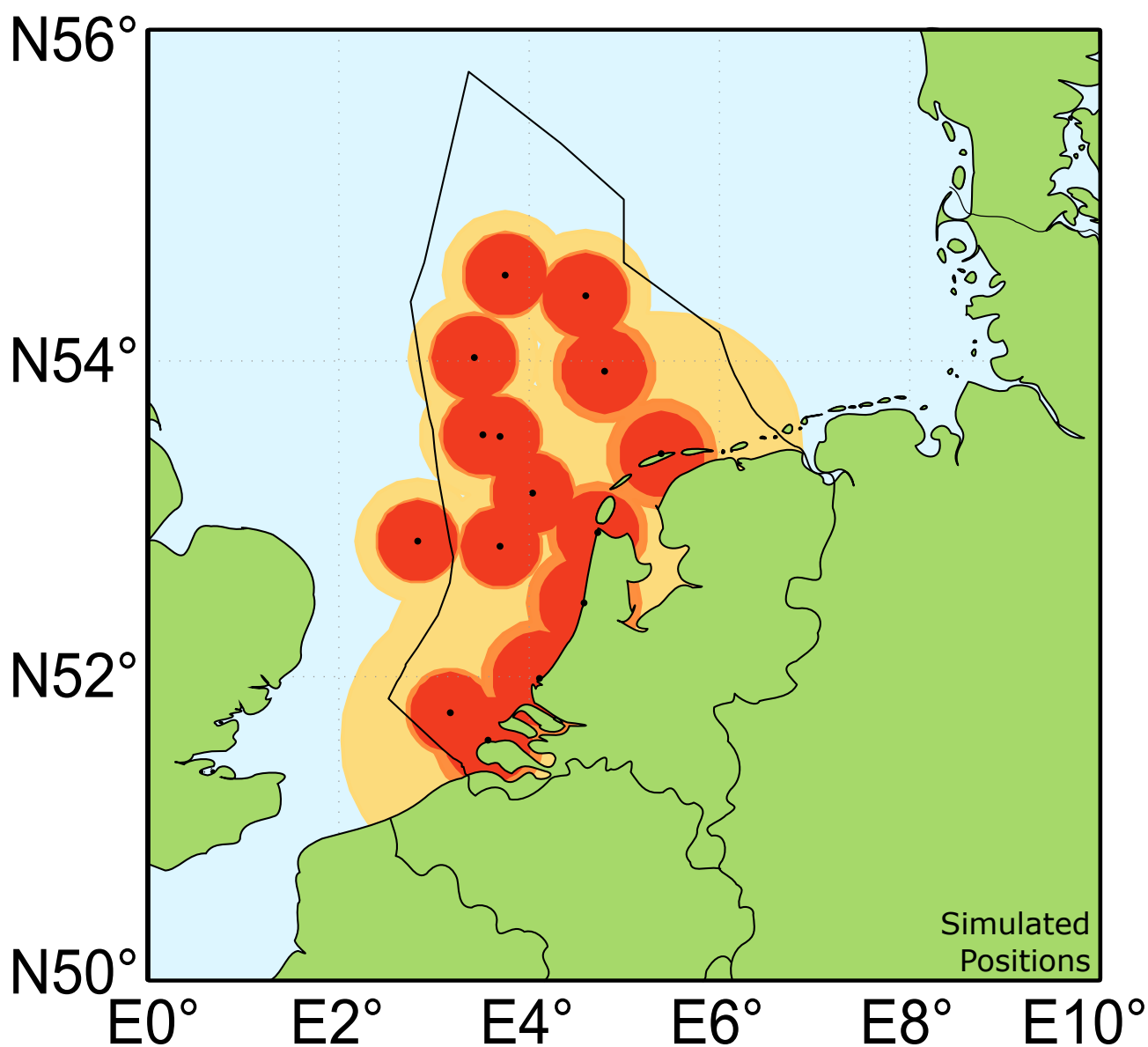
Maximum detection range for a target (antenna) at height (m):

| 5 | 10 | 20 |

Surface-based duct

Radar

Maximum detection range for a target (antenna) at height (m):

Elevated duct

AIS

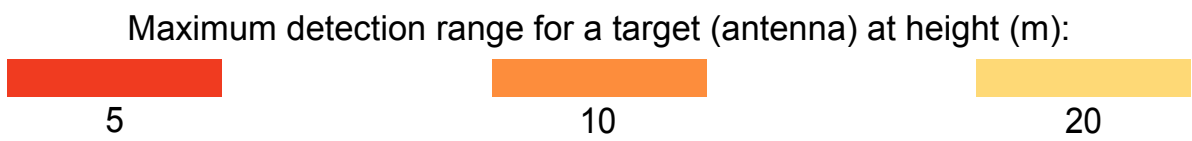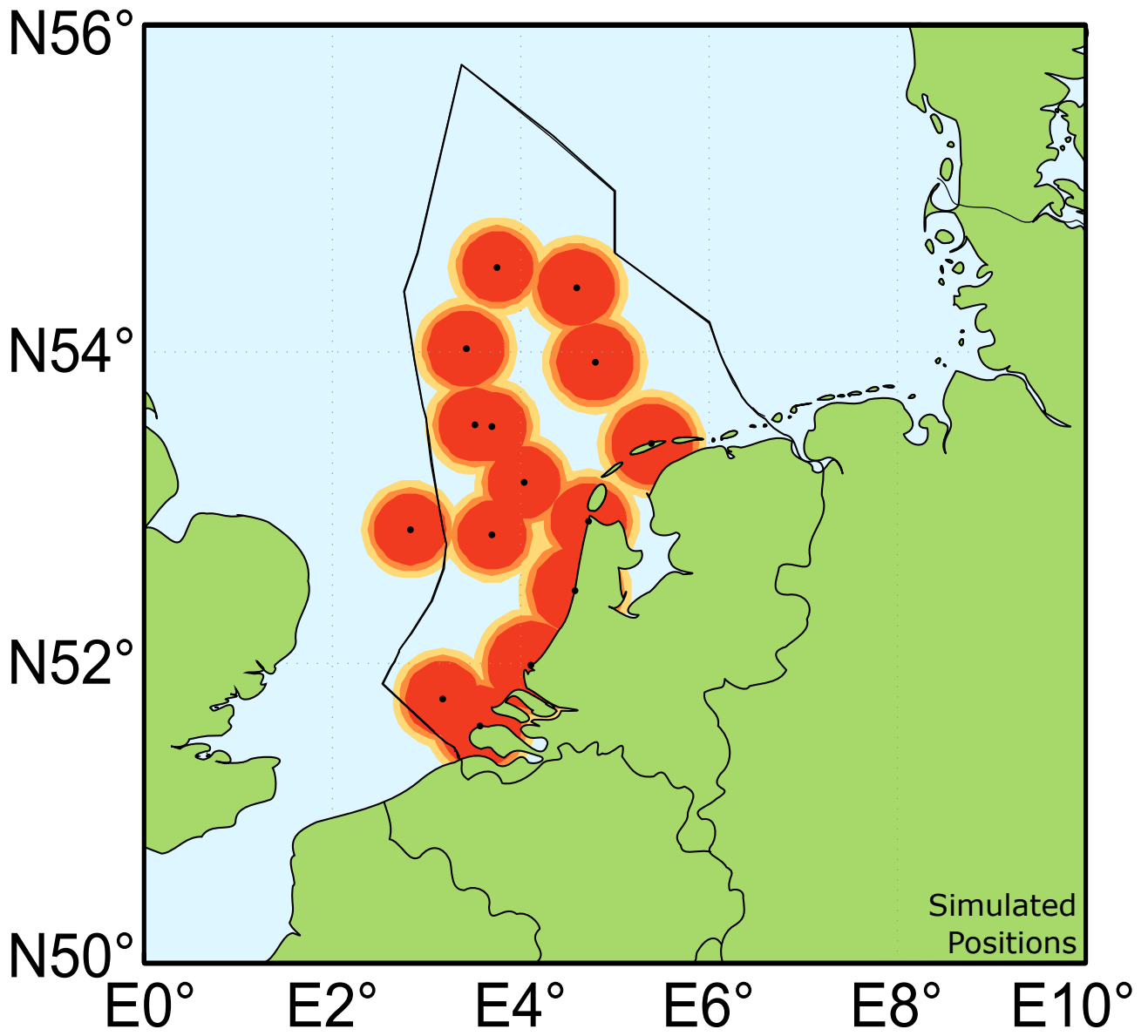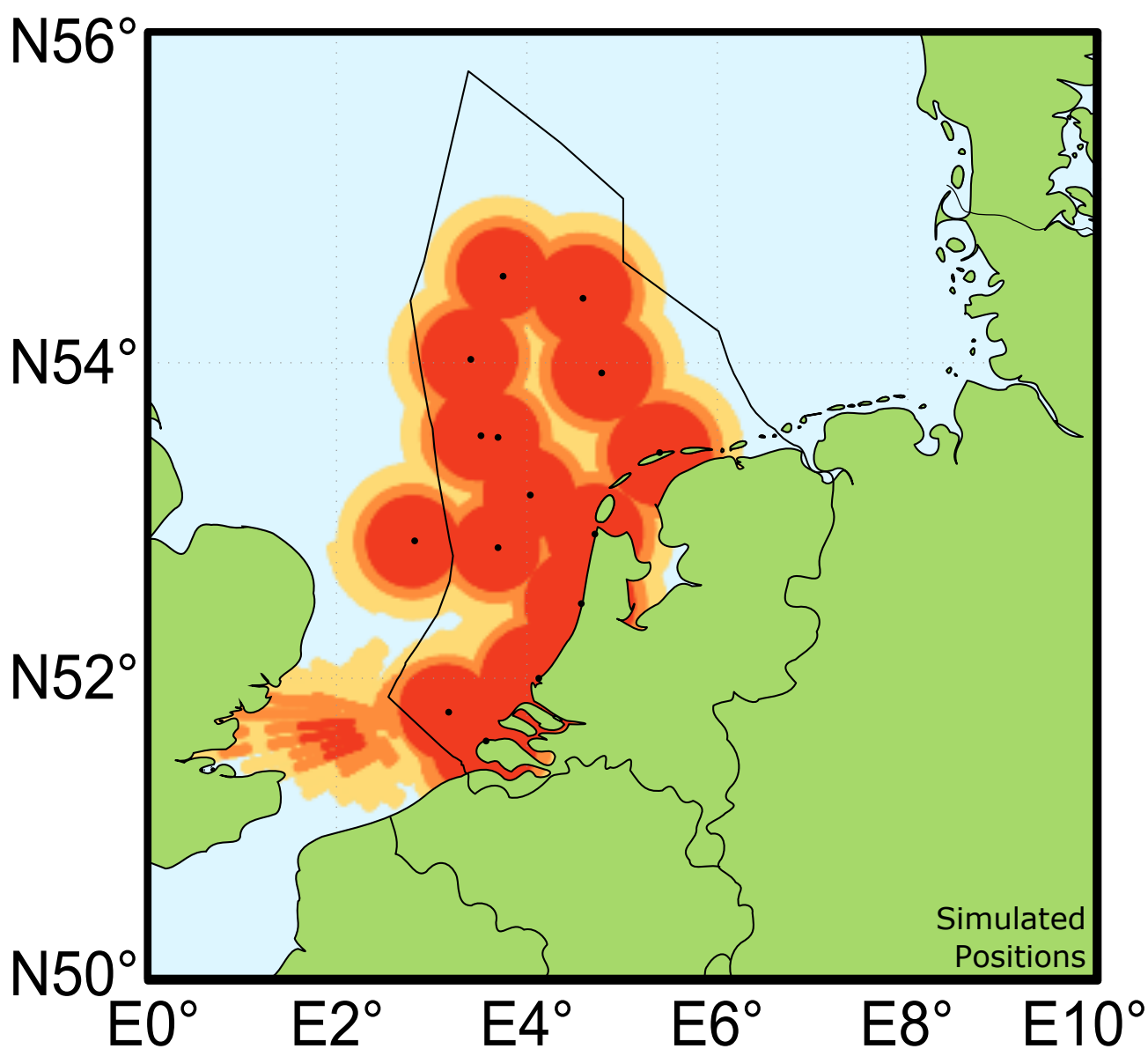Maximum detection range for a target (antenna) at height (m):

| 5 | 10 | 20 |

Elevated duct

Radar

Maximum detection range for a target (antenna) at height (m):

5   10   20

Real evaporation duct

AIS

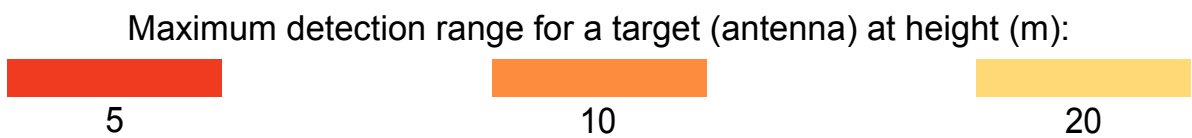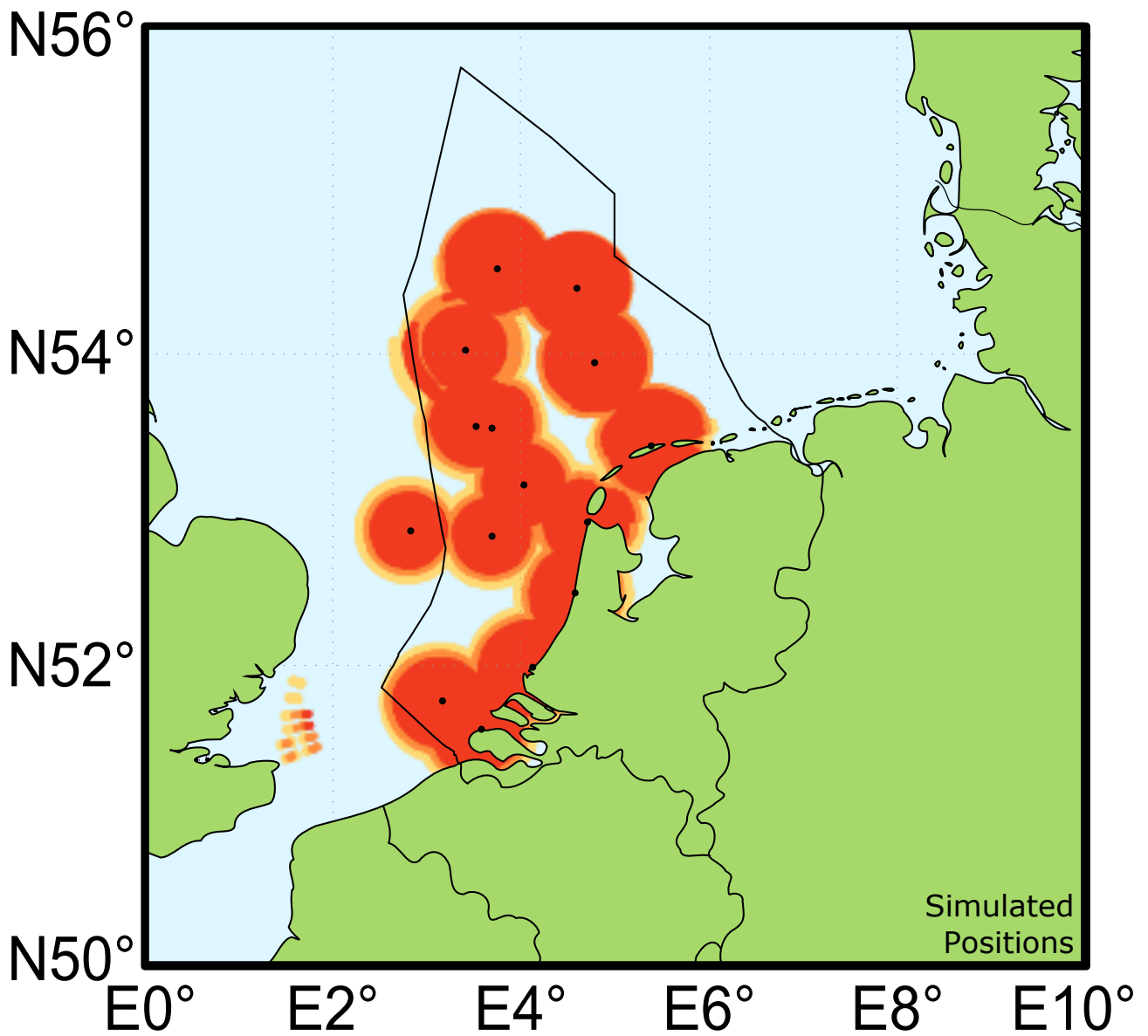Maximum detection range for a target (antenna) at height (m):

| 5 | 10 | 20 |

Real evaporation duct

Radar

Maximum detection range for a target (antenna) at height (m):

5   10   20

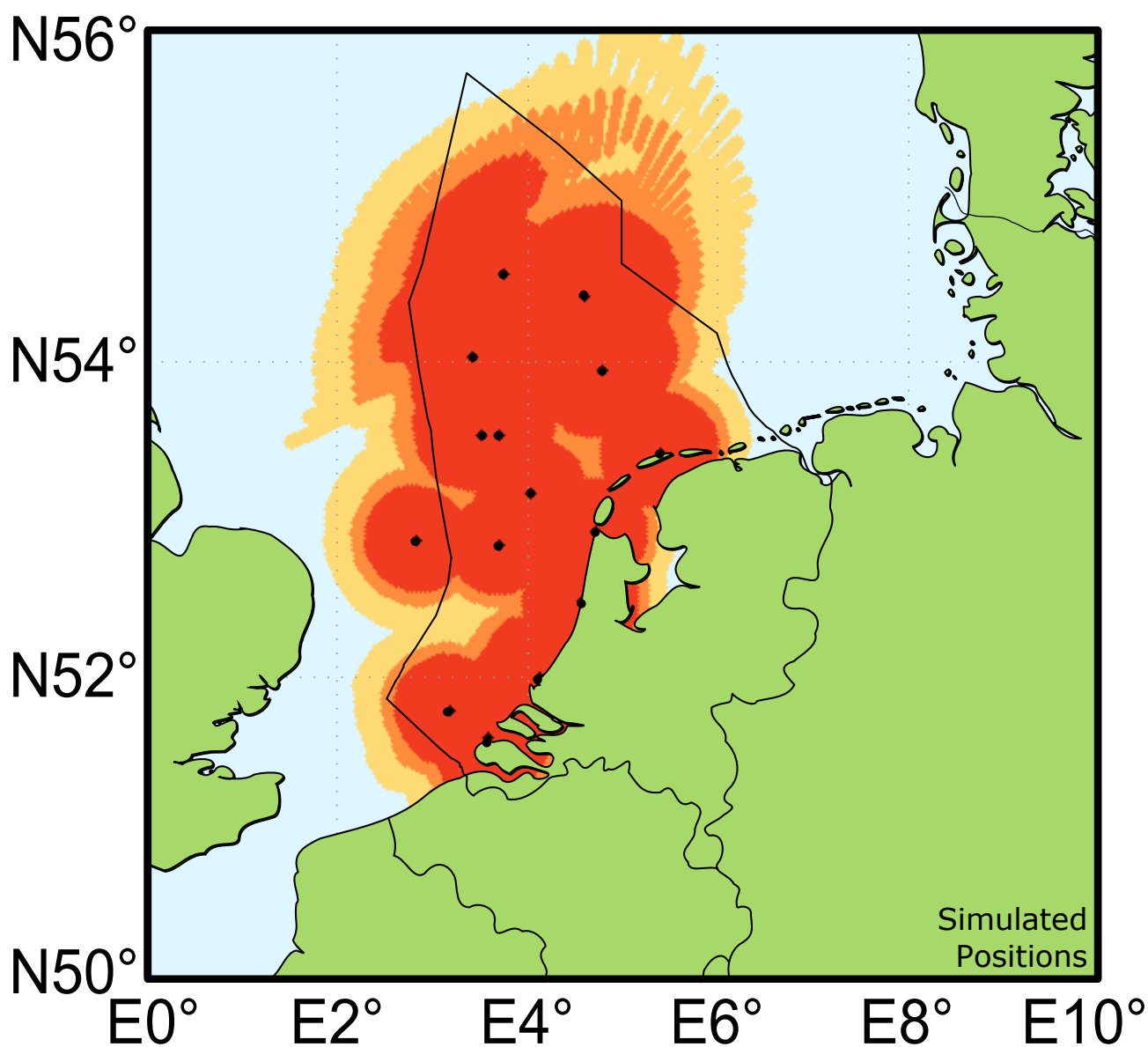# Real elevated duct

AIS

Simulated
Positions

Maximum detection range for a target (antenna) at height (m):
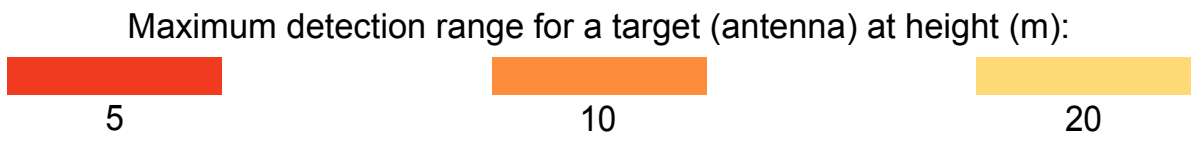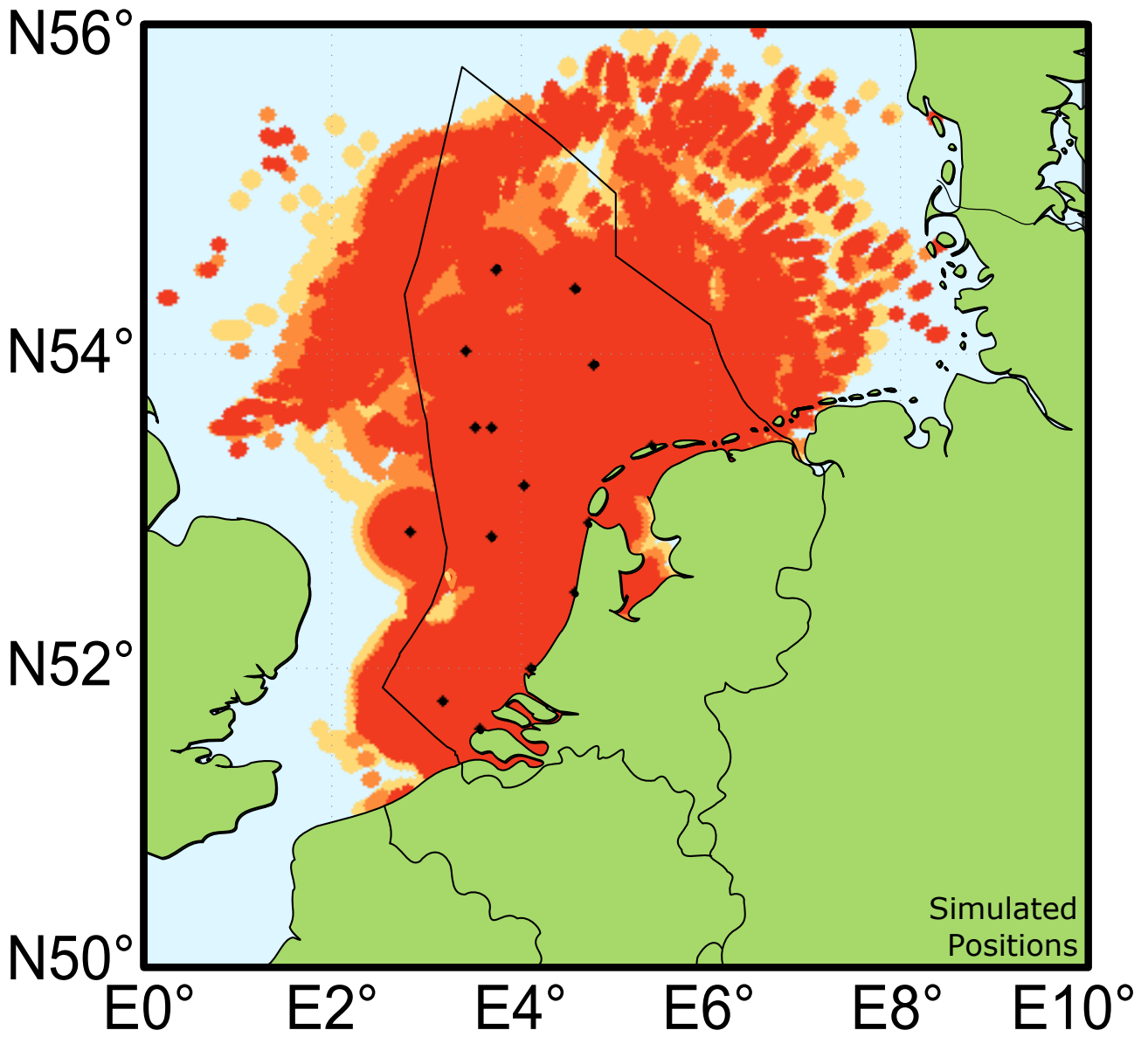
5   10   20

Real elevated duct

Radar

Appendix F

Line of sight

The line of sight detection range gives an indication of the detection range when only the curvature of the earth is taken into account. It shows the maximum detection range between a target and a receiver without the smooth surface of the earth blocking the signal. The formula for this is:

$$R_{max} = \alpha \left(\sqrt{h_{radar}} + \sqrt{h_{target}} \right) \tag{F.1}$$

with R_{max} the maximum detection range in either km or NM, h_{radar} being the radar antenna height in m, h_{target} being the target height in m, and α being the factor to take into account the curvature of the earth. In theory, α would only depend on R_{max} being in either kilometres of nautical mile, but it can be adjusted in case different sensor systems are used. For radar, α is 3.57 or 1.93 and for AIS, α is 4.17 or 2.25 for R_{max} in km or NM respectively. (See figure F.1)
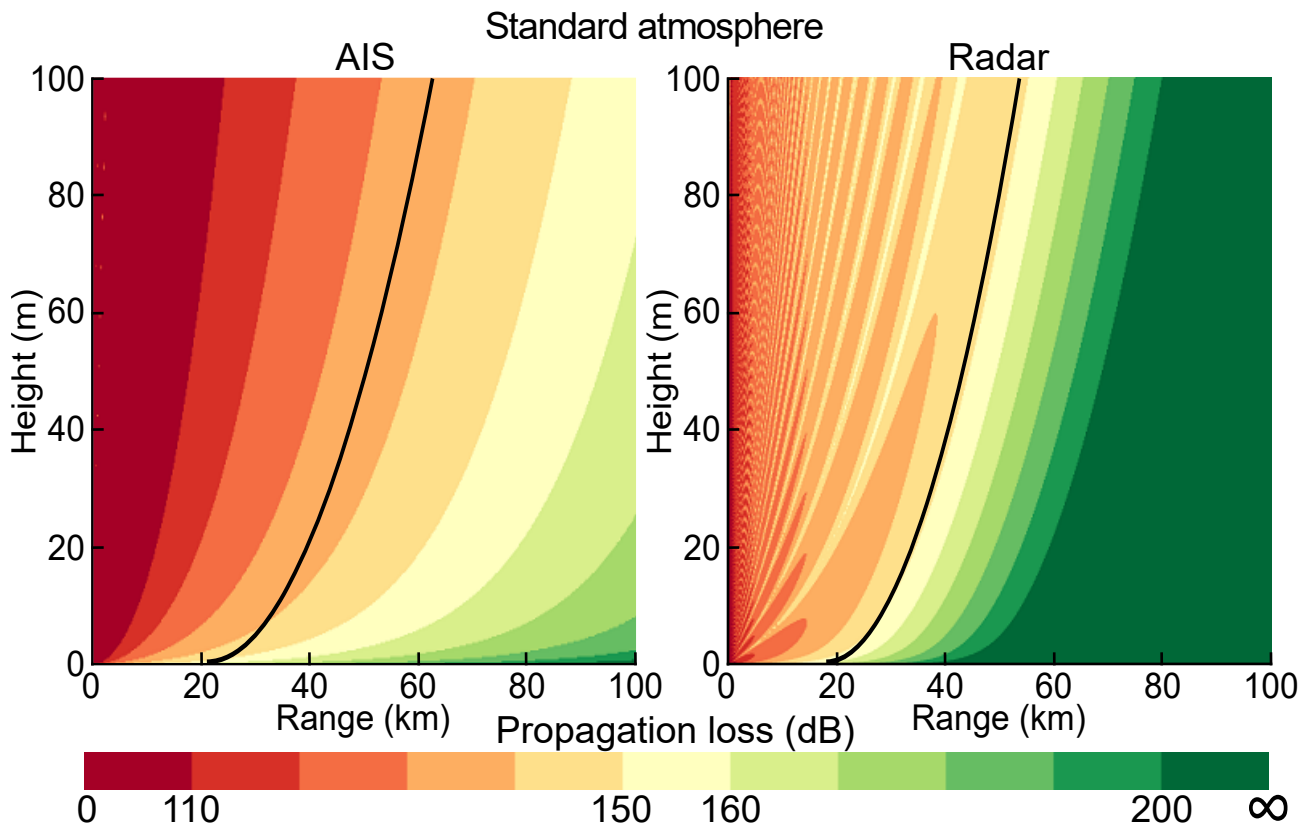

Figure F.1: Propagation loss in standard atmosphere with a black line that corresponds to the line of sight maximum detection range.

Table F.1: Detection ranges for both AIS and coastal radar for two antenna heights based on the line of sight detection range formulas.

	AIS				Radar			
Antenna height	39.8 m		50 m		39.8 m		50 m	
Target height	Range (km)	(NM)	Range (km)	(NM)	Range (km)	(NM)	Range (km)	(NM)
Line of sight								
5 m	35.6	19.2	38.8	20.9	30.5	16.5	33.2	18.0
10 m	39.5	21.3	42.7	23.0	33.8	18.3	36.5	19.8
20 m	45.0	24.3	48.1	26.0	38.5	20.8	41.2	22.3

Appendix G

All ranges

This appendix contains a summary of all detection ranges stated within this thesis.

Table G.1: Detection ranges for both AIS and coastal radar for two antenna heights during different conditions.

	AIS				Radar			
Antenna height	39.8 m		50 m		39.8 m		50 m	
Target height	Range (km)	(NM)	Range (km)	(NM)	Range (km)	(NM)	Range (km)	(NM)
Standard atmosphere								
5 m	31.5	17.0	34.5	18.6	23.5	12.7	26	14.0
10 m	37	20.0	40.5	21.9	27	14.6	31	16.7
20 m	49.5	26.7	53.5	28.9	32.5	17.5	36.5	19.7
Evaporation duct								
5 m	31.5	17.0	34.5	18.6	33	17.8	34	18.4
10 m	37.5	20.2	40.5	21.9	22	11.9	25	13.5
20 m	50	50	53.5	28.9	32.5	17.5	36.5	19.7
Standard surface duct								
5 m	69.5	37.5	77.5	41.8	101.5	54.8	73.5	39.7
10 m	91	49.1	101	54.5	111.65	60.3	93.35	50.4
20 m	136.5	73.7	147	79.4	124.95	67.5	104.53	56.4
Surface-based duct								
5 m	28	15.1	30	16.2	21.5	11.6	24	13.0
10 m	30.5	16.5	38	20.5	26	14.0	28	15.1
20 m	45.5	24.6	104	56.2	30.5	16.5	33	17.8
Elevated duct								
5 m	55	29.7	64.5	34.8	24.5	13.2	27	14.6
10 m	75.5	40.8	86	46.4	29.5	15.9	32	17.3
20 m	120	64.8	132	71.3	35	18.9	38	20.5